Shape and Deformation Analysis of the Human Ear Canal

Darkner, Sune

Publication date:
2009

Document Version
Publisher's PDF, also known as Version of record

Shape and Deformation Analysis of the Human Ear Canal

Sune Darkner

Kongens Lyngby 2008
IMM-PHD-2008-204

Technical University of Denmark
Informatics and Mathematical Modelling
Building 321, DK-2800 Kongens Lyngby, Denmark
Phone +45 45253351, Fax +45 45882673
reception@imm.dtu.dk
www.imm.dtu.dk

IMM-PHD: ISSN 0909-3192

Summary

This thesis presents work on the analysis of the dynamic behavior of the human ear canal. The work is based on two studies designed during the project, a pilot study with 30 normal hearing subjects and a main study with 42 hearing impaired subjects, all hearing-aid users. The main focus is on the extraction and analysis of the shape and deformation of the ear canal due to movements of the mandible, leaning over, and turning of the head. Methods for surface registration with focus on non-rigid registration are presented, as well as a wide range of statistical methods used for analyzing the shapes and deformation fields.

The results show that the ear canal changes shape significantly in all subjects and that the deformation is more complicated than previously described in the literature. It is shown that the deformation at specific locations in the ear is significantly correlated to comfort issues reported by the hearing-aid users. In addition, this thesis presents an unpublished analysis that relates shape and deformation. This enables clinicians to identify hearing-aid users that have a higher risk of problem related to deformation. In addition, the work should provide valuable information that can be used in future designs of hearing aids.

Resumé

Denne afhandling præsenterer et arbejde med analyse af de dynamiske egenskaber ved den menneskelige ørekanal. Arbejdet er baseret på to studier gennemført under projektet, et pilotstudie med 30 deltagere, alle normalthørende, og et hovedstudie med 42 deltagere, alle høreapparatbrugere. Fokus er lagt på at udtrække og analysere deformationer forårsaget af bevægelse af kæben, af at bukke sig ned, og af at dreje hovedet. Metoder til overfladeregistrering, med fokus på ikke-rigid registrering er præsenteret sammen med en bred vifte af statistiske metoder til brug for analyse af former og deformationer.

Resultaterne viser, at ørekanalen ændrer form signifikant hos alle personer, og at denne ændring er mere kompliceret end tidligere rapporteret i litteraturen. Det bliver påvist, at formændringen specifikke steder kan relateres til komfortproblemer, rapporteret af høreapparatbrugere. Endvidere præsenteres ikke-publicerede resultater som relaterer form og deformation til hinanden. Dette kan sætte klinikere i stand til at identificere den gruppe af brugere, der har en højere risiko for komfortproblemer relateret til deformationer. Endvidere giver arbejdet en værdifuld viden der kan bruges i fremtidige design af høreapparater.

Preface

This thesis was prepared at Informatics and Mathematical Modeling, the Technical University of Denmark and Oticon Research Centre Eriksholm in partial fulfillment of the requirements for acquiring the Ph.D. degree in engineering. The project is the result of a cooperation with Forsknings- og innovationsstyrelsen (FIST).

The thesis deals with shape changes or deformations of the human ear canal. Through the use of advanced surface registration algorithms and statistical methods for high dimensional data, the deformation of the ear canal is quantified and correlations with shape and comfort issues are explored.

The thesis consists of a summary report and a collection of six research papers written during the period 2005–2008, and published elsewhere.

Funding of the project was provided by the Oticon Foundation and FIST (former VTU).

The project was supervised by Prof. Rasmus Larsen (IMM) in collaboration with Rasmus R. Paulsen (IMM/Oticon), Ole F. Olsen (Oticon) and Prof. Polina Golland (CSAIL M.I.T.).

Lyngby, August 2008

Sune Darkner

List of Submitted and Published Papers

This is a list of the papers prepared during the project. It includes the papers included in this thesis and additional published papers. The included papers were chosen due to the coherence between them and with the main subject of the thesis. The additional paper includes original work but has been excluded from the thesis for clarity reasons and are cited instead. Each paper is listed with the chapter in which it occur and corresponding reference. Papers not included in the thesis is listed with reference. All paper are referenced through out the thesis with the general reference.

Journal

- L. H. Clemmesen and S. Darkner, Classification in Longitudinal Studies, Medical Image Analysis, (Submitted) (Chapter 13([23]))

Conference

- S. Darkner, M. R. Sabuncu, P. Golland, R. R. Paulsen, and R. Larsen. Analysis of surfaces using constrained regression models. In Medical Image Computing and Computer Assisted Intervention- MICCAI 2008, LNCS. New York, USA, Springer, September 2008. to appear. (Chapter 9 ([42]))

- S. Darkner, R. R. Paulsen, and R. Larsen. Analysis of deformation of the human ear and canal caused by mandibular movement. In Medical Image Computing and Computer Assisted Intervention MICCAI 2007, pages 801-808, B, oct 2007. Brisbane, Australia, Springer Lecture Notes. (Chapter 10 ([40]))

- S. Darkner, M. Vester-Christensen, R. R. Paulsen, and R. Larsen. Non-rigid registration of 2D manifolds in 3D Euclidian space. In Joseph M. Reinhardt and Josien P. W. Pluim, editors, Proc. Medical Imaging 2008: Image Processing, volume 6914, page 69142R. SPIE, 2008. (Chapter 11 ([43]))

- S. Darkner, D. Witzner Hansen, R. R. Paulsen, and R. Larsen. Robust registration for change detection. In Josien P. W. Reinhardt, Joseph M.; Pluim, editor, Proc. SPIE Medical Imaging 2007: Image Processing, volume 6914, pages 69142T-69142T-8. SPIE, April 2008.(Chapter 12 ([44]))

- S. G. H. Erbou, S. Darkner, J. Fripp, S. Ourselin, and B. K. Ersbøll. Estimation of shape model parameters for 3D surfaces. In 5th IEEE International Symposium on Biomedical Imaging, pages 624−627, may 2008. (Chapter 14 ([55]))

Additional Papers

- S Darkner, M Vester-Christensen, R Larsen, R R. Paulsen, and C Nielsen. Automated 3D rigid registration of open 2D manifolds. In Proc. From Statistical Atlases to Personalized Models Workshop, MICCAI 2006, pages 19-22. ([38])

- F. Kahraman, M. Gokmen, S. Darkner, and R. Larsen. An active illumination and appearance (aia) model for face alignment. In Proceedings of the CVPR 2007, IEEE Computer Society Workshop on Biometrics, pages 1-7. IEEE Computer Society, jun 2007. ([88])

- S. Darkner, M. Vester-Christensen, R. Larsen, and R. R. Paulsen. Evaluating a method for automated rigid registration. In Josien P. W. Pluim and Joseph M. Reinhardt, editors, Proc. SPIE Medical Imaging 2007: Image Processing, volume 6512, page 651225. SPIE, 2007. ([41])

- M. Vester-Christensen, S. G. Erbou, S. Darkner, and R. Larsen. Accelerated 3D image registration. In Joseph M. Pluim, Josien P. W.; Reinhardt, editor, Proc. SPIE Medical Imaging 2007: Image Processing, volume 6512, page 65121W. SPIE, mar 2007. [164]

Acknowledgements

I thank my supervisors Rasmus Larsen, Rasmus R. Paulsen and Ole F. Olsen for encouraging discussions and guidance through the project. A special thanks goes to Claus Nielsen from Oticon for a very honest, fruitful and devoted collaboration, and the help in acquiring all of my data. I have really enjoyed all the discussions and wacky ideas we've worked on, and the project has really benefitted from your experience and knowledge of the subject.

A special thank goes to my family. My wife Frederikke and my son Zacharias whom both have put up with a lot, especially around paper deadlines, but also for coming along with me to Boston during my visit to M.I.T. Thanks to my family for support and encouragement during the project.

Thanks to all my colleagues at Eriksholm. It has been a truly great experience working with you. Thanks for very good discussions and feedback on the project, it really helped a lot. Special thanks to Sørent Laugesen for proofreading a lot of my stuff, in particular this thesis.

Thanks to 3D lab, Tron Darvann, Nuno Herman, Per Larsen and Svend Kreiborg for providing me with data on the anatomy of the human head and giving me access to a surface scanner.

Thanks to all the people in the image group at IMM, Bjarne K. Ersbøll, Henrik Aanes, Andreas Bærentzen, Martin Vester-Christensen, Søren Erbou, Mads F. Hansen, Michael S. Hansen, Hildur Olafsdottir, Jeppe Frisvald and the rest of the group.

Thanks to Polina Golland at M.I.T. for letting me stay with her group for 6 months. Thanks to Mert Sabuncu, Boon Thye (Thomas) Yeo, Wanmei Ou, Danial Lashkari, Yongwook (Bryce) Kim, Archana Venkataraman, Serdar Balchi, Tamar Riklin Raviv and Koen van Leemput for inspiring discussion and feedback at M.I.T.

I would like to thank Ingelise Pedersen, Zenia Lausten, Lars Næsby and Momirka Dasic Vulevic at ITE Lab, Oticon for helping me with the scanning of the impressions.

Finally I would like to thank Oticon, the Oticon Foundation and FIST for supporting the project financially.

Contents

Part I

Shape and Deformation Analysis of the Human Ear Canal

Chapter 1

Introduction

This thesis addresses the problem of shape changes to the ear canal due to movement of the mandible as well as some restricted movements of the head e.g. turning of the head and leaning over. This is important because these shape changes are a major cause of discomfort for hearing aid user. Many hearing aids are made from a hard acrylic material and are a not able to accommodate the shape changes and thus acoustical feedback and discomfort can occur. Based on a study specifically designed for this project, advanced statistical methods are applied to reveal novel discoveries about the human ear and how and where shape changes occur.

1.1 Scope

The original scope of the project was to uncover how the ear and canal deforms during jaw movement. This was during the project extended to include two other common movements of the head. The scope was extended due to the fact that hearing impaired test subjects during interviews and small talk mentioned problems related to these specific motions. The task has not been trivial since no data existed and a study for that specific purpose needed to be designed from scratch. The design of the study included gathering information about anatomy and knowledge about comfort-related problems due to the movements

of interest. Knowledge of comfort-related problems was gathered extensively throughout the project by participation in fitting sessions with hearing aid users and discussions and interviews with users. This process was carried out in close collaboration with clinical audiologist Claus Nielsen at the Oticon Research Centre Eriksholm.

While gathering all this background information a parallel course with development and implementation of registration methods was followed. It was realized quite early on that automatic procedures for registration were essential due to the potential huge amount of data. No methods that accommodated the special properties of the ear data could be identified, thus methods had to be adapted and developed to accommodate these. Finally, suitable methods for data analysis had to be identified and consequently the thesis has very wide scope. The scope ranges from anatomy through computer graphics to surface registration and regression, machine learning, classification, hypothesis testing and optimization, with each of these topics as a research area in itself.

1.2 Purpose

The purpose of this project is to give the reader insight into how the human ear canal changes shape with movement of the mandible, turning of the head and leaning over, three very common movements. Furthermore it gives the reader insight into the design of the study and how the data where collected as well as an overview of the classes of methods used to analyze the ear data. Besides the original published work, the thesis contains a new analysis of how shape and deformation is correlated and an unpublished analysis of the deformations caused by turning of the head and leaning over respectively. The goal is to give a complete picture of a very complicated subject and to contribute to the knowledge base that eventually will create better comfort for hearing aid users by enabling better design of future solutions.

1.3 Custom Hearing Aid Production

In order to give the reader the right prerequisites for reading the thesis, a brief introduction to the process of making a hearing aid is described. Custom hearing aids are cast after the customers ear. Today this process is done by obtaining an impression from the customers ear by injecting a composite silicon material that sits while in the ear of the customer (figure 1.1). The resulting cast is then shipped to a production facility where the impression is scanned in a 3D surface

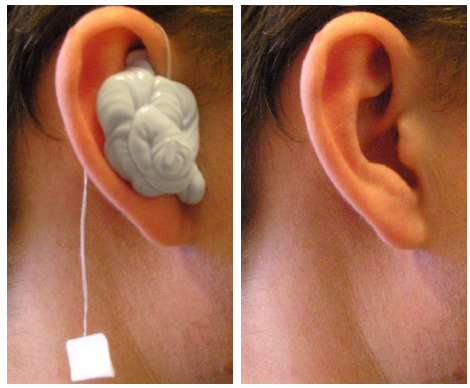

(a) (b)

Figure 1.1: An ear with impression material and an ear without. This figure shows the extend of the impression in Pinna, which only includes the Concha.

scanner. This is the modality of the data used in this thesis if not stated otherwise. After the scanning the hearing aid is modelled digitally and the final shell is printed using SLA, a laser based printing process that solidifies a photopolymer epoxy resin. The electronics including the speaker, amplified and the lid mounted with microphones and battery drawer, also called a faceplate, is then placed and fitted manually to the printed shell. The result is a CIC (Completely In the Canal) or ITE (In The Canal) that precisely fits the customers ear in the position the impression was obtained (figure 1.2).

1.4 About Oticon

The William Demant Holding Group was founded in 1904 by Hans Demant. Hans Demant, whose wife had a hearing loss, went to London to get a hearing aid for his wife. That very same year, he became a hearing instrument agent and founded the company Oticon. After Hans Demant's death in 1910, his son William took over the business. In 1957, William and his wife Ida Emilie donated the Demant family's shares in the company to the Oticon Foundation. The Oticon Foundation's general aim is charity with particular emphasis on helping people with a hearing impairment, and today the Oticon Foundation is the main shareholder in William Demant Holding A/S which is listed on the OMX and is in the C20 index [3]. Oticon is the largest of the 3 hearing aid manufactures in Denmark which together has approximately 40% of the world market for hearing aids. The other two Danish companies are GN Resound

Figure 1.2: A CIC (Completely In the Canal)hearing aid. It is the smallest if the ITE's (In The Canal)).

and Widex which is privately held. In 1977 Research Centre Eriksholm was established with the purpose of doing research within hearing, not specifically aimed at technology but with a broader perspective. Today approximately 25 people are employed at Eriksholm, which is located in Helsingor more than 40 km from the headquarters.

1.5 Background and Motivation of the Project

Modern hearing aids contains some of the most advanced and durable electronics and some of the best and most robust algorithms for directionality, noise reduction and feedback cancellation. As the technology evolved the production of the encasing and the way they were fitted physically remained the same. In spite of the state of the art technology some hearing aid styles are made from hard acrylic material unable to absorb shape changes of the ear and canal. The introduction of the SLA production technique and scanning of the impressions i.e. a digitization of the production has enabled shape analysis on ear canals. The first to do so was Paulsen [120] who used scannings of ear impressions to explore the shape of the ear and the possibilities in the production environment such as finding the optimal insertion path etc. This thesis takes its offset in his work, with the main focus on the dynamic shape changes that potentially cause problems for hearing aid users.

The dynamic behavior of the ear canal is challenging for some hearing aid-users, because it causes the hearing aid to fall out of the ear, and can make the ear canal sore or go into acoustical feedback. The acoustical feedback occurs due

to the fact that when the ear changes shape the hearing aid does not fit the ear perfectly anymore and a so called false vent occurs. This can potentially cause the finely tuned hearing aid to go into feedback. Even though very good feedback cancellation algorithms have been developed, the hearing aid still makes a squeaking noise. As the electronics are becoming smaller and smaller and the market reports that customers often desire an invisible hearing aid, the hearing aids are becoming smaller and smaller. This places them deeper into the ear canal and gives them smaller surface area, thus, they can more easily slip out of the ear, a problem called retention in audiology.

In the past three years a new type of hearing aid have come into the market. It is the so called RITE (Receiver in the ear), both as an open fitting (i.e. no acoustical seal) or as a closed fitting with a so called micro mold. These new solutions are cosmetically very attractive and are due to their design almost invisible. The experiences are still few, but, retention seems to be the designs Achilles heel. Thus, the knowledge of the dynamic behavior could improve the design.

1.6 Thesis overview

To guide the reader, a short overview of the contents of the thesis is given.

1.6.1 Part I

Chapter 2 This chapter introduces the anatomy of the human ear and canal and the surrounding tissue in order to create a basic understanding of the physical domain. The potential causes of the deformation are introduced and explained.

Chapter 3 This chapter introduces the data sets collected in this study, along with an existing data set, made available from the production at Oticon. The data sets are described in detail with emphasis on the main study, which also includes a questionnaire.

Chapter 4 An extensive review of previous work within the field of ear deformation is provided. This includes studies of the deformation of the human ear

canal, techniques that minimizes the effects of the deformation, some product designs that accommodate shape changes to the ear canal and shape modeling.

Chapter 5 An overview of the methods used for shape analysis is given. The methods are constrained regression techniques such as the ridge regression and the elastic net along with classification via the support vector machine. Generalizations of penalties to the support vector machine are introduced plus the support vector domain descriptor. The methods are put in common optimization framework.

Chapter 6 An introduction to registration in general is given with specific focus on some of the methods used and developed in this thesis. The loss function, norm, and constraints or regularization are discussed, in particular the formulation of the regularization, as either implicit or explicit. The optimization of the registration is discussed and a relationship to regression is established. As an example of a constraint, the shape model is introduced, turning the fitting of a shape model into a constrained registration problem.

Chapter 7 This chapter provides an overview of the application of the shape analysis methods and the registration techniques with respect to the ears in this study. An overview of the published work is given with short description of the contents of each paper as well as a presentation of the latest unpublished work on the shapes and deformation fields.

Chapter 8 This chapter summarizes and discuses the results. An overall conclusion of the results and the project is presented.

1.6.2 Part II

This part of the thesis describes the application of some of the methods to the data sets in terms of original work published during the course of the Ph.D project.

Chapter 9 This paper was written during my 6 moths stay with Polina Golland at CSAIL, M.I.T. in Boston, USA. It deals with constrained regression

analysis of reported acoustical feedback from hearing aid users onto deformation field associated with the surfaces. The paper is included because it shows that deformation and feedback is related and that it is possible to identify the correlated regions of the deformation field. The paper was written together with Mert R. Sabuncu, Polina Golland, Rasmus R. Paulsen and Rasmus Larsen.

Chapter 10 This paper derives a shape and deformation model. Furthermore, it investigates correlation between shape and deformation, shape and gender. The paper shows through large scale hypothesis testing, that all ears in the study has significant deformation. The paper has been included in the thesis because it show that every subject in the study experiences significant deformation. The paper was written with Rasmus Larsen and Rasmus R. Paulsen.

Chapter 11 This paper describes the non-rigid registration algorithm developed during the project. The method is based on distance maps which turns out to have properties that increase the computational speed of the algorithm. The algorithm described is for pairwise registration. It is included because it describes the basic frame work for all the registration performed during the project and thus, forms the basis of most of the statistical analysis. The paper was written with Rasmus R. Paulsen and Rasmus Larsen.

Chapter 12 This paper suggests a robust method for rigid registration for change detection. The method is based on rigid and non-rigid registration and large scale hypothesis testing combined with the mean shift algorithm. The basic idea is to identify outliers, in this case changing areas, and iteratively exclude them from the rigid registration. It has been included because it presents an interesting application of large scale hypothesis testing and clustering to registration. This paper was prepared together with Dan W. Hansen, Rasmus R. Paulsen and Rasmus Larsen.

Chapter 13 This paper describes an extension to the support vector machine. In longitudinal studies data have a certain structure and in the case of the ear impressions we have several observations from the same individual with differen properties or pathologies. By using this particular structure, a data driven constraint is derived, which is then generalized to operators for both an ℓ_1 and ℓ_2 penalty. The paper is included because it shows an interesting extension of the support vector machine based on the properties of the data set itself, with a general extension of operator based constraints. Furthermore, it contains a successful classification of open and closed mouth ear impressions. This paper

is submitted to Medica Image Analysis and was prepared together with Line H. Clemmesen.

Chapter 14 This paper shows how the fitting of the shape model can be written as a registration problem of the mean shape constrained by the modes of variation from the model. This paper connects shape models with registration in an elegant way and is therefor included in the thesis. The paper was prepared in collaboration with Søren Erbou, Jürgen Fripp, Sebastien Ourselin, and Bjarne. K. Ersbøll

Appendix This includes the application submitted to and approved by the research ethical committee and the developed questionnaire used in the main study.

1.6.3 Figures

Some of the figures are 2D projections of 3D surfaces and can be some what difficult to read. The projections used are those which are thought to be the most informative. However, to help the interpretation along the number of projections used for results have been limited to 3 when results are displayed in chapter 7 (se figure 1.3). There is the into the ear projection as in figure 1.4(a), the canal view (figure 1.4) and the inside out view (figure 1.4(c)).Other projection will occur as well in other chapters, however these are the prevailing projections.

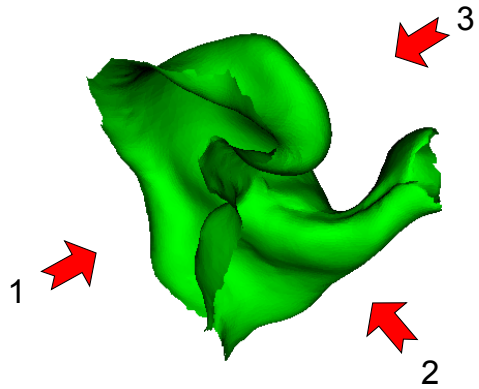

Figure 1.3: The directions of the 3 major projections in relation to an ear impression..

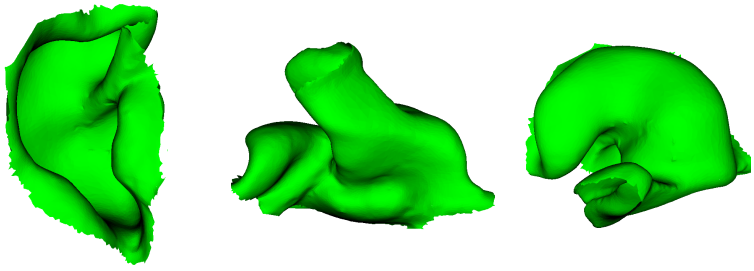

(a) Into the ear (b) Canal (c) Inside out

Figure 1.4: The 3 most frequently used projections. (a) Into the ear, (b) from the canal and (c) the inside out view (out of the ear).

Chapter 2

Anatomy

To create a proper foundation for understanding the dynamic behavior of the human ear, a basic understanding of the anatomy and functioning of the mandible in relation to the ear is required. Insight into the anatomy has helped strengthen the development of methods aimed at analyzing the problem at hand. It provides very good information for the validation process and helps keeping a sound and critical view on the outcome of different methods and analysis. That is, knowledge of the anatomy will assist in evaluating the results whether or not the results correspond well to the actual physical properties of the ear and the surrounding tissue. The following is a summary based on information from Andreasen et al. [5], Netler [106] supported by the histological sectioning provided by Sorensen et al. [145]. Figure 2.1 shows in very high detail the physiological properties of the tissue in the Pinna (the visible part of the human ear) and in and around the ear canal all the way into the hearing nerve.

2.1 The Human Ear

The human ear is a very complex organ which can be divided into three parts: The outer ear, which is everything from the Pinna to the tympanic membrane (the eardrum), the middle ear which is from the tympanic membrane to the

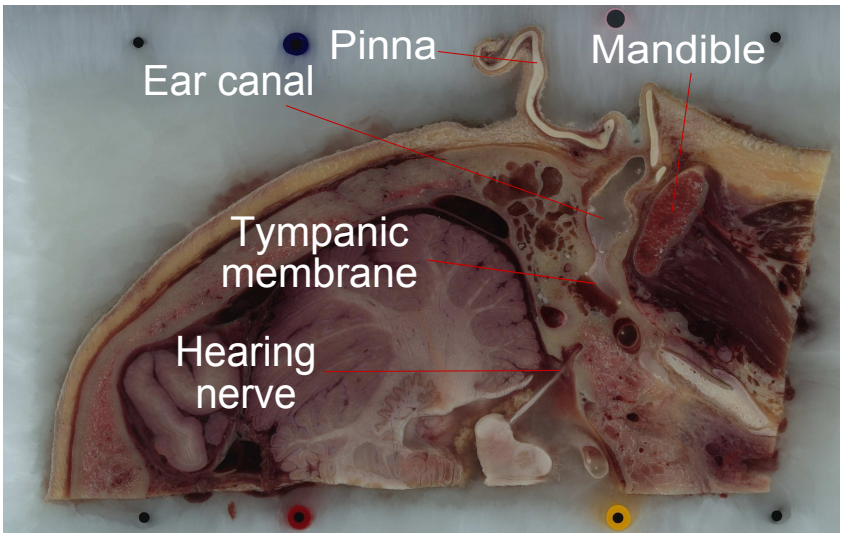

Figure 2.1: Histological section of the human ear from pinna to cochlea. The data is a part of the work published by Sorensen et al. [145]

oval window and the inner ear which is the cochlea and the hearing nerve etc. see figure 2.2. This thesis considerers only the outer ear, in particular the soft part of the outer ear, which is the only place in the ear where deformation can occur and where most hearing aids are placed. The outer part of the human ear and canal consists of the pinna (figure 2.3) and the canal. The canal can be divided into two parts, the inner part, terminated by the tympanic membrane and embedded in the mastoid, called the bony part of the canal and the outer soft part which is made up of cartilage and fat covered with a thin layer of skin. The pinna, the visible part of the ear, is made of cartilage and is situated on top of the mastoid. The ear canal is in general a very hostile environment especially for hearing aids, it is very humid and protected by an antiseptic wax with the ability to clean the canal. The first soft part of the ear canal is not particularly sensitive. Most people are able to place head phones and clean their ears without to much discomfort. In contrast, the bony part of the canal is extremely sensitive. Due to the potential painful procedure of obtaining an impression including any of the bony part of the canal this is not included in the data set. For the remainder of this thesis, when referring to an impression or data of the ear, this includes only the cymba concha, cavum concha, tragus and anti tragus and the soft part of the canal (figure 2.3). The soft part of the canal usually has two distinct features the first and the second bend (figure 2.4(a)). However, in some cases the canal is more or less straight and the second bend is almost invisible or non-existing (figure 2.4(b)).

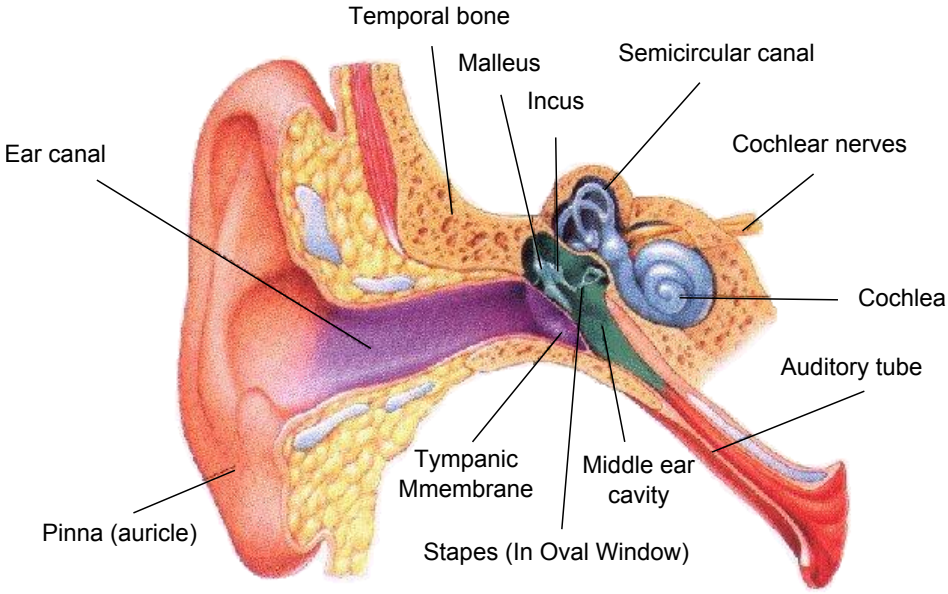

Figure 2.2: The human ear from pinna to cochlea.

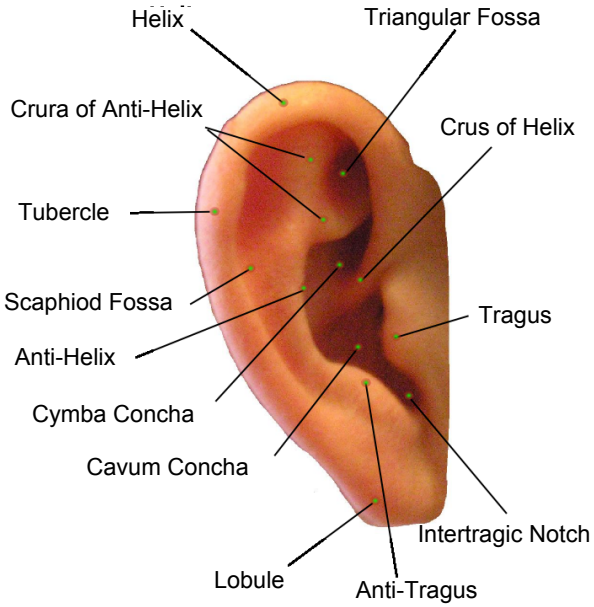

Figure 2.3: The outer human ear i.e. pinna.

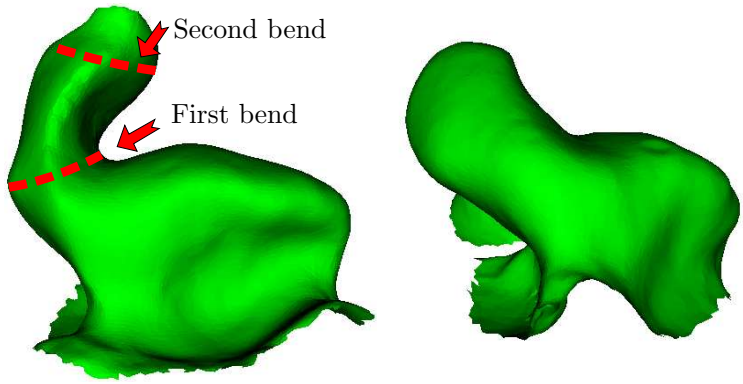

(a) Normal (b) Open jaw

Figure 2.4: (a) The two bends on the scanning of an ear impression. (b) An example where the first bend is there but some what difficult to exactly point out and where the second bend is invisible. This is not due to the length of the impression it is simply the anatomy of that specific ear canal.

2.2 Causes of Deformation

The following describes the causes believed to affect the shape of the ear. Most were observed during visits to the clinic talking to hearing aid-users and have subsequently been included in the main study.

2.2.1 Movement of the Mandible

The Mandible and the mandibular joint are situated on the anterior side of the canal. The joint is one of the most complex joints in the body and allows for movement with more degrees of freedom than most other joints. This is vital for understanding how the mandible moves in relation to the ear canal, see figure 2.6. This movement influences significantly how the tissue around displaces. The mandible is not attached directly to the skull but is held in place by a tendon and has a sliding joint with a cartilage disc between the condyle of the mandible and the skull. Figure 2.6 shows the temporo mandibular joint. When this disk is damaged by injury or by simple wear and tear the pathology Temporo Mandibular Joint Disorder (TMJD) occurs Cooper [27], Ewing [56], Hampton [73]. This pathology is present in approx. 15% of the adult population according to Dierks [46], and can in extreme cases make clicking noises when the person moves the jaw. When the mouth is closed, the mandible is as close to the ear

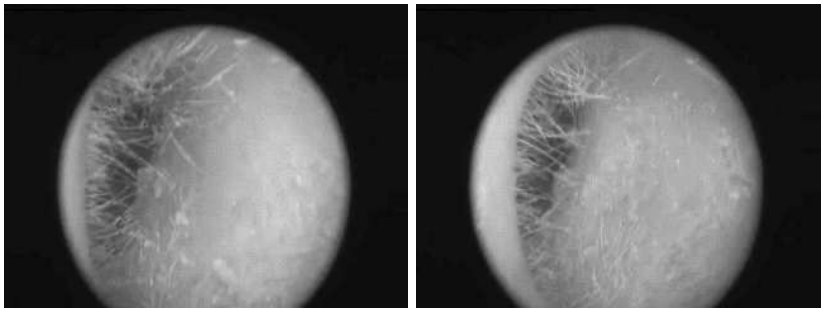

(a) Open (b) Closed

Figure 2.5: (a) The ear canal with the jaw closed. (b) The ear canal with the jaw opened from the right ear.

canal as it can be. As the mouth is opened, the mandible in front of the canal moves forward and a void is created in front of the canal. When a person chews, talks or in general moves the mandible this void is filled by the surrounding tissue, and as the ear canal is embedded in this tissue the movement or shifting causes the ear canal to change shape. Movies acquired at Eriksholm has revealed that not only does the canal change shape, but the collapse of the tissue inwards into the void causes the entire concha to shift and deform, see figure 2.5. The deformation is not taken up significantly by the tissue due to the fact that soft tissue is almost incompressible (Gross [70]). On the posterior side and top of the soft part of the canal the mastoid is situated: a bony structure in which the hearing and balance organs are embedded. The space between the mastoid and the canal is very small and filled with tissue. In addition, the mastoid is assumed to have a stabilizing effect so this side of the canal is only expected to deform very little trough forces propagated through the tissue close to the ear canal wall.

2.2.2 Gravity

Because the outer ear and canal mainly consists of soft tissue, it is believed that other factors may cause deformation of the ear and canal. One of these is gravity which affects the ear when the head for instance is slightly bend forward like when leaning over. It is a well known fact [85, 90] that as humans get older the cartilage degenerates, and since the average hearing aid user is in the mid 70'ties it is expected that this also will have an impact on the amount of deformation of the ear. This hypothesis receives some support from the fact that some hearing aid users report feedback problems when vacuum cleaning,

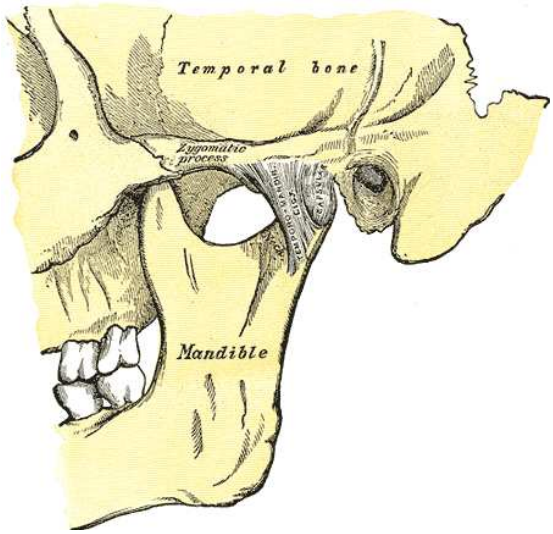

Figure 2.6: The mandibular joint taken from Standring and Ellis [146]

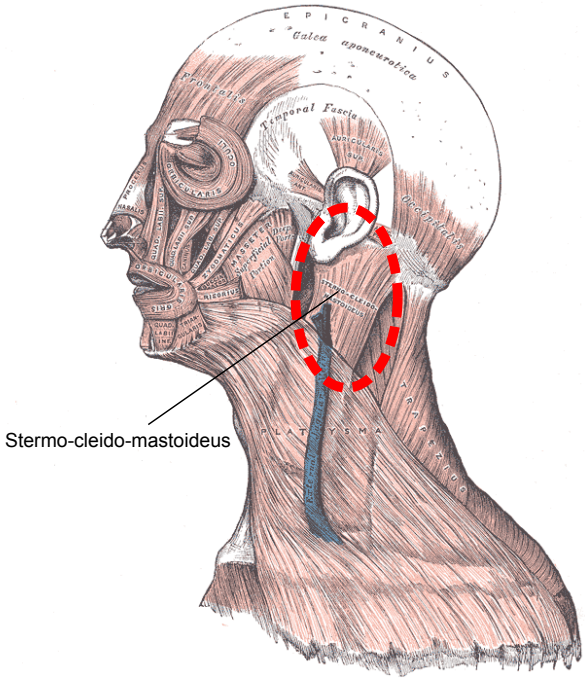

Figure 2.7: The muscles of the neck taken from Standring and Ellis [146]. The stemocleidomastoid muscle is circled in red.

lawn mowing or picking up something from the floor.

2.2.3 Turning the Head

Another not so obvious factor is the neck muscles attached to the skull. One of the largest and strongest neck muscles is attached to the skull just beneath the concha to the mastoid (figure 2.7): the stemocleidomastoid muscle. It is believed that this muscle could also have an impact on the shape of the ear and canal causing it to change shape. Such a deformation will occur when the subject turns his/her head, which is a very common movement, especially in conjunction with localization of sound.

Chapter 3

Data

This chapter describes the data sets used in this thesis, and how they where collected. Knowledge about the data and collection process is important to understand the limitations and possibilities.

A study to investigate the main hypothesis was designed involving some crucial decisions that impacted the possibilities in the final analysis. Several limitations had to be handled including time frame, man hours and access to test subjects plus their willingness to participate. Realizing this at a very early stage led to the decision of making two data sets, where one was a pilot study including ear impressions only that where collected from normal hearing people and the main study consisting of ear impressions and a questionnaire collected from hearing aid users. The pilot study was used to get data and experience for use in the development of the registration methods and to get a feel for the data. The pilot study gave a lot of experience with respect to the data and provided interesting and useful information that helped in the design and setup of the main study. In addition many hours were spend in the clinic listening to hearing aid users reporting their experiences in relation to comfort issues. A lot of effort was put into discussing possible setups and configurations of the study to cover most cases of comfort related deformations the easiest way with audiologist Claus Nielsen taking the limitations into account. One of the problems that had to be taken into account was the number of impressions that can be collected at on time. Since the material injected exerts some pressure to

the ear canal, the limit of impressions that can be taken from one ear during a session is approximate four. In addition, the number of possible visits was limited to one, thus, the natural boundary of the number of impressions where given in advance. Therefore the conditions for taking the impressions had to be considered carefully.

3.1 Collection Process

The data collection process was carried out at Eriksholm by audiologist Claus Nielsen who has more than 20 years of experience. The data was collected in a fashion that resembles normal practice. However, due to the extensions of the study as mentioned in section 1 an application to the research ethical committee was written and approved (appendix A). The data used in this thesis are ear impressions normally used for the production of hearing aids. The impressions have all been made by the same audiologist with extra care to make sure they are as consistent and deep in the ear as possible. The impression material is a silicone composite material that is mixed with a hardener prior to injection in to the ear and canal. The canal is blocked at the entrance to the bony part with a cotton ball to ensure that the material injected stays in the soft part. The material sits for 3-5 minutes after which the impression can be removed. The impressions where then scanned in a 3Shape [1] legato surface scanner specially designed for scanning ear impressions. The resulting scanned impression is a triangulated open surface with 8-15000 vertices, depending on smoothness and size of the impression.

3.2 Shape Representation

Shapes can be represented in numerous ways and we will briefly discuss some of the most common. Some of the basic representations are directly dependent on the modality of the data while others are derived from the original representation. The ear shapes are directly acquired as triangulated meshes as an approximation to a continuous surface. The representation consists of vertices and faces and are a single connected open 2D manifold in 3D Euclidian space, see figure 3.1. Other representations include point clouds where no connectivity is included, which is a subset of the type of data the surfaces represent. Other data such as organs extracted from images are closed surfaces. Such surfaces can be extracted using some segmentation scheme and then marching cubes [100] to extract the surface. Alternatively manual segmentation can be applied; however, in 3D such a task is almost infeasible for larger data set. Often

these surfaces contain 10^6 points and equally many faces, thus, some compact representation is desirable. Principal component analysis (PCA) and related methods have are often used for subspace projection. Other methods include Medial Sheets/Axis (MREP) [130], spherical harmonics [92], wavelets [71, 171], graph representation through the Laplace operator [13] or Laplace-Beltrami operator [109], level sets (Osher and Sethian [117])or other implicit surfaces such as radial basis functions(Dinh et al. [47]). Each representation has it advantages and disadvantages and based on that and the application some reasonable representation is chosen. In this thesis three shape representations are used: a point cloud/surface for statistics, a surface for correspondence and an implicit surface for registration purposes.

3.3 The Pilot Study

The pilot study included 30 subjects; 9 female and 21 males. Two impressions were obtained from each subject:

1. Subject sitting upright with closed relaxed jaw as the reference position.
2. Open mouth, obtained with the use of a bite block for surgery to ensure consistent opening of the jaw between subjects, see figure 3.2.

These two impressions allow for the calculation of a deformation field caused by jaw movement. This is a snapshot of the difference between the two positions, i.e. not continuous mapping between the two positions. The study provided data as well as important information about how the main study should be designed and what kind of data should be included. Also included in this data set are two impressions of the same single subject in the same position to investigate the reproducibility of the impressions.

3.4 Main Study

Based on the experiences from the pilot study, the main study was set up in the following way: The goal was to get 40-50 hearing aid users (42 participated), and obtain 4 impressions from each test subject, one in each in conditions. In addition to this a questionnaire was developed based on clinical experiences as well as informal discussions with hearing aid users in the clinic.

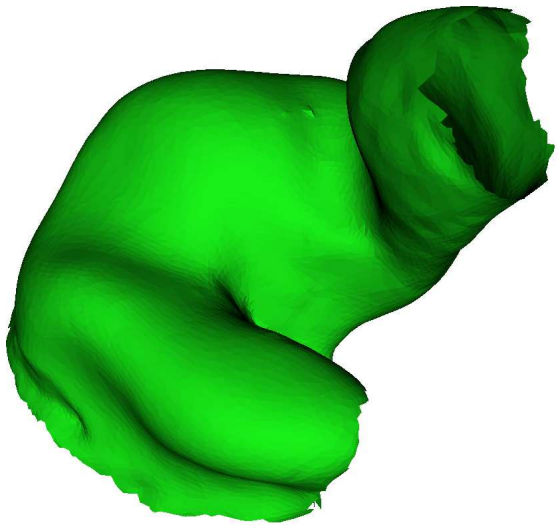

(a) Surface

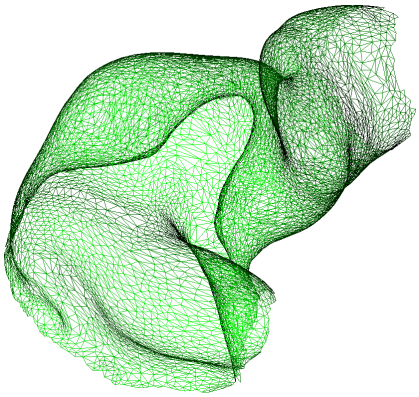

(b) Mesh

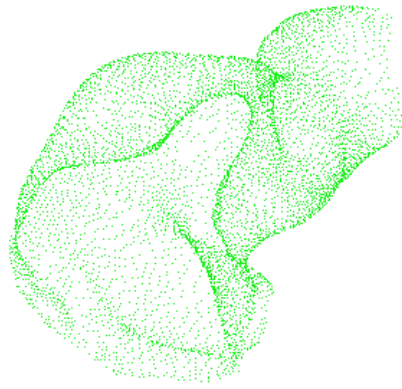

(c) Points

Figure 3.1: 2 of representations used for the surfaces (a and b) the surface and corresponding mesh and (c) the point cloud representation

Figure 3.2: A bite block used to ensure consistent opening of the jaw between test subjects.

3.4.1 Ear Impression Data

As mentioned in chapter 2, different factors are suspected to contribute to acoustic feedback. With this in mind the experiment was designed in such a way that most of these causes could be covered. The following 4 position during impression taking where included in the study:

1. Normal upright position with closed relaxed jaw (figure 3.3(a)).

   - As in the pilot study this was chosen as the reference impression from which the deformation field is calculated.

2. Open jaw (figure 3.3(b)).

   - This impression represents the deformation that occurs when a person chew or talks etc.

3. Leaning over (figure 3.3(c)).

   - To represents vacuum cleaning etc. People have reported acoustical feedback while mowing the lawn or vacuum cleaning.

4. Head turned to the left (figure 3.3(d)).

   - A very common movement and suspected to influence the shape of the ear since one of the large muscles in the neck is attached to the skull just beneath Concha.

(a) Normal (b) Open jaw (c) Leaning over (d) Turn

Figure 3.3: The four different positions for acquisition of impressions in the main study. (a) is the normal position, (b) is with jaw opened, (c) leaning over and (d) with the head turned to the opposite side of the impression.

3.4.2 Questionnaire

In order to be able to investigate if the deformation of the ear really causes any problems, a questionnaire was designed. The entire questionnaire can be found in appendix B. The first part is collection of demographic data such as age, gender, type of hearing aid (ITE or BTE), age of the hearing aid device, and TMJD. In addition to this a self report from the subject were requested on different subjects. It was decided that the questionnaire should not take more than 5 minutes to fill in and should not exceed more than 2 A4 pages. This decision was made in order to ensure that the questionnaire would not deter the subject from participating in the study.

The answers to the questions are designed to be categorical. This mean that they are binomial or multinomial [87] and can be analyzed using logistic regression. Some questions are ordered as to severity or degree, others are unordered and some are binary yes or no questions. The questionnaire contains questions about retention (the hearing aid falling out of the ear), acoustical feedback, the cause of acoustical feedback, physical discomfort and cause, satisfaction with respect to appearance of the hearing aid and the comfort. When a cause is to be reported room is left for comments and other causes not included in the list. The reason for letting the user specify the reason for the problem rather than just having 'other' as an option was that the actual reason might be something interesting providing new insight to the problem. In order to ensure the quality and readability of the questionnaire a psychologist from the human resource department of Oticon validated the questionnaire and a small pilot study on 5 subjects were conducted. This process spawned the idea of including questions about visual appearance.

3.4.3 Test Subjects

The subjects recruited for this study are not a good representation of the average hearing aid-user. They are a part of a larger group of hearing aid-users that on a regular basis participate in experiments at Eriksholm Research Centre. In general they are more alert and have a lower average age. In addition these people have fewer problems in general than the average population since extra care and consideration are given to the test subjects hearing aid Jensen and Nielsen [86]. In fact, this group represent very close to what could be classified as a best case scenario, where in contrast if people from real clinics had been recruited for the study, more cases of the different problems would most likely have been reported. The age difference is quite large and cover from 25-93 years of age, thus, some of the subject have limited mobility of the different joints in particular the neck which of cause will affect the consistency of impressions of type 3 and 4. However, the audiologist was very aware of this problem and has made a significant effort to get as consistent data as possible under the given circumstances.

3.4.4 Intended Analysis

The data set serves three purposes, (i) to find correlations between the questionnaire response and the shape or deformation, (ii) investigate the shape and deformation independently of the questionnaire data by using subspace projection such as the PCA and look for correlations, and (iii) look at the questionnaire data independently and look for answers to specific problems. Some of the analysis have already been published ([23, 40, 42]) and some are for future studies such as a closer investigation of the questionnaire data.

3.5 Production Data Set

The final data set used is a set of 178 impressions from the production environment. This set is basically an extraction of anonymized left ear impressions from the US production environment of Oticon inc. This data set was acquired to validate a rigid registration algorithm for open manifolds (Darkner et al. [43]).

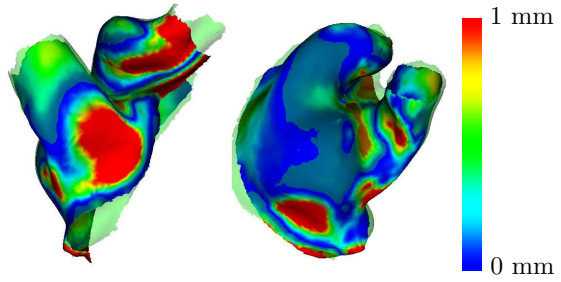

Figure 3.4: The difference between two impressions of the same ear. The data has been obtained from the production environment of Oticon.

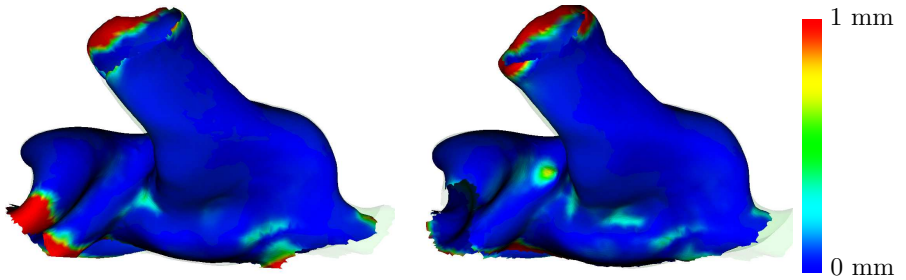

(a) Verification 1 (b) Verification 2

Figure 3.5: The difference between a reference impressions and 2 repeated impressions of the same ear. As can be seen the differences are very small due to the fact that extra care has been taken. The main cause of difference are small air bubbles that are inclosed by the impression material during injection.

3.6 Sources of Error

The way the impressions have been obtained will, no matter how careful the audiologist is, introduce some errors. When impressions are made, the material is injected into the subject's ear with a syringe with either manual or mechanical pressure. The viscosity of the material will affect the shape of the ear in some way causing deformation. In some cases this deformation can be quite severe, hence careful considerations and precautions where made in order to avoid this during the acquisition process. By looking at remakes from the production environment insight into of the true scale of this problem can be obtained. Figure 3.4 shows the difference, however, the difference may include the difference between open and closed mouth. Repeated measures show that the difference between impression even when extra care is taken can be up to 0.2 mm (figure 3.5).

3.6.1 MR Data

To evaluate how much the injection of the impression material distorts the shape of the ear, an experiment was set up. By acquiring MR data from the same individual with and without impression material it was hypothesized that the deformation caused by the impression material could be quantified. However, it turned out that the resolution of the images was to low and the contrast between the impression material and the tissue to poor to do an accurate segmentation. The experiment was carried out at Herlev Hospital in collaboration with Arnold Skimminge.

Chapter 4

Previous Work

The field of ear dynamics is very narrow and only few people have published within this field. This section focuses on previous work within the clinical subject of this thesis, the dynamic behavior of the ear canal. There have been several studies on the subject of changes of the ear canal due to movement of the mandible. The main part of these has been based on ear impressions and some on MRI or CT scan data. Most of the studies are motivated by commercial aspects such as a particular device or remedy towards feedback, and only few of the published papers are peer reviewed. The belief of most of the authors is that the most significant cause of deformation of the ear canal is movement of the mandible and that this deformation causes acoustical feedback. One of the first was Oliviera et al. [115] that based on measurements of ear impression and on MRI data described changes in the width and height of the ear canal with jaw movement. It was concluded that the canal changes shape but only in one direction - the transversal (horizontal) plane and the magnitude of the deformation is a function of the angle of opening. As most other studies except from Grenness et al. [69] the study did no take the concha into account. Oliviera [113] and B. Ballachanda [8] confirmed the claims by Oliviera et al. [115]. Oliviera and Hoeker [114] then investigated volume changes as a function of depth in the canal. The study was based on MRI scans of a number of individuals. Oliviera et al. [116] extended the number of subjects from Oliviera et al. [115] and showed that 51% of the subjects had a volume change of more than 10% including positive and negative changes. All measurements by Oliviera

have been done manually either assisted through software or with a calliper. Grenness et al. [69] have published the most thorough study on the dynamics of the ear canal. This study is based on manual measurements of ear impressions using a digitizing device. The study includes the Concha and assumes that it is stable. The study shows that significant deformation do occur and it is some what more complex that previously claimed by Oliviera et al. [115].

From Shape Changes to Comfort Due to the belief that acoustical feedback is caused by movement of the mandible, Pirzanski and Berge [127, 128, 129][126] did a series of studies with the intension of establishing a standard procedure for impression taking that should reduce the number of remakes due to physical discomfort. The general conclusions were that the digitized modeling fails to result in better hearing aids, and that in order to reduce the remake rate of hearing aids, impressions should be taken with the mouth open. The study in Pirzanski [126] involved 50 audiologists and more than 2000 impressions. The impressions were obtained with a variety of impression materials with different viscosities.

Countermeasures Different countermeasures have been proposed to deal with the problems caused by shape changes in the canal, some by Olivera and some by Creel et al. [37] who describes a hearing aid made from a softer material that can flex with the movement of the ear canal. It is supposed to give a better level of comfort and help reduce the feedback that normally occurs with traditional ITE. However, there are several drawbacks (not included in the paper) and therefore this is not the standard way that hearing aids are made today. Sebotek introduced a soft tip to receiver in the ear hearing aids that also failed and recently a new hearing aid the lyric [2] has com to the market which sits in the bony part of the ear canal.

Shape The Ph.d. thesis of R. Paulsen Paulsen [120] and paper [123] was partially on the shape of the ear. An average ear was made as well as a shape model and an minimal hearing aid. Using the ear model Paulsen et al. [124] showed that models and methods for surface analysis can be used in hearing aid production, in this case for the placement of faceplates. In Paulsen et al. [122] it was shown that shape analysis can reveal gender related differences such as size. Finally Egolf et al. [54] investigated the accuracy of ear impressions. The accuracy was measured using CAT-scans to verify and validate the impressions taken. All measurements were made on cadavers.

Chapter 5

Shape Analysis

This chapter deals with analysis of shapes. This is one of the most important subjects in this work, since the goal is to quantify the shape changes of the ear canal. There are several approaches to this problem and some of applied methods will be reviewed supplemented by a brief overview of other related methods.

5.1 Introduction

Shape analysis is extracting information about shape or shape change and representing it in some compact form. Shapes tend to be observations in a very high dimensional space, like the data in this thesis which is 15000 dimensional observations. The need for dimensionality reduction methods are therefor eminent and several approaches exist - often in the form of a shape model. The idea is to come up with interpretable projections into some subspace. Compact representations open possibilities for analysis through standard statistical methods, however, methods for more direct analysis have also been developed or adapted from statistics, machine learning and data mining based on regularization like Tikhonov [158]

$$\|\mathbf{A}\mathbf{x} - \mathbf{b}\|_2^2 + \lambda\|\mathbf{L}(\mathbf{x} - \mathbf{x}_0)\|_2^2 \tag{5.1}$$

where x_0 is the reference or bias point for the penalty term. This includes methods such as the ridge regression[80] and the support vector machine [163].

5.2 Shape Model

The most common way of analyzing shape spaces (Dryden and Mardia [49]) is through a shape model (Cootes et al. [33]). This is traditionally done by minimizing the Procrustes distance between all shapes through procrustes analysis [49]. A mean shape can then be calculated from a space where all affine transformations have been removed. Principal Component Analysis (PCA) (Pearson [125]) is then performed on the covariance matrix of the data itself. The shapes can then be characterized by the Principal Components through a projection of the shapes onto the successive orthogonal modes of variation. Any shape can then be reconstructed through the principal components as follows.

$$\hat{\mathbf{x}} = \hat{\boldsymbol{\mu}} + \boldsymbol{\Phi}\mathbf{b} \tag{5.2}$$

Where $\hat{\boldsymbol{\mu}}$ is the estimated mean shape and $\boldsymbol{\Phi}$ is the principal components and $\mathbf{b}$ the loading for the generated shape $\hat{\mathbf{x}}$. The primary reason is to obtain a compact representation governed by the variance in the training set. The components are not necessarily easy to interpret and in order to get better interpretability several other projections have been suggested. Among these are factor analysis (Kaiser [89]) or varimax rotation, Maximum autocorrelation factorization (MAF)(Larsen [95], Switzer [153]),independent component analysis (ICA)[83], truncated PCA (Cadima and Jolliffe [22]), sparse PCA (SPCA) (Zou et al. [174]) or Principal Geodesics Analysis (PGA) ([59, 60, 152]). Cootes and Taylor [30, 31, 32], Cootes et al. [34] introduced both the active shape model and the Active Appearance Model (AAM) (Cootes and Taylor [29]). Extension that included texture in its representation is thoroughly discussed in Stegmann [148] like colors and compact bases. Other variations include [96] where the texture representation is extended to include wavelets and wedgelets, and Kahraman et al. [88] who extended the Appearance Model (AM) to include lighting conditions. The models can be used as a machine learning approach to segmentation like in Lanche et al. [94], Ólafsdóttir et al. [111, 112], Rueckert et al. [135], Sjöstrand et al. [142], Stegmann and Skoglund [149], Stegmann et al. [150], where different approaches have been used to segment the heart, corpus callosum or the breast in order to extract knowledge or to do actual measuring for diagnostic purposes such as cancer screening or blood flow measurements such as perfusion.

5.2.1 Deformation Model

The approach from the shape modeling can be used to analyze the deformation field, however, the direction and magnitude of the deformation is very important and closely coupled to the shapes themselves. Procrustes analysis should therefore be used with care. In addition, scaling will remove the metric of the deformation, a very important parameter in this context. Thus, the most straight forward approach would be to omit scaling or to rely on the registration (chapter 6). Several approaches for decomposition and analysis of the deformation are possible, such as doing decomposition on a vector consisting of both the shape and the deformation, deformation independently or letting one of the features drive the decomposition i.e. shape or deformation.

5.3 Regression

Regression is used to examine the correlation between a predictor and a specific response. The standard linear regression model

$$\mathbf{Y} = \mathbf{E}(\mathbf{Y}|\mathbf{X_1}, \ldots, \mathbf{X_p}) + \varepsilon \tag{5.3}$$

i.e.

$$\mathbf{Y} = \beta_0 + \boldsymbol{\beta}\boldsymbol{X} + \varepsilon \tag{5.4}$$

models the response $\mathbf{Y}$ with noise $\varepsilon \in N(0, \sigma^2)$ and a linear combination of some predictors $\mathbf{X_1}, \ldots, \mathbf{X_p}$. This approach assumes $n \geq p$ where n is the number of observation and p the dimensionality of the predictors and a quadratic loss function, thus the solution can be found through Ordinary Least Squares (OLS) $\boldsymbol{\beta} = (\mathbf{X}^t\mathbf{X})^{-1}\mathbf{X}\mathbf{Y}$ The data in this thesis are high dimensional and consists of only few observation, i.e. no unique solution exists using ordinary least squares. Regressions can be applied in conjunction with some subspace projection technique like the PCA (Darkner et al. [40]) where PC where regressed onto gender and deformation PC. However, an explaining characteristic of the PC are implicitly assumed, which most likely is not the case. Alternatively point wise regression can be used. The point wise regression is a regression model fitted to each observation, however, this method ignores any co-variability between variables in the data, thus, valuable information about co-variances is lost. Sjöstrand et al. [144] illustrates the differences between this approach and constrained or regularized regression.

5.3.1 Non-linear Regression

In some cases the data cannot be described with a simple linear model either because the responses are categorical or simply because the model is inadequate. The most common way to handle this is to transform the data and then apply the linear model to the transformed data. Examples of this approach is the Generalized Linear Model (GLM), kernel regression or fitting a set of nonlinear functions to the data such as splines etc.

5.3.2 GLM and Logistic Regression

The GLM is a relaxation of the linear model in equation 5.5 by relaxing on the Gaussianity assumption of the noise term ε, making no assumptions about the distribution. The GLM is written as follows

$$E(Y|X) = f^{-1}(\boldsymbol{\beta X}) \tag{5.5}$$

where f^{-1} is the canonical link function. The GLM assumes that the data comes from the exponential family of distributions such as the binomial, Poisson etc. The standard regression model fits the GLM frame if the data is transformed using the identity transform.

To model other distributions the use of a link function is employed. The purpose is to map the response into some space where the standard linear model can be applied. In the case of the binomial distribution the probability ratio or the odds of the outcome is modelled through the canonical link function

$$logit(p_i) = Y_i = \frac{P_i}{1 - P_i} = \exp^{\beta_0 + \boldsymbol{\beta X}} \tag{5.6}$$

or

$$E(\frac{Y_i}{n_i}|\mathbf{X_i}) = p_i = f(X_i) = \frac{1}{1 + \exp^{-Z}}, \qquad Z = \boldsymbol{\beta X} \tag{5.7}$$

where $Y_i \in B(n_i, p_i)$. The model is used to model the chance of death given a certain drug dose or categorical data such as yes/no answers. The link function has the nice property that it maps any value of Z from infinity to minus infinity to the interval $]0:1[$, thus a probability of a given outcome. The model that is fitted has the following form

$$\log\left(\frac{p_i}{1 - p_i}\right) = \beta_0 + \boldsymbol{\beta}\mathbf{x_i} + \epsilon_i \tag{5.8}$$

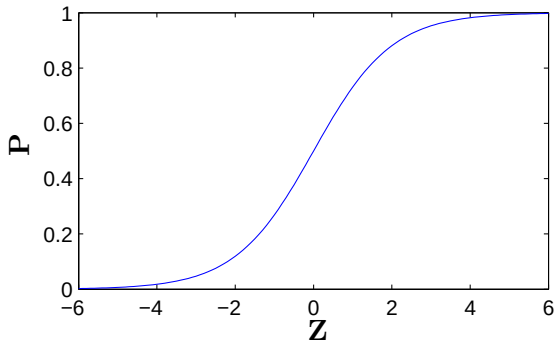

Figure 5.1: The logit mapping of Z

and as mentioned no assumptions is made about ε. This model can be used to do point wise regression on surface for a certain pathology as by Darkner et al. [42] where the technique is applied to investigate the effect of deformation of the human ear canal due to movement of the mandible on acoustical feedback. Exchanging Z with $f(x)$, an analytical function, the model becomes identical to a single layer neural network Haykin [78].

5.3.3 Regularized Regression

To analyze data where $p \gg n$ constraints on the solution space can be introduced. By decreasing the degrees of freedom on the model, the solution becomes unique and obtainable. The solution space reduction can be viewed in several ways. From an optimization point of view the degrees of freedom in solution space is reduced. From a Bayesian learning theory point of view a prior on the solution is enforced, hence forcing the solution in a particular direction.

5.3.3.1 Ridge penalty

Ridge regression (Hoerl and Kennard [80]) is a well known way of reducing the degrees of freedom in a model. The penalty itself is on the regression parameters in the form of an ℓ_2-norm penalty on the magnitude of the regression coefficients. The model can be written as follows

$$\mathbf{Y} = \beta_0 + \boldsymbol{\beta}\mathbf{x} + \varepsilon_i, \quad \text{s.t. } \|\boldsymbol{\beta}\|^2 < \rho \tag{5.9}$$

$$argmin\|\mathbf{Y} - \boldsymbol{\beta}\mathbf{X}\|^2 + \xi\|\boldsymbol{\beta}\|^2 \tag{5.10}$$

where ξ is a regularization constant that controls the amount of regularization. The ridge regression identifies correlation between predictors and distributes regression parameters more equally. The regularization is basically a Tikhonov regularization and the degrees of freedom can be estimated from the eigenvalues of

$$\boldsymbol{\lambda} = eig(\mathbf{X}^t\mathbf{X}) \tag{5.11}$$

$$df = \sum_i \frac{\lambda_i}{\lambda_i + \xi} \tag{5.12}$$

This optimization problem can be solved using quadratic programming, however, the constraint can also be formulated as a prior on the regression coefficients $\boldsymbol{\beta}$ gaussian. Optimization and solutions to the problem will be reviewed in section 5.5.

The ridge penalty penalizes large coefficients as it is a quadratic penalty, however small coefficients are virtually unaffected by the penalty. The effect is that correlated coefficients are given equal weight because this is the most optimal solution with respect to the penalty assuming that their explanatory value is the same.

5.3.3.2 Lasso

Even though the ridge penalty offers some dimensionality reduction, it is still desirable to get explicit variable selection. This can of course be obtained by standard techniques such a forward/backward stepwise regression by sequentially including/excluding, respectively, parameters in the model. This is, however, virtually impossible for data sets with a very large amount of variables and other and better methods are needed. Variable selection or shrinkage through the ℓ_1-norm is used in the LASSO by Tibshirani [156], which replaces the ℓ_2 in equation 5.9 and 5.10 with the ℓ_1 penalty

$$\mathbf{Y} = \beta_0 + \boldsymbol{\beta}\mathbf{x} + \varepsilon_i, \quad \text{s.t. } |\boldsymbol{\beta}| < \rho \tag{5.13}$$

$$argmin\|\mathbf{Y} - \boldsymbol{\beta}\mathbf{X}\|^2 + \xi|\boldsymbol{\beta}| \tag{5.14}$$

The equivalent Bayesian formulation as a prior on the regression parameters is a Laplace distribution, however, one of the easiest way of solving the optimization problem is through quadratic programming. But as can be seen from figure 5.2 the penalty has a discontinuity at $\beta_i = 0$ which has to be handled. Well known approaches include estimating $\boldsymbol{\beta}_+$ and $\boldsymbol{\beta}_-$ or reformulating the penalty to a constraint where $\boldsymbol{\beta} \geq \rho$ and $\boldsymbol{\beta} \leq -\rho$. As with the ridge penalty this method obviously reduces the degrees of freedom and as shown by Zou et al. [175], this corresponds exactly to what you would expect, i.e. the *df* is equal to the number of non-zero variables in the model.

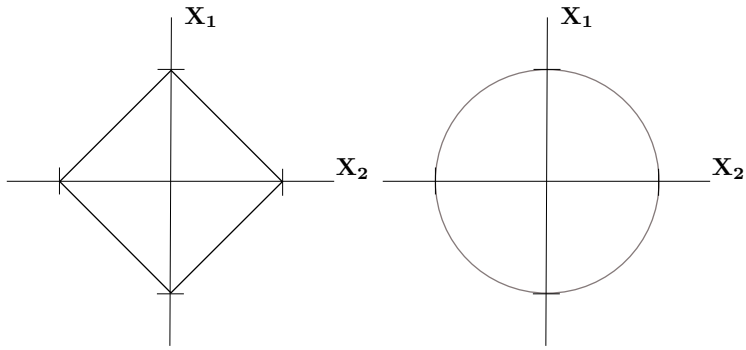

(a) ℓ_1 penalty (b) ℓ_2 penalty

Figure 5.2: (a) The ridge penalty in 2D (b) The LASSO penalty in 2D

5.3.3.3 Elastic Net

Combining the ridge penalty and the LASSO yields a regression model that emphasizes correlation and makes variable selection at the same time. The model was introduced by Zou and Hastie [173] and can be written as follows

$$\mathbf{Y} = \beta_0 + \boldsymbol{\beta}\mathbf{x} + \varepsilon_i, \quad \text{s.t. } \|\boldsymbol{\beta}\|^2 < \rho_1, \quad |\boldsymbol{\beta}| < \rho_2 \tag{5.15}$$

which gives the following minimization problem

$$argmin\|\mathbf{Y} - \boldsymbol{\beta}\mathbf{X}\|^2 + \xi_1\|\boldsymbol{\beta}\|^2 + \xi_2|\boldsymbol{\beta}| \tag{5.16}$$

It is obvious from the previous methods that the equivalent prior to the elastic net must be a combination of a Gaussian and a Laplacian. The optimization and solution can be found through convex optimization using quadratic programming (QP) or EM which will be discussed in 5.5.

5.3.3.4 Generalizations and Their Constraints

Several other constraints exist that are familiar with the above methods and the most of them can be summarized into the following generalized constrained regression model.

$$\mathbf{Y} = \beta_0 + \boldsymbol{\beta}\mathbf{x} + \varepsilon_i, \quad \text{s.t. } \|\mathbf{A_1}\boldsymbol{\beta}\|^2 < \rho_1, \quad |\mathbf{A_2}\boldsymbol{\beta}| < \rho_2 \tag{5.17}$$

which gives the following minimization problem

$$argmin\|\mathbf{Y} - \boldsymbol{\beta}\mathbf{X}\|^2 + \xi_1\|\mathbf{A_1}\boldsymbol{\beta}\|^2 + \xi_2|\mathbf{A_2}\boldsymbol{\beta}| \tag{5.18}$$

where $\mathbf{A_1}$ and $\mathbf{A_2}$ are matrices that define some operation on $\boldsymbol{\beta}$ like the fused lasso Tibshirani et al. [157] where $\mathbf{A_2}$ would be the numerical first order differential operator. Alternatively one could think of the second order or the graph laplacian for the surface that basically would ensure similarity in a given neighborhood, that is,

$$\mathbf{A}_2 = \begin{bmatrix} 1 & -1 & 0 & \dots \\ & \ddots & \ddots & \\ \dots & 0 & 1 & -1 \end{bmatrix} \quad or \quad \mathbf{A}_2 = \begin{bmatrix} -1 & 2 & -1 & 0 & \dots \\ & \ddots & \ddots & \ddots & \\ \dots & 0 & -1 & 2 & -1 \end{bmatrix} \tag{5.19}$$

5.3.4 Constrained GLM

It is evident that the above constraints can be applied to the GLM and in particular to the logistic regression model. Several papers have been written on the subject and several approaches to the formulation and variants exist. le Cessie and van Houwelingen [97] describes the ridge penalty applied to the logistic regression. Genkin et al. [62] describes the prior for both the ridge and the lasso penalties as well as a way to do optimization. The combined prior of the Laplace and Gaussian distribution is described in the original paper by Zou and Hastie [173]:

$$\log\left(\frac{p_i}{1-p_i}\right) = \beta_0 + \boldsymbol{\beta}\mathbf{x_i} + \epsilon_i, \quad \text{s.t. } \|\boldsymbol{\beta}\|^2 < \rho, |\boldsymbol{\beta}| < \xi \tag{5.20}$$

5.4 Classification

Classification and regression are closely linked together and in some cases implicitly defined by each other. The logistic regression can be interpreted as a classifier. The output can be interpreted as the probability for a given input of belonging to a certain class, however, much simpler models exist. This section gives an overview of some of the methods with main focus on Support Vector Machines.

5.4.1 Multi Class Classifiers

One of the easiest methods is the k-nearest neighbors [76] which basically is a majority vote in the local area of a new observation. There is the classification

and regression tree extensively described by Breiman et al. [19] which subdivide the domain hierarchically and is governed by a trade-off between complexity and accuracy. The basic approach can be very simple but the method can be extended with a variety of discriminators and basis functions like in Darkner et al. [39] where the use of wedgelets (Donoho [48]) is applied. Other methods include Linear Discriminant Analysis (LDA) and Quadratic Discriminants Analysis (QDA) both described in Hastie et al. [76]. The LDA assumes the same covariance matrix for all classes whereas the QDA does not. Fishers discriminant analysis maximizes the ratio of the between-class variance over the within class variation. The neural network is a an approach that uses a hierarchy of functions to discriminate. The neural network is often very good at classification but the resulting model is very hard to interpret. An extensive introduction is found in Haykin [78]. Boosting, uses the combined power of a series of weak classifiers, where ADABoost [76] is probably the best known algorithm.

5.4.2 Support Vector Machines

The support vector machine is one of the most versatile classification methods that originates from the separating hyperplane (Duda et al. [50]). The main difference from other classification methods is that it focuses on the point of separation rather than on the distribution of the two classes, hence, it makes no assumptions about the distribution of the classes to be separated. Furthermore, the plane of separation is a function of some of the observations themselves, i.e. the support vector, hence, the name support vector machines (SVM). As this is a good example of a quadratic programming problem the solution of the problem will be derived as an example. The separating hyperplane is formulated as follows. Given a set of observations $\mathbf{X}$ the two classes are encoded as $Y_i \in \{1, -1\}$ respectively. The separating hyperplane is written as

$$\boldsymbol{Y} = \boldsymbol{\beta}^t \mathbf{X} + \beta_0 \tag{5.21}$$

and in the case of separable classes the optimal separating hyperplane is the hyperplane that maximizes the distance to the closest observations which is equal to minimizing the Euclidian norm of $\boldsymbol{\beta}$. The problem for the separable case can be formalized as follows

$$\begin{aligned} &\min \|\boldsymbol{\beta}\|^2 \\ &st. \quad \mathbf{Y}(\mathbf{X}\boldsymbol{\beta} + \beta_0) \geq 1 \end{aligned} \tag{5.22}$$

figure 5.3(a) show the optimal separating hyperplane. The two classes are totally separable and the shortest distance to the plane of separation is maximized. It is rarely the case that two classes are separable, hence, the separating hyperplane needs to take such cases into account, and thus become the support vector

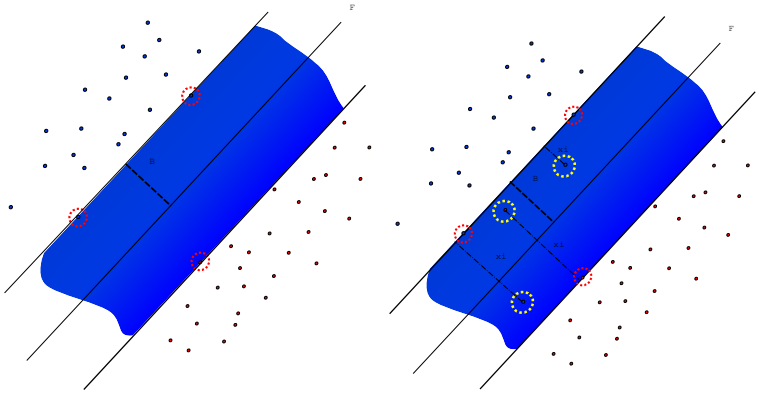

(a) (b)

Figure 5.3: The separating hyperplane with (a) separable classes, (b) non-separable clases

machine. In order to handle misclassification, an extra variable is introduced: the slack variable ξ, which relaxes on the separability of the two classes. Figure 5.3(b) shows this relaxation compared to the case in figure 5.3(a). The support vector machine optimization problem is thus formulated as follows with starting point in equation 5.22

$$\begin{aligned} &\min \|\boldsymbol{\beta}\|^2 + C\sum_{i=1}^{N}\xi_i \\ &st. \quad \mathbf{y}_i(\mathbf{x}_i\boldsymbol{\beta}+\beta_0) \geq 1-\xi_i, \quad \xi_i \geq 0 \quad \forall i \end{aligned} \tag{5.23}$$

The problem in equation 5.40 is a convex function of $\boldsymbol{\beta}$. In addition, the constraints are linear; thus, the constrained optimization problem can be written using Lagrange multipliers. The Lagrangian function is written as follows

$$\begin{aligned} L_P(\boldsymbol{\beta},\beta_0,\alpha) \quad = \quad & \frac{1}{2}\|\boldsymbol{\beta}\|^2 + \gamma\sum_{i=1}^{n}\xi_i \\ & -\sum_{i=1}^{n}\alpha_i[y_i(\mathbf{x}_i^t\boldsymbol{\beta}+\beta_0)-(1-\xi_i)] - \sum_{i=1}^{n}\mu_i\xi_i \end{aligned} \tag{5.24}$$

The optimum is the saddle point of minimizing $\boldsymbol{\beta}$, β_0, and ξ and maximizing α. Thus, the optimal solution can be found by differentiation with respect to

$\boldsymbol{\beta}$, β_0 and ξ and setting the derivatives equal to 0 which are given by

$$\frac{\partial L_P(\boldsymbol{\beta}, \beta_0, \alpha)}{\partial \boldsymbol{\beta}} : \quad \boldsymbol{\beta} = \sum_{i=1}^{n} \alpha_i y_i \mathbf{x}_i \tag{5.25}$$

$$\frac{\partial L_P(\boldsymbol{\beta}, \beta_0, \alpha)}{\partial \beta_0} : \quad 0 = \sum_{i=1}^{n} \alpha_i y_i \tag{5.26}$$

$$\frac{\partial L_P(\boldsymbol{\beta}, \beta_0, \alpha)}{\partial \xi_i} : \quad \alpha_i = \gamma - \mu_i \tag{5.27}$$

The Lagrangian dual can now be obtained by substituting equation 5.25-5.27 in equation 5.24

$$L_D(\boldsymbol{\alpha}) = \sum_{i=1}^{n} \alpha_i - \frac{1}{2} \sum_{i=1}^{n} \sum_{j=1}^{n} \alpha_i \alpha_j y_i y_j \mathbf{x}_i^t \mathbf{x}_j \tag{5.28}$$

In addition the Karush-Kuhn-Tucker (KKT) (Karush [91]) conditions introduce the following constraints

$$\alpha_i (y_i (\boldsymbol{x}_i^t \boldsymbol{\beta} + \beta_0) - (1 - \xi_i)) = 0 \tag{5.29}$$

$$\mu_i \xi_i = 0 \tag{5.30}$$

$$y_i (\boldsymbol{x}_i^t \boldsymbol{\beta} + \beta_0) - (1 - \xi_i) \geq 0 \tag{5.31}$$

The maximization of equation 5.28 is the same as minimizing $-L_D(\boldsymbol{\alpha})$. The coefficients of $\boldsymbol{\beta}$ are given by equation 5.25 and the KKT conditions implies that only the observations with non-zero coefficients are included (support vectors). Thus,

$$\hat{\boldsymbol{\beta}} = \sum_{i=1}^{n} \hat{\alpha}_i y_i \mathbf{x}_i \tag{5.32}$$

The bias β_0 can be estimated from the support vectors (SV) that lie exactly on the margin i.e. $\hat{\xi}_i = 0$ (equation 5.29). The resulting classification function or decision function can be written as

$$\text{sign}(\boldsymbol{x}^t \boldsymbol{\beta} + \beta_0) \tag{5.33}$$

5.4.3 The 'Kernel Trick'

A well known procedure for improving the fitted linear model is to do a basis expansion. Suppose that we choose some transformation of $\mathbf{x}$ such as $h(\mathbf{x})$ with the inner product $< \cdot, \cdot >$. Equation 5.28 can be rewritten as

$$L_D(\boldsymbol{\alpha}) = \sum_{i=1}^{n} \alpha_i - \frac{1}{2} \sum_{i=1}^{n} \sum_{j=1}^{n} \alpha_i \alpha_j y_i y_j < h(\mathbf{x}_i), h(\mathbf{x}_j) > \tag{5.34}$$

Rewriting equation 5.33 by inserting equation 5.32 the following is obtained

$$\begin{aligned} f((x)) &= \text{sign}\left(\boldsymbol{x}^t \sum_{i=1}^{n} \alpha_i y_i \mathbf{x}_i + \beta_0\right) \\ &= \text{sign}\left(\sum_{i=1}^{n} \alpha_i y_i \boldsymbol{x}^t \mathbf{x}_i + \beta_0\right) \\ &= \text{sign}\left(\sum_{i=1}^{n} \alpha_i y_i < h(\mathbf{x}), h(\mathbf{x}_i) > + \beta_0\right) \end{aligned} \tag{5.35}$$

In fact this means that if the kernel is a symmetric inner-product kernel (the reader is referred to [140] p. 42 or [78] p. 331) a basis expansion can implicitly be achieved through the kernel $\mathbf{K}(\mathbf{x}_i, \mathbf{x}_j) =< h(\mathbf{x_i}), h(\mathbf{x}_i) >$. One requirement is that $\mathbf{K}(\mathbf{x}_i, \mathbf{x}_j)$ also known as the Gram matrix must have full rank. A few examples of kernels are presented here

$$\text{polynimial} \qquad (\mathbf{x}^t \mathbf{x} + 1)^p \tag{5.36}$$

$$\text{Radial basis functions} \qquad \exp\left(-\frac{1}{2\sigma^2}\|x - x_i\|^2\right) \tag{5.37}$$

5.4.4 Extensions and Regression in the SVM Framework

The SVM is well known to give very good results for classification of text, images etc. Nevertheless several extensions and modification have emerged. The weighted SVM (WSVM) (Liu et al. [99]) takes unequal class sizes into account through reweighing of the slack variables ξ by the inverse of the class size ratio:

$$\begin{aligned} &\min \|\boldsymbol{\beta}\|^2 + C \sum_{i=1}^{N} s_q \xi_i \\ &st. \quad \mathbf{y}_i(\mathbf{x}_i \boldsymbol{\beta} + \beta_0) \geq 1 - \xi_i, \quad \xi_i \geq 0 \quad \forall i \end{aligned} \tag{5.38}$$

sn is the ratio parameter for the classes, $q = \{1, 2\}$. Feature selection through the lasso penalty was suggested Bradley and Mangasarian [18] using the ℓ_1 rather than the ℓ_2 penalty on $\boldsymbol{\beta}$

$$\begin{aligned} &\min |\boldsymbol{\beta}| + C \sum_{i=1}^{N} \xi_i \\ &st. \quad \mathbf{y}_i(\mathbf{x}_i \boldsymbol{\beta} + \beta_0) \geq 1 - \xi_i, \quad \xi_i \geq 0 \quad \forall i \end{aligned} \tag{5.39}$$

Another extension is the Feature Vector Machine (FVM) (Li et al. [98]) that analyzes the feature space and generates sparse solutions there. The doubly constrained SVM (Wang et al. [165]) is basically imposing the lasso constraint in the parameters as well to create a sparse solution in $\boldsymbol{\beta}$. 5.22

$$\begin{aligned} &\min \|\boldsymbol{\beta}\|^2 + |\boldsymbol{\beta}| + C\sum_{i=1}^{N}\xi_i \\ &st. \quad \mathbf{y}_i(\mathbf{x}_i\boldsymbol{\beta} + \beta_0) \geq 1 - \xi_i, \quad \xi_i \geq 0 \quad \forall i \end{aligned} \tag{5.40}$$

One of the problems with the ℓ_1-norm is that the kernel trick cannot be applied. Clemmesen and Darkner [23] used constraints formulated by the data itself both for the ℓ_1-penalty and the ℓ_2 such as the Orthogonality Constrained SVM (OC-SVM) that enables the kernel trick to be used. The method assumes some similar dependence between the observations that are paired and uses this information to reduce variability of solutions with up to a factor of 50. However, great care should be taken since the constraint in the kernel space does not necessarily makes sense. The problem formulation for an additional data driven ℓ_2-penalty can be stated as follows

$$\begin{aligned} &\min \frac{1}{2}\|\boldsymbol{\beta}\|^2 + \gamma\sum_{i=1}^{n}\xi_i + \frac{\lambda}{2}\|\boldsymbol{\beta}^t\mathbf{A}\|_2^2 \\ &\text{s.t.} \quad y_i(\mathbf{x}_i^t\boldsymbol{\beta} + \beta_0) \geq 1 - \xi_i, \quad \xi_i \geq 0 \quad \forall i \end{aligned} \tag{5.41}$$

Following the method from the derivation of the SVM is obtained

$$L_D = \sum_{i=1}^{n}\alpha_i - \frac{1}{2}\sum_{i=1}^{n}\sum_{j=1}^{n}\alpha_i\alpha_j y_i y_j \mathbf{x}_i^t(\mathbf{I} + \lambda\mathbf{A}^t\mathbf{A})^{-1}\mathbf{x}_j \tag{5.42}$$

It is seen that a data driven constraint is equivalent to a linear kernel made up of the data and that it is symmetric and in most cases has full rank unless two observations coincide. The method is not limited to data driven constraints, and the use of the operators in 5.19 can be applied.

$$L_D = \sum_{i=1}^{n}\alpha_i - \frac{1}{2}\sum_{i=1}^{n}\sum_{j=1}^{n}\alpha_i\alpha_j y_i y_j K((\mathbf{I} + \lambda\mathbf{A}^t\mathbf{A})^{-1/2}\mathbf{x}_i, (\mathbf{I} + \lambda\mathbf{A}^t\mathbf{A})^{-1/2}\mathbf{x}_j) \quad . \tag{5.43}$$

For the ℓ_1 constraint the problem is formulated as follows

$$\begin{aligned} &\min \frac{1}{2}\|\boldsymbol{\beta}\|^2 + \gamma\sum_{i=1}^{n}\xi_i + \lambda\sum_{k=1}^{m}\delta_k \\ &\text{s.t.} \begin{cases} -\delta_k \leq \boldsymbol{\beta}^t\mathbf{a}_k, \quad \delta_k \geq \boldsymbol{\beta}^t\mathbf{a}_k \quad \forall k \\ y_i(\mathbf{x}_i^t\boldsymbol{\beta} + \beta_0) \geq 1 - \xi_i, \quad \xi_i \geq 0 \quad \forall i \end{cases} \end{aligned} \tag{5.44}$$

and the dual has the following form

$$\begin{aligned} L_D &= \sum_{i=1}^{n}\alpha_i - \frac{1}{2}\sum_{i=1}^{n}\sum_{j=1}^{n}\alpha_i\alpha_j y_i y_j \mathbf{x}_i^t\mathbf{x}_j - \sum_{k=1}^{m}\sum_{i=1}^{n}\alpha_i y_i(\rho_k' - \rho_k)\mathbf{x}_i^t\mathbf{a}_k \\ &\quad -\frac{1}{2}\sum_{k=1}^{m}\sum_{l=1}^{m}(\rho_k' - \rho_k)(\rho_l' - \rho_l)\mathbf{a}_k^t\mathbf{a}_l \end{aligned} \tag{5.45}$$

It is clear that this allows for the kernel trick, but the use of operators are restricted to spaces where the expansion is known.

5.5 Optimization

For regression problems there are some general approaches to find the solution. For normal regression, the ordinary least squares (OLS) is the obvious solution. However, dealing with constrained regression models and non-linear model makes optimization a little more difficult. Solutions to these problems can be found through Maximum Likelihood methods which can be solved through Maximum A Posterior (MAP) via Expectation Maximization (EM) or Newton methods. However the problems can also be viewed as an optimization problem. The SVM formulation is not unique for the SVM but rather a problem that falls into the category of constrained optimization. The SVM falls into the category QP a group of problems which is a subset of the group of convex optimization [79][110] problems called second order cone programming and has Linear programming (LP) as a subset of it self. The general form of the QP offers a wide range of possibilities for the use of loss functions. The support vector machine uses the hinge loss function with the possibility of implementing the Huber norm [82], the sum of squared differences (SSD) etc. The general QP can be written as follows

$$F(x) = \mathbf{x}^t\mathbf{H}\mathbf{x} + \mathbf{f}^t\mathbf{x} \tag{5.46}$$

$$\text{s.t.} \quad \boldsymbol{A}\boldsymbol{x} \geq b, \quad \boldsymbol{B}\boldsymbol{x} = c, \quad \mathbf{l} \leq \boldsymbol{x} \leq u \tag{5.47}$$

It is easy to se that the formulation of the constrained regression problem described in the previous section fall into the QP domain. The problems can be solved through the KKT system with an interior point method, active set or conjugated gradient methods [110]. The two following examples illustrate how a regression and a one class classifier, the support vector domain descriptor (SVDD [141]) can be stated in this framework.

5.5.1 Ridge Regression via QP

To bring regression into the context of QP the primal problem of the ridge regression in equation 5.9 is stated here. The derivation of the Wolfe dual is omitted but can be performed in analogy to that of the SVM:

$$\min_{\boldsymbol{\beta},\boldsymbol{\xi}} \quad \frac{1}{2}\|\boldsymbol{\beta}\|_2^2 + \frac{\lambda}{2}\sum_i \xi^2 \tag{5.48}$$

$$\text{s.t.}(y_i - \boldsymbol{X_i}\boldsymbol{\beta}) = \xi_i, \qquad \forall i \tag{5.49}$$

reformulating using lagrangian multipliers yield

$$L_P(\boldsymbol{\beta}\,\boldsymbol{\alpha},\boldsymbol{\xi}) = \frac{1}{2}\|\boldsymbol{\beta}\|_2^2 + \frac{\lambda}{2}\sum_i \xi^2 + \sum_i \alpha_i(y_i - \boldsymbol{\beta}\boldsymbol{X_i} - \boldsymbol{\xi}) \tag{5.50}$$

differentiation of $L_P(\boldsymbol{\beta}\,\alpha)$ with respect to it variables yield

$$\frac{\partial L_P(\boldsymbol{\beta}\,\boldsymbol{\alpha},\boldsymbol{\xi})}{\partial \boldsymbol{\beta}} = \boldsymbol{\beta} - \sum_i \alpha_i \boldsymbol{X_i} = 0 \tag{5.51}$$

$$\frac{\partial L_P(\boldsymbol{\beta}\,\boldsymbol{\alpha},\boldsymbol{\xi})}{\partial \xi_i} = \lambda\xi - \alpha_i = 0 \tag{5.52}$$

The Wolfe dual can now be formed by insertion

$$\max_{\alpha} \quad L_D(\boldsymbol{\alpha}) = 1/2\sum_{i,j}\alpha_i\alpha_j < \mathbf{X}_i, \mathbf{X}_j > + \frac{1}{\lambda 2}\sum_i \alpha_i^2 - \sum_i \alpha_i y_i \tag{5.53}$$

5.5.2 Support Vector Domain Descriptor SVDD

Support Vector Domain Descriptor is a one class classifier that, as previous models can be formulated as a QP. It is a hypersphere rather than a hyperplane that surrounds the observation optimizing on a tradeoff between radia and outliers as shown in figure 5.4 Using the formulation presented by Sjöstrand et al. [143] the SVDD is written as follows

$$min. \quad \sum_i \left(\|\mathbf{x}_i - \mathbf{a}\|^2 - R^2\right)_+ + \lambda R^2 \tag{5.54}$$

where $(\cdot)_+$ is the hinge loss function, a function that is positive if the argument is positive and zero otherwise. This in turn leads to the following optimization problem

$$min. \qquad R^2 + \lambda\sum_i \xi_i \tag{5.55}$$

$$st. \qquad \|\mathbf{x_i} - \mathbf{a}\|^2 \leq R^2 + \xi_i, \qquad \xi_i \geq 0, \qquad \forall i \tag{5.56}$$

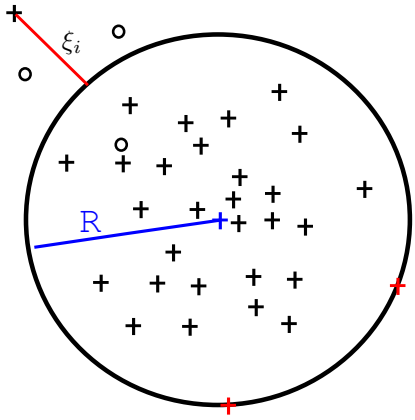

Figure 5.4: The SVDD is basically a one class classifier relying in the hinge loss function and penalizing outliers. The resulting classifier is a tradeoff between the error of having outlier vs. the size of the descriptor.

The idea is to minimize the radius subject to a penalty for each observation belonging to the the class that is classified as an outlier (figure 5.4). By introducing λ the tradeoff between small radius an more outliers is controlled see Sjöstrand and Larsen [141] for an analysis of the regularization path.

5.6 Validation and Regularization

Most of the methods in this chapter require user input in the form of tuning the regularization parameter. A series of techniques exist for optimal selection of the regularization parameters. The most straight forward method is n-fold cross validation, where the parameter is optimized on $N-\frac{N}{n}$ samples and tested on the remaining, in n configurations. The application has become much easier since the introduction of the possibility of calculating the entire regularization path for SVM (Hastie et al. [77]) and SVDD (Sjöstrand and Larsen [141]) which both estimates the model for all possible values of the regularization parameters. The approach has been extended to other methods as well (Park and Hastie [119]). Other approaches exist for selection of regularization parameters such as Bayes Information Criterion (BIC) Schwarz [138] given by

$$BIC = n \ln\left(\frac{RSS}{n}\right) + k \ln(n) \tag{5.57}$$

where n is the number of samples, k is the number of parameters in the model and RSS the residual sum of squares. The best model is the on with the lowest score i.e. BIC favors simple models with good fit. Alternatively Akaikes Information Criteria (AIC) (Akaike [4]) can be used which is given by

$$AIC = 2k - 2\ln(L) = 2k - n(\ln\left(\frac{2\pi RSS}{n}\right) + 1) \tag{5.58}$$

with L as the maximized likelihood of the model. Last the L-curve (Hansen [75]) which is closely related to Tikhonov regularization [158]. In general the problems in the QP as had the form of equation 5.1 with $\mathbf{L} = \mathbf{I}$ and $x_0 = 0$

$$\|\mathbf{Ax} - \mathbf{b}\|_2^2 + \lambda\|\mathbf{x}\|_2^2 \tag{5.59}$$

The L-curve is a plot of $\|\mathbf{Ax} - \mathbf{b}\|_2^2$ versus $\|\mathbf{x}\|_2^2$ as a function of λ in log-log scale.

5.6.1 Hypothesis and Permutation Testing

When using regression models it is valuable to know if the used model indeed explains the data, and if so with what of significance. For this use hypothesis testing is applied (see Conradsen [26] for a thorough introduction). The goal is to evaluate the null hypothesis $H_0 : \theta \in \Theta_0$ versus the alternative $H_1 : \theta \in \Theta_1$. Usually H_0 is the 'negative' outcome, i.e. that the chosen model is not significantly different given the distribution it belongs to, with H_1 is the alternative that in fact it belongs to a different distribution. Many hypothesis tests exist depending on the purpose and the goal. In the work of this thesis only two versions have been used explicitly. The first is the Likelihood ratio, used to evaluate the goodness of fit given the degrees of freedom in the given model compared to the model that only includes bias.

$$\Lambda = \frac{L(\boldsymbol{\beta}|\mathbf{X})}{L(\beta_0|\mathbf{X})} \tag{5.60}$$

where the numerator $L(\boldsymbol{\beta})$ is the log-likelihood of the fitted model. A convenient result is that $-2log(\Lambda)$ approximately follows a χ^2 distribution with n degrees of freedom, where n is the difference in model complexity between the models. For high dimensional data such as the scanned ear impressions, simultaneous hypothesis testing is desirable, especially if a map of the significance of the deformation is desired. For this purpose a regression model could be fitted at each point through the pointwise regression or ridge regression and a z score could be calculated. Another approach is that suggested by Efron [52] that with a little abuse can be utilized to estimate the significance of the given deviation

from H_0 by estimating the empirical H_0 from the data and then use either the estimated distribution directly or the false discovery rate (FDR) (Efron and Tibshirani [53]).

A third way of evaluating the model is a permutation test. Good examples are Horn [81] or Terriberry et al. [154] and Nichols and Holmes [107]. The first is very useful for model selection in conjunction with PCA or factor analysis and is applied in [40], the latter for detecting differences.

Chapter 6

Registration and Correspondence

In order to perform statistical analysis on the shapes a common reference frame has to be established. To do so, the shapes need to be registered to each other such that a given point on a given shape has a corresponding point on any other shape in the data set. This section describes registration in general and many of the approaches that have formed the basis of the methods developed, employed and published during the study. The main contributions are in two papers, one describing a rigid registration framework and another describing a non-rigid registration framework. The methods has since their publication been refined and developed further into groupwise registration; an extension that will be described in this chapter.

6.1 The Transformation

Registration is creating correspondence between similar objects where. Hence, the key element is bringing observations into a common reference frame. This is in principle done through the estimation of a function in some space that maps

one observation onto another. This can be formulated as follows:

$$\min_{\mathbf{W}} \quad \|\mathbf{W}(\mathbf{X}) - \mathbf{Y}\|_p^l \tag{6.1}$$

$$\text{s.t.} \quad \mathbf{R}(W)$$

$$\min L(\mathbf{W}(\mathbf{X}), \mathbf{Y}) + \lambda R(\mathbf{W}) \tag{6.2}$$

Where L is the loss function, distance or similarity measure and R is the regularization. The registration problem is often very ill posed, hence, the regularization is essential for obtaining a unique solution when solving for W. A good example is the smoothness of curvature of the warp in the case of the Thin Plate Spline (TPS) [16]. The function W defines the correspondence but is often represented by a discrete set of points with a corresponding transformation. Other formulations such as Bayesian interpretations Tu et al. [161],Darkner et al. [38],Maximum Likelihood Estimation (MLE) Roche et al. [134] or Therions demons (Thirion [155]) exist, where the focus in this study has been the formulation in equation 6.2 and Baysian like interpretation. The simplest way of estimating W but often the most labor intensive is manual labeling where landmarks are manually placed by an expert, referred to as expert annotation. The Expert is assumed to have superior knowledge of the given object, hence have less variability compared to others. Another class of methods is the semiautomatic methods that depends on expert annotations to define sparse correspondences and uses these to guide the generation of correspondence or registration for the rest of the domain. Several methods exist for this type of registration like Bookstein [16] that uses a thin plate spline (TPS) to interpolate. This brings us back to the core of the subject. The TPS basically introduces a constraint or regularization on the deformation between the points.

6.2 Features and Similarity Measure

To create the correspondence, a set of features and a similarity measure has to be identified or defined, which is used to measure the distance or similarity between shapes or images. In addition, a norm of the similarity measure must be chosen, which has an impact on the choice of optimization method.

6.2.0.1 Norm

The norm can be considered as measure of similarity. The ℓ_2-norm has a high weight on outliers and does not prioritize perfect matches, where as the ℓ_1 norm give equal penalty to all differences. This means that in contrast to the ℓ_2-norm,

a large sum of small differences will out weigh a few major outliers. Other norms such as the Huber norm (Huber [82]), a combination of the ℓ_1 on small values and ℓ_2 on large value etc. The general form of the norm is given as

$$\|\mathbf{x}\|_p = \sqrt[p]{\sum |x_i|^p}, \qquad p \in]0; \infty] \tag{6.3}$$

6.2.1 Features and Similarity

Selecting the right similarity measure depends to a high degree on the modality or representation and features of the objects. The features include points [6], gradients [104], curvature[167][51], filter banks [171] etc. A very common choice is the expert annotation which implies a transformation at certain points. These selected features are then compared under the given similarity measure and define the warp in principle. The similarity measure can in the case of the expert annotation be the ℓ_1-norm on the differences, the sum of squared difference (SSD) typically on the Euclidian norm (see figure 6.1) or the procrustes distance [49] between the points. The procrustes distance is a common distance measure for landmarks. The corresponding transformation removes scaling, translation and rotation leaving only shape variation. In some applications a combination of features is used where both points and the underlying image is used. Alternatively, a combination of surface and image features can be applied such as that proposed by Postelnicu et al. [131]. The additional features are then often used as an extra constraint. For some modalities like X-ray, CT, MRI or real world images the variation in intensities and contrast can be quite pronounced especially between modalities. Thus, a similarity measure that can accommodate these changes is usually employed rather than a preprocessing step that adjusts for intensity and contrast such as mutual information, as suggested by Wells et al. [168] and Studholme et al. [151].

6.2.1.1 Modality of the Ears

2D surfaces in 3D Euclidian space are not noisy or biased as the images, however, they often have very little information as in the case of the ear impressions where no texture is available. In addition, the curvature is highly irregular across the population, thus, not applicable in this context. For 2D manifolds embedded in 3D Euclidian space several different approaches have been suggested. Most manifold of this kind are parameterized by a triangulated mesh. Due to the properties and very fast search techniques such as the KD-tree (Whitted [169]), the iterative closest point method (Besl and McKay [15]) is a very common choice, to which a lot of extensions like Fitzgibbon [58], Granger and Pennec

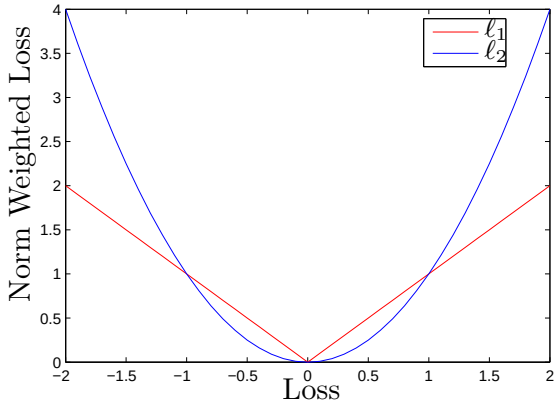

Figure 6.1: The loss or similarity under the ℓ_1-norm and SSD respectively

[67], Rusinkiewicz and Levoy [137] exist. For ICP the feature is the set of closest points between the two surfaces to be registered, however point to surface could also be used. Other methods rely on different features such as wavelets [171] or curvature [45] in addition. Another approach is to used a mapping to a topological equivalent entity such as a sphere, disc [166] or a cylinder, however, such a mapping require either that the surface is closed for use of the sphere or that the edges are in correspondence (for the use of the cylinder). For open manifolds with non coinciding edges this approach can be somewhat difficult without manual intervention in the form of an expert adding landmarks for guidance. Another well defined measure for closed surfaces are difference of level sets (Hansen et al. [74])(figure 6.2), however, the level set is not a smooth function and is not differentiable everywhere and is not defined everywhere for open surfaces. This can be handled by using pseudo level sets like the distance map as in Yamany et al. [170], Darkner et al. [43] and [38] where the outcome of [38] is evaluated in [41].

6.3 Optimization

Having defined an appropriate distance measure for the given modality, the problem in 6.2 has to be solved. As mentioned, all kinds of interpretations exist. Two formulations and optimization procedures and methods will be discussed. Before discussing how to reach the solution to the problem, the regularization and the way it enters the solution space is discussed.

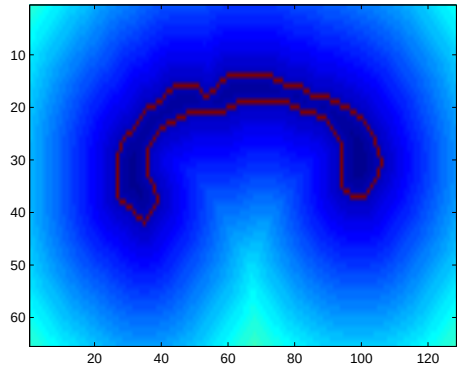

Figure 6.2: The distance map of a 2D contour extracted from an image, here the corpus callosum

6.3.1 Regularization

There are two general ways that the problem can be regularized. One solution is to limit directly the degrees of freedom (DOF) of the solution space. One example of such a regularization scheme is the rigid registration, where the solution space is restricted to rotation and translation i.e. 6 DOF. Other more elaborate methods are the B-spline used by Rueckert et al. [135], Vester-Christensen et al. [164] or the basis used by Cootes et al. [36] where the solution space is limited to the respective basis functions. Alternatively, the constraint can enter through the regularization term. An example of this is the constraint of matching points that can be enter in two ways, either as a soft constraint, where the L is allowed to be nonzero or hard where the distance measure in the points are forced to become 0, i.e. $L(W(X), Y) = 0$. More elaborate constraints such as volume preservation [72], fluid or elastic constraint (Bro-Nielsen and Gramkow [20]) fit the formulation of the registration problem in equation 6.2. Another constraint that has found its way into registration is the requirement that W is diffeomorphic. The constraint ensures that W is a smooth 1 to 1 mapping. Several papers discuss these mapping and the reader is referred to Nielsen et al. [108] Cootes et al. [35], Modersitski [104] Durrleman et al. [51] among others.

6.3.2 Solving the Registration Problem

The impact of the norm is quite significant and depends on several factors and should therefore be considered carefully. As mentioned, registration is an ill-

posed problem so in order to solve the problem and obtain a solution a prior or a constraint is imposed on the solution to the problem. The constraints come in many forms but all restrict the freedom of the function W. One of the simplest cases is 2D rigid registration where only 3 degrees of freedom is allowed. Depending on all the choices made about similarity measure, norm, and degrees of freedom a suitable optimization procedure must be selected.

To solve the registration problem the use of Newton Methods and approximations like the Gauss-Newton method are often used. By reformulating equation 6.2 and assuming that the constraint is imposed by limiting the solution space it can be written as

$$\min(F(W(X,p)) - Y) + R \tag{6.4}$$

Where F is the evaluation of X warped by the function W with the parameters p. Linearizing the loss function by a Taylor expansion yields the solution to the regularized Gauss-Newton as follows

$$\Delta\mathbf{p} = \mathbf{H}^{-1}(\Delta\mathbf{F}\frac{\partial\mathbf{W}}{\partial\mathbf{p}})^t(\mathbf{Y} - \mathbf{F}(\mathbf{W}(\mathbf{X},\mathbf{p}))) \tag{6.5}$$

$$\mathbf{H} = (\Delta\mathbf{F}\frac{\partial\mathbf{W}}{\partial\mathbf{p}})^t(\Delta\mathbf{F}\frac{\partial\mathbf{W}}{\partial\mathbf{p}}) + (\frac{\partial^2\mathbf{R}}{\partial\mathbf{p}^2}) \tag{6.6}$$

Optimizing using a reduced space such as the b-spline basis, rigid etc. the regularization term disappears and the following is obtained

$$\Delta p = H^{-1}(\Delta F\frac{\partial W}{\partial p})^t(Y - F(W(X,p))) \tag{6.7}$$

$$H = (\Delta F\frac{\partial W}{\partial p})^t(\Delta F\frac{\partial W}{\partial p})) \tag{6.8}$$

If $\mathbf{H}$ is singular, it can be replaced by $\mathbf{I}$ turning the optimization into gradient descend or $\mathbf{H} + \lambda\mathbf{I}$. These formulations of the optimization problem turns into a linear equation provided that the second derivative or the Gauss-Newton approximation to the second derivative can be calculated. Several methods exist and depending on the size of the problem iterative methods such as BFGS, Levenberg-Markvard, conjugated gradient (CG), gradient descend, BiCG ,BiCGSTAB minres, etc [12] can be used to solve the system in combination with line search [7]. One interesting method that potentially could be useful if the hessian is really complicated to evaluate is the inverse compositional algorithm by Baker and Matthews [10].

6.3.3 Bayesian Interpretation

The other approach is more similar to a random walk approach where an energy term is set up for each configuration and a prior on the transformation. Assum-

ing that a registration of I_1 to I_2 is desired, and the desired transformation is denoted W. In the Bayesian framework this becomes

$$P(W|I_1, I_2) = \frac{P(W)P(I_1|I_2, W)}{P(I_1|I_2))} \tag{6.9}$$

Since $P(I_1|I_2)$ is independent of W, i.e constant, the system can be reformulated as

$$P(W|I_1, I_2) \propto P(W)P(I_1|I_2, W) \tag{6.10}$$

The registration problem becomes

$$\hat{W} = arg\min_W E(W) = arg\min_W -\log(P(W)) - log(P(I_1|I_2, W)) \tag{6.11}$$

This equation is the same as equation 6.2 with the regularization term $P(W)$, i.e the prior and $P(I_1|I_2, W)$ the loss function. This can of cause be solved using either a MAP approach through EM [76] or a MRF approach, which in the case of uniform prior turns into a random walk, hence, ICM becomes a steepest descend Darkner et al. [38].

6.3.4 Optimization of Regression and Classification Models

It is obvious that the optimization strategies described above can be used to solve the regression and classification problems from chapter 5. For instance, in the Bayesian interpretation it is easy to see where the prior of 5.15 5.20, 5.9 etc. can enter. Its a little bit more difficult with the Newton methods due to the lack of differentiability of the ℓ_1-penalty on the parameters.

6.4 Registration Strategies and Computational Complexity

To obtain faster convergence and ease computation numerous strategies exist both for registration and for optimization. For the registration it is a challenge to avoid bias in the final atlas, i.e. the final reference created. Some strategies exist to circumvent this problem. Additionally, 3D data are often very large and even algorithms with reasonably low complexity become very slow. Methods have been developed to handle this as well, methods that in no way are unique to image and surface registration but will be presented in this context here.

6.4.1 Pairwise and Groupwise Registration

It is well known that many registration algorithms are very slow and often dictates the strategy involved in solving the problem. One of the major issues is whether to do template registration, i.e. pair wise registration or to do group wise registration. If a large population is to be co-registered and the choice of procedure is pair wise, then the choice of template will bias the registration and the mean towards the template itself. Some of this effect can be circumvented by recalculating the mean image or shape after each registration of the group and repeat the registration to the mean until convergence. However, this procedure is very slow and a much better approach is to do group wise registration. The group wise registration is in theory somewhat more complicated. Given N shapes to be co-registered, the following can be written

$$\min L(\mathbf{W}(\mathbf{X}), \mathbf{Y}) + \lambda R(\mathbf{W}) \tag{6.12}$$

becomes

$$\min L(\mathbf{W}(\mathbf{X_n}), \frac{\mathbf{1}}{\mathbf{N}} \sum_{\mathbf{n}} \mathbf{W}(\mathbf{X_i})) + \lambda R(\mathbf{W}) \tag{6.13}$$

It is very clear that $\frac{1}{N}\sum_n W(X_i)$ is dependent on $W(X_i)$. However if N is large enough $\frac{1}{N}\sum_n W(X_i)$ can be assumed to be a constant. This makes the scheme very similar to normal registration and can be perceived as a de-blurring of the atlas. Balci et al. [11] use an extension of this by assuming an independent Gaussian distribution at each point and then model the uncertainty at each variable in the problem by dividing by the variance a follows

$$\min L\left(\mathbf{W}(\mathbf{X_n}), \frac{\mathbf{1}}{\mathbf{N}} \sum_{\mathbf{n}} \frac{\mathbf{W}(\mathbf{X_i})}{\sigma^{\mathbf{2}}}\right) + \lambda R(\mathbf{W}) \tag{6.14}$$

This will have the effect of emphasis on variables that are consistent. However, this will also in my experience slow down the optimization and requires a significantly higher number of iterations compared to equation 6.13.

6.4.2 Optimization Strategies

Since the number of calculations for a full image or shape can be very high, scalespace techniques are applied. The approach is simple but very effective. By blurring the image or distance measure like in the Gaussian pyramid (Burt et al. [21]) through sub-sampling and perform registration using the blurred features, a high level deformation field can be obtained. The image or shape that arises from this transformation and the original observation is then sub sampled but

at a higher resolution than the previous iteration and so on. The approach serves two purposes, first it reduces the number of computations needed due to the sub-sampling, and secondly it has a regularizing effect on the resulting transformation. The use of this approach is widespread, and used among others in [135],[164],[43].

6.5 Shape Models and Registration

Having established the framework for registration, a good example of a registration algorithm with a meaningful prior or regularization term is the Active Shape Model ASM. Assume a point linear distribution model

$$\hat{\mathbf{x}} = \hat{\boldsymbol{\mu}} + \boldsymbol{\Phi}\mathbf{p} \tag{6.15}$$

For simplicity the search space is limited to this linear model. Thus, the Gauss-Newton estimate in equation 6.8 of the Hessian with the parameters p becomes

$$\frac{\partial W}{\partial p} = \boldsymbol{\Phi} \tag{6.16}$$

$$H = (\Delta F \boldsymbol{\Phi})^t (\Delta F \boldsymbol{\Phi}) \tag{6.17}$$

This approach is thoroughly described by Erbou et al. [55].

Chapter 7

Application of Methods to the Ears

This chapter gives an overview of the applications of the methods in the previous chapters, first by giving an overview of the published and submitted papers. Secondly, some of the unpublished results from the work that forms the basis of this thesis are described. These include a shape model and a deformation model with respect to the three conditions for impression taking described in chapter 3, as well as an investigation into a more true model of the deformation.

7.1 Summary and Comments on Published Work

Ten papers, 9 conference and 1 journal has been written during the project. This section provides a very brief summary of each paper with a few comments. Among these paper are some that address issues concerning the ear data including registration and shape and deformation analysis. The remaining papers are on topics and methods closely related to the project. The papers have been divided into two groups: registration and shape analysis.

7.1.1 Registration

Previous work with ear data by Paulsen [120] used expert annotations to obtain correspondence across the population and combined Markov Random Field modification of non-rigid registration by geometry constrained diffusion [6] with Iterative Closest Point(ICP). However, the annotation procedure in this study would become very extensive due to the fact that 200 impressions had to be annotated by an expert, which was almost intractable. Based on this fact, it was decided to develop an automatic algorithm for registration of the surfaces.

7.1.1.1 Automated 3D Rigid Registration of Open 2D Manifolds Darkner et al. [38]

This paper is a first proof of concept on the loss function which is published as a rigid registration algorithm with a Gibbs sampler [132] for optimization with a uniform prior. The formulation has the advantage of allowing for different loss functions and the possibility of adding simulated annealing in order to avoid local minima. As it turns out there are no local minima and the Iterated Conditional Modes (ICM)[14] achieves the minimum. As for the choice of distance measure the ℓ_1 norm on the distance map and the difference of the distance maps gives the best registration for the purpose, which may be described as intra-subject change quantification. In addition, as discussed in previous chapters, the ℓ_1-norm weighs all differences equally which has a noise reducing effect.

7.1.1.2 Evaluating a Method for Automated Rigid Registration Darkner et al. [41]

The rigid registration approach in [38] is evaluated and compared to ICP for robustness in this paper, where it outperforms ICP (as implemented in VTK [84]) on the ear data. A reasonable explanation is that the formulation of sampling the distance map rather than using the parameterizations of the surface has an effect similar to that of a Gaussian pyramid [21].

7.1.1.3 Non-rigid Registration of 2D manifolds in 3D Euclidian space Darkner et al. [43](Chapter 11)

The rigid registration algorithm is extended to non-rigid registration in this paper using the basis functions suggested by Cootes et al. [36] instead of the B-spline in [135]. The chosen formulation uses difference of distance maps as loss function, which has some attractive properties that makes computation very fast. The method forms the basis of the work presented in [40] and an extension to group wise registration is introduced and used in [42]. This is feasible due to the fast computation of approximations to derivatives etc. The timing is approximately 8 hours for 84 surfaces on a 2.2 GHz XEON machine taking up only 500 MB of memory and one kernel.

7.1.1.4 Robust Registration for Change Detection Darkner et al. [44](Chapter 12)

To enhance outlier detection and improve intra subject registration the method presented in this paper was developed. By using large scale hypothesis testing [52] and mean shift [24] for outlier detection in a non-rigid registration framework a set of inliers used for the registration is obtained. The set of outliers are discarded from the rigid registration part of the algorithm. The algorithm seems promising; however, experiments point towards the fact that perhaps too much of the surface is changing for the algorithm to be robust for the ear impression data. That is, in some cases the ear deforms to such an extent that the part classified as outliers become inliers and vice versa, causing the algorithm to become unstable.

7.1.1.5 Estimation of Shape Model Parameters for 3D Surfaces Erbou et al. [55](Chapter 14)

The registration and fitting of shape models come full circle in this paper, where the fitting of the shape model is formulated as a registration problem. The solution is found through limiting the search space of the registration problem to the principal components of a shape model, as described in the previous chapter. The method has not been applied to the ear impressions but rather to porcine pelvic bone surfaces and images.

7.1.1.6 Accelerated Image Registration Vester-Christensen et al. [164]

This paper introduces the application of the inverse compositional algorithm for 3D image registration. The constraints or basis functions of the warp are the functions introduced by Cootes et al. [36] and used in [43]. The paper won a poster price at SPIE 2007 as a noteworthy presentation.

7.1.2 Shape Analysis

Based on the registration and the resulting correspondences, analysis of the shapes was performed. Some of the most simple yet very powerful analysis tools have provided insight into the deformation of the human ear canal.

7.1.2.1 Analysis of Deformation of the Human Ear and Canal Caused by Mandibular Movement Darkner et al. [40](Chapter 10)

This paper presents a study (based on the pilot study, se section 3.3) that show the true complexity of the deformation fields in contrast to what previously have been reported [69, 115]. In fact, the whole ear deforms and not just the canal which is in very good correspondence with the anatomy. In addition, it is shown that the deformation of the ear is strongly correlated with the shape and that the magnitude of the deformation seems to be related to gender. This corresponds very well to research made within forensics where the size of the mandible can be used to determine the sex of a subject with up 80% accuracy (Giles [63], Graw [68]). Finally, by using large scale hypothesis testing on each deformation field it is shown that all individuals without exception have significant deformation due to movement of the mandible. However, it is worth noticing that due to the soft properties of the tissue, this does not imply that every one has some kind of deformation-related comfort issue. The results show that the deformation varies significantly, from around 0.2 mm to above 2 mm.

7.1.2.2 Classification in Longitudinal Studies Clemmesen and Darkner [23](Chapter 13)

This paper presents an extension to the Support Vector Machine (SVM) that uses the special relationship between the open and closed mouth impressions.

The method has an extended regularization term that uses the fact that observations are paired to regularize the obtained solution. The method shows that it can classify the two groups, open and closed mouth 100% correctly with n-fold cross validation and at the same time reduce the variation of the solution by a factor of 50. Furthermore, the paper introduces a generalization of the ℓ_1 and ℓ_2 constraints to the support vector machine for operators.

7.1.2.3 Analysis of Surfaces Using Constrained Regression Models Darkner et al. [42] (Chapter 9)

As the main study was completed it became possible to investigate if there was a correlation between acoustical feedback and the deformation of the ear and canal. Using classification and regression methods such as the SVM and the logistic regression with ℓ_1 and ℓ_2 penalty on the regression parameters, i.e. the elastic net, the correlation between acoustic feedback and deformation is addressed in this paper. The study reveals that significant correlation between acoustic feedback and deformation caused by jaw movement exists and that the best and most consistent model to uncover this correlation is the Logistic elastic net. The underlying data, of course, gives the possibility of creating a shape model and a deformation model. A shape model was published in [43] and used as validation of the algorithm. However, in Darkner et al. [42] the registration procedure was extended and the resulting shape model can be found in section 7.2.

7.1.2.4 An Active Illumination and Appearance (AIA) Model for Face Alignment Kahraman et al. [88]

This paper introduces a combined illumination and appearance model where the modes of variation have been made orthogonal with respect to each other. Due to the fact that illumination and appearance are parameterized in the texture space the models can be build orthogonal via Gram-Schmidt process. Once such a model is fitted to a new observation, the illumination and appearance parameter are easy to read out since these are independent and have separate loadings. This paper is a result of a collaboration with Fathi Kahraman during his visit to our group at IMM, DTU, during 2005 and 2006.

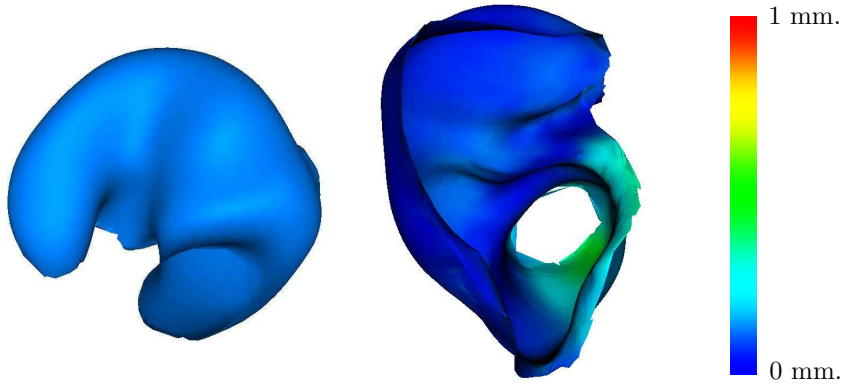

(a) Mean Shape (b) Mean Deformation

Figure 7.1: The mean shape and mean deformation from jaw movement.

7.2 Unpublished Results

In this section the unpublished results will be presented. These results are very recent and the opportunity to publish them in the right forum has not yet arisen. However, in the context of this thesis these results are very important, because they shed light on the major modes of variation of deformation of the human ear and canal, which is the main topic of this thesis. Note that the scale of the deformations in the rest of the chapter is the same, thus colorbars are only displayed with the mean deformation in general.

7.2.1 Shape

In order to examine the shape variation a shape model has been build as in [40]. The mean shape can be seen in figure 7.1 and the first 3 modes of variation can be seen in figure 7.2. Such a model has previously been described by Paulsen et al. [123] and can be used in the design of mechanical parts for hearing aids. In addition it can be used as in [40] and [122] to test for correlation between shape and gender. This model is based on groupwise registration whereas the model in [40] is based on pairwise registration. As mentioned in chapter 5, good interpretations of the principal components are hard to give and in this case they are a mixture of many factors including size and the shape of the canal. Nevertheless, it gives a good overview of the complexity of the shape variation between individuals. By using Horn's parallel analysis [81] we can se 10 components include information (se figure 7.3). Notice that the shapes are

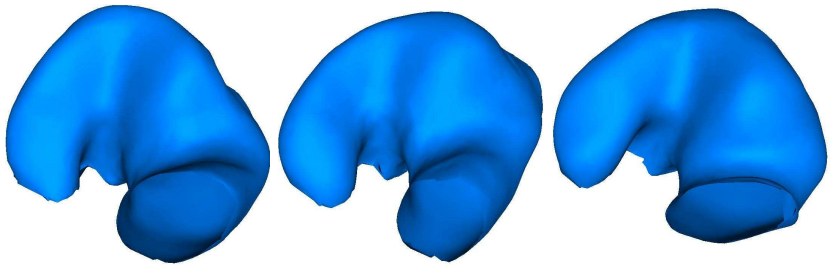

(a) Shape $+3\sigma PC_1$ (b) Shape $+3\sigma PC_2$ (c) Shape $+3\sigma PC_3$

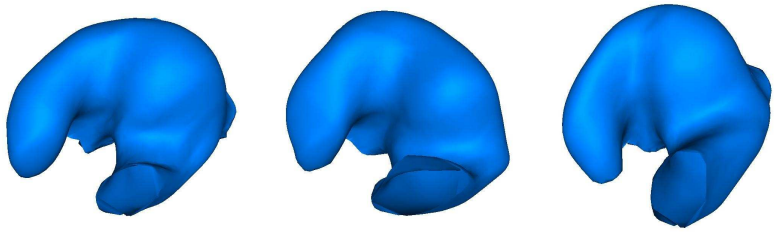

(d) Shape $-3\sigma PC_1$ (e) Shape $-3\sigma PC_2$ (f) Shape $-3\sigma PC_3$

Figure 7.2: The 3 first modes of variation for the shape, i.e. the mean shape +/- 3 σ of the given component

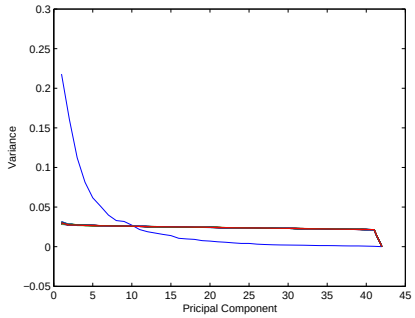

Figure 7.3: Horn's parallel analysis of the shape model. The conclusion is that the first 10 modes are significant and they explain 82% of the total variation.

not procrustes aligned since we believed that the registration is sufficient and as a consequence size is also included in the model.

7.2.2 Deformation

So far, as described in chapter 4, the research has been focused on the shape of the ear and deformation due to jaw movement. But as stated in chapter 3 several hearing aid users have reported problems related to feedback in other situations where jaw movement is not involved. This leads to the very obvious question: Are there any other causes of deformation? The main study was extended to examine some of theses potential causes and the resulting deformation fields are presented here.

7.2.2.1 Jaw Movement

Jaw movement is the only cause of deformation that has been investigated so far. By observing the average deformation and the modes of variation (figure 7.4 and figure 7.1(b)) it is obvious, as stated in [40], that the deformation is quite complicated and not confined to the canal (as claimed in [115]) although the largest deformation occurs here. The deformation is very consistent with the anatomy, especially the second principal component 7.4(b) and 7.4(e), which exactly represents the deformation caused directly by the mandible. The other components are side effects of the shifting of the tissue caused by movement of the mandible. It is also clear from figure7.4 that concha is not stable as stated by Grenness et al. [69]

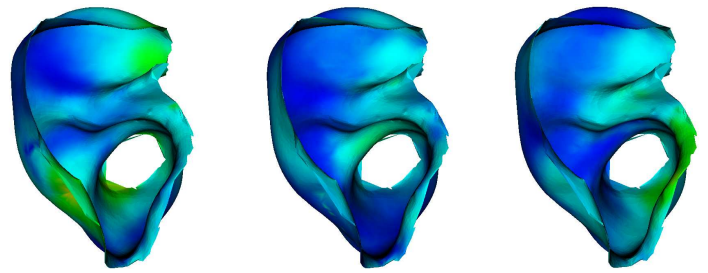

(a) Def. $+2\sigma PC_1$ (b) Def. $+2\sigma PC_2$ (c) Def. $+2\sigma PC_3$

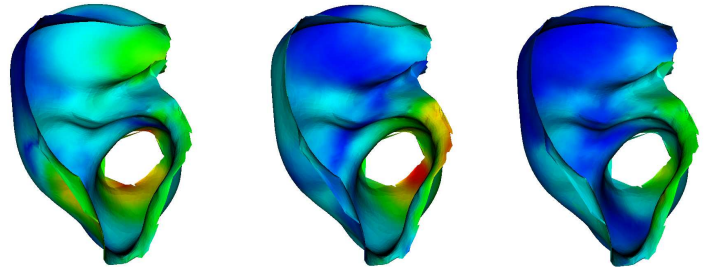

(d) Def. $-2\sigma PC_1$ (e) Def. $-2\sigma PC_2$ (f) Def. $-2\sigma PC_3$

Figure 7.4: The first 3 modes of variation of the deformation field from jaw movement. The scale is the same as in figure 7.15(a) and 7.5. Notice the extent and magnitude of the deformation to the concha in all 3 components.

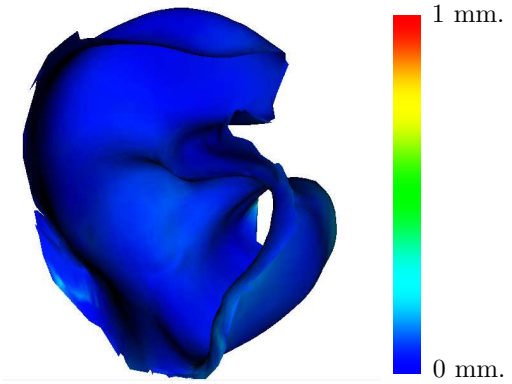

Figure 7.5: The mean deformation from leaning over.

7.2.2.2 Leaning Over

In figure 7.5 the average deformation caused by leaning over is shown. The deformation is not very pronounced but nevertheless present and reported to be able to cause acoustical feedback. It could be speculated that the deformation is only the catalyst for feedback and that the real cause could be a poor fit, the shape of the canal etc. A closer look at the major modes of variation (figure 7.6) reveals that some subtle deformation exist and that the deformation of the tragus may be enough to cause acoustic feedback. However,the informal talks have indicated that these problems only occur in few subject.

7.2.2.3 Turning the Head

As can be seen in figure 7.7, the deformation caused by turning of the head is on average the largest of the three with a maximum value of 0.82 mm, almost twice the maximum of the deformation caused by jaw movement. This is very surprising and has a magnitude that can cause acoustic feedback. It seems to be primarily the canal that changes shape whereas the concha only deforms slightly. Also tragus and anti-tragus seems to be deforming quite significantly, in particular in some of the modes of variation (figure 7.9). Thus, a very possible way of checking if this potentially can cause problems is by observing a given subject's tragus and anti-tragus during turning of the head. This is an extreme position and it does not occur with the same frequency as jaw movement, however, it does occur for instance when driving a car.

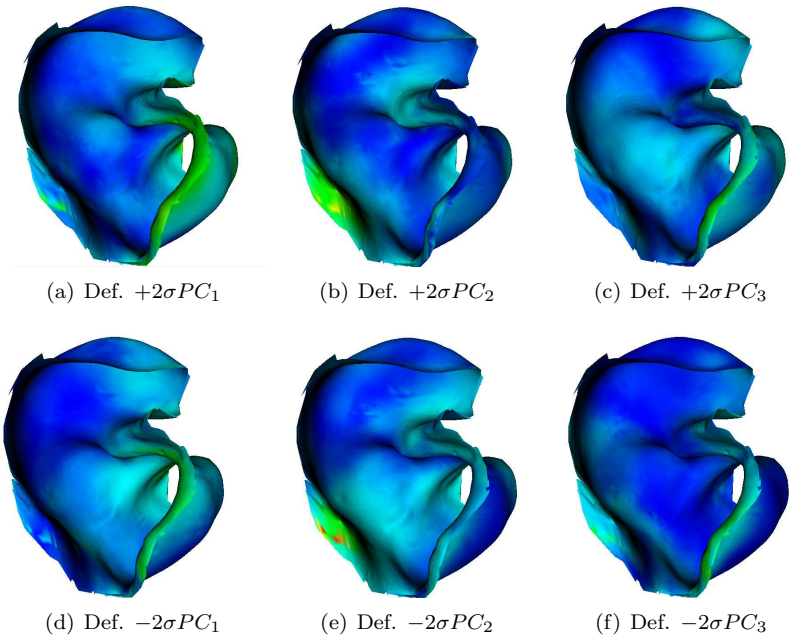

(a) Def. $+2\sigma PC_1$ (b) Def. $+2\sigma PC_2$ (c) Def. $+2\sigma PC_3$

(d) Def. $-2\sigma PC_1$ (e) Def. $-2\sigma PC_2$ (f) Def. $-2\sigma PC_3$

Figure 7.6: The first 3 modes of variation of the deformation field from leaning over.

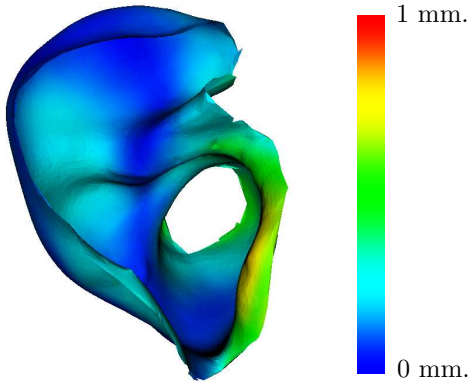

Figure 7.7: The mean deformation from turning the head.

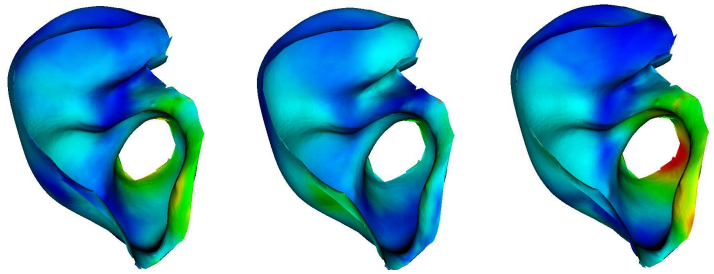

(a) Def. $+2\sigma PC_1$ (b) Def. $+2\sigma PC_2$ (c) Def. $+2\sigma PC_3$

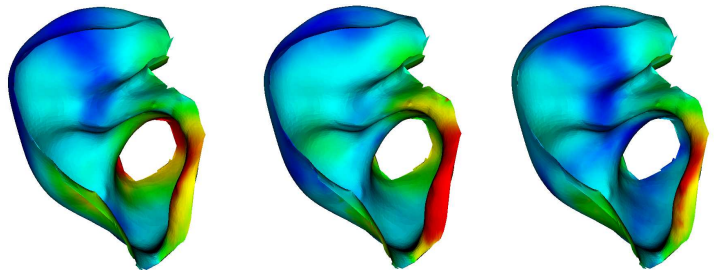

(d) Def. $-2\sigma PC_1$ (e) Def. $-2\sigma PC_2$ (f) Def. $-2\sigma PC_3$

Figure 7.8:

Figure 7.9: The first 3 modes of variation of the deformation field from turning the head.

7.2.3 Shape and Deformation

To reveal how the deformation and the shape are correlated a combined model normalized with respect to the variance is derived. The resulting model, which is based on a PCA shows the correlation between the particular deformation and the shape. The two different measures used in the model: the shape and deformation, are normalized with respect to their variance [147] as follows

$$\frac{\sum_j \lambda_{dj}}{\sum_i \lambda_{si}} \tag{7.1}$$

where λ_d are the eigenvalues of the covariance matrix of the deformation and λ_s the eigenvalues of the covariance matrix of the shapes. As it turns out, the shape is dominated by the deformation on the first modes, i.e. the modes of variation for the shape follows the deformation. We examine all three types deformations in the following sections.

7.2.3.1 Jaw Movement

Deformation caused by jaw movement is the only deformation type examined in other studies. However, the correlation with the shape has to the best of my knowledge never been explored. Figure 7.10 visualizes this correlation. On average (figure 7.1(a)), the most pronounced deformation is, as previously reported, between the first and the second bend and has the form of a bump right next to the mandible. The maximum deformation has a magnitude about 0.4-0.45 mm, which is a relatively subtle deformation. Building the combined model, Horn's parallel analysis identifies the number of components that can be distinguished from noise to 13 components or approximately 30% of the eigenvectors. The use of linear PCA does not normally give good interpretability. However, when looking for a certain shape that is highly correlated with a particular deformation it turns out that this method gives good results. As figure 7.10 shows the second principal component can be interpreted at the magnitude of the deformation and it is obvious from the shape part of the component that this is highly correlated with the shape of the canal. In general, the shape of the canal seems to be a good indicator of potential problems caused by deformation, when looking across all three components. This result can be used in the clinic to spot potential problematic ears, or at least in conjunction with good common sense help achieving better customer satisfaction.

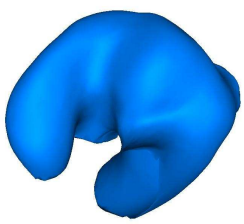

(a) Shape part of $+3\sigma PC_1$

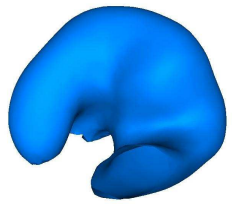

(b) Shape part of $+3\sigma PC_2$

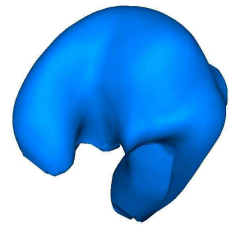

(c) Shape part of $+3\sigma PC_3$

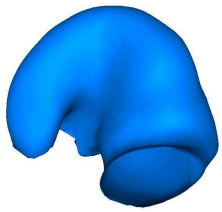

(d) Shape part of $-3\sigma PC_1$

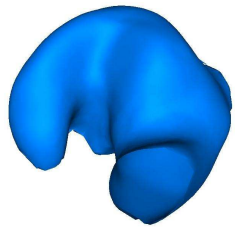

(e) Shape part of $-3\sigma PC_2$

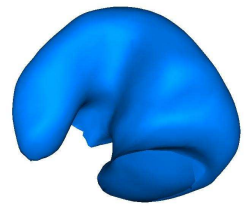

(f) Shape part of $PC_3 - 3\sigma$

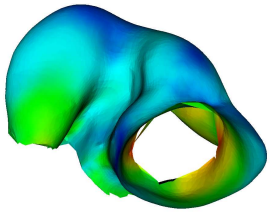

(g) Def. part of $+2\sigma PC_1$

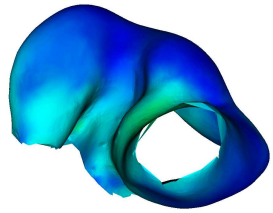

(h) Def. part of $+2\sigma PC_2$

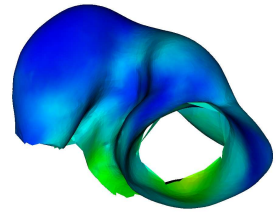

(i) Def. part of $+2\sigma PC_3$

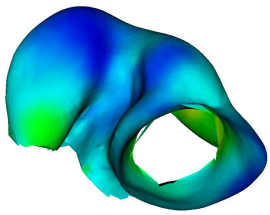

(j) Def. part of $-2\sigma PC_1$

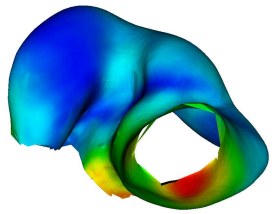

(k) Def. part of $-2\sigma PC_2$

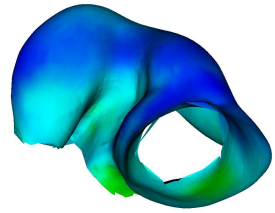

(l) Def. part of $-2\sigma PC_3$

Figure 7.10: The first 3 modes of variation with respect to normalized shape and deformation variation due to jaw movement, i.e. their covariation. 7.10(a)-7.10(f) show the shape and below are the corresponding deformations. The second component is interesting since it seems to relate the magnitude of the deformation with the shape of the canal. 7.10(a),7.10(d),7.10(g) and 7.10(j) are PC 1 and so forth.

7.2.3.2 Leaning Over

The changes caused by leaning over are so subtle that it is hard to find any really good explanation for changes, except for the size and shape of the canal, see figure 7.11. Looking across the three modes of variation it seems that the bigger the ear, the more deformation. However, there is no really clear pattern and any firm conclusions would be premature.

7.2.3.3 Turning the Head

Turning of the head has been the big surprise in this study. Not only does it actually cause the ear to deform when the head is turned, it is also causes the largest deformation. Figure 7.12(a),7.12(d),7.12(g) and 7.12(j) shows that a large deformation close to the bony part seems to be correlated with the size of the canal. Figure 7.12(c),7.12(f),7.12(i) and 7.12(l) explains that small ears with a upward bend of the canal also seem to be subject to deformation close to the bony part around the second bend. In both cases the canal seems to become more circular when deformation occurs, as in the case with jaw movement.

7.2.4 Closer to the True Deformation Field

To evaluate if the approximation of linearity in the deformation field holds, a simple experiment was carried out. Instead of just two impressions, five were obtained with increasing opening of the jaw (figure 7.13).

Figure 7.14 shows the corresponding deformation caused by that particular opening. The deformation is not entirely linear, but reasonably close. The position with 4 blocks is beyond the deformation in the full data set, where 3 approximately corresponds to the angle of opening used in the study. As can be seen from figure 7.15(a)) and figure 7.15(b), the deformation caused by 1-3 blocks is almost linear, which is a good indication that a linear interpolation between the two positions is adequate.

7.3 Empirical Validation of Registration

Validation of registration algorithms is not particularly easy. To justify the use of the registration algorithm used in this thesis, a registration of ears including

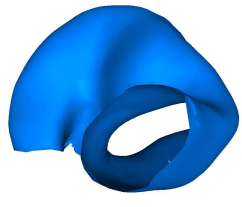

(a) Shape part of $+3\sigma PC_1$

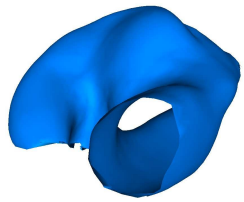

(b) Shape part of $+3\sigma PC_2$

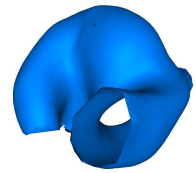

(c) Shape part of $+3\sigma PC_3$

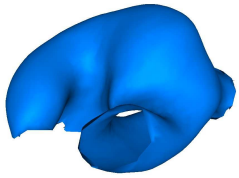

(d) Shape part of $-3\sigma PC_1$

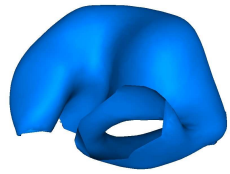

(e) Shape part of $-3\sigma PC_2$

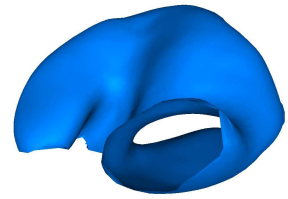

(f) Shape part of $-3\sigma PC_3$

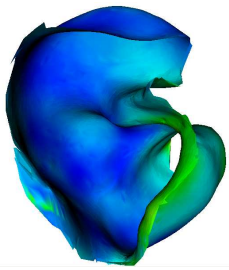

(g) Def. part of $+2\sigma PC_1$

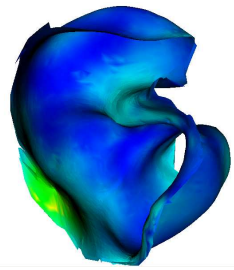

(h) Def. part of $+2\sigma PC_2$

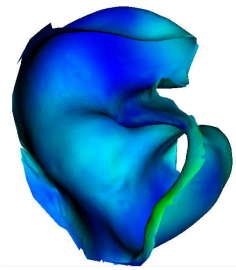

(i) Def. part of $+2\sigma PC_3$

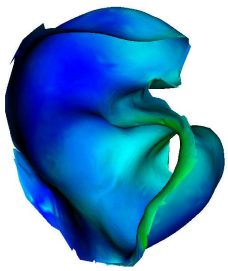

(j) Def. part of $-2\sigma PC_1$

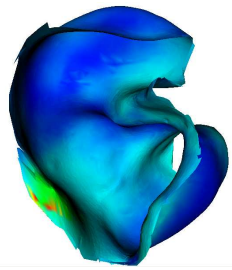

(k) Def. part of $-2\sigma PC_2$

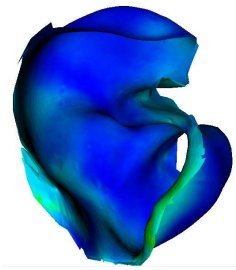

(l) Def. part of $-2\sigma PC_3$

Figure 7.11: The first 3 modes of variation with respect to normalized shape and deformation variation due to leaning over, i.e. their covariation. 7.11(a)-7.11(f) are the deformation and below are the corresponding deformations. 7.11(a),7.11(d),7.11(g) and 7.11(j) are PC 1 and so forth.

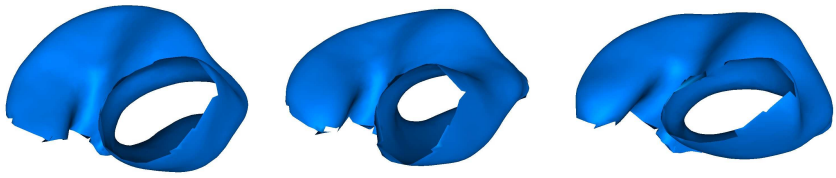

(a) Shape part of $+3\sigma PC_1$ (b) Shape part of $+3\sigma PC_2$ (c) Shape part of $+3\sigma PC_3$

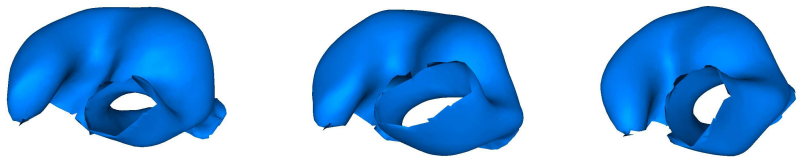

(d) Shape part of $-3\sigma PC_1$ (e) Shape part of $-3\sigma PC_2$ (f) Shape part of $-3\sigma PC_3$

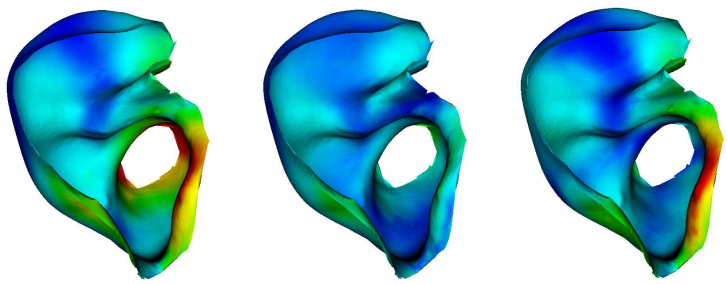

(g) Def. part of $+2\sigma PC_1$ (h) Def. part of $+2\sigma PC_2$ (i) Def. part of $+2\sigma PC_3$

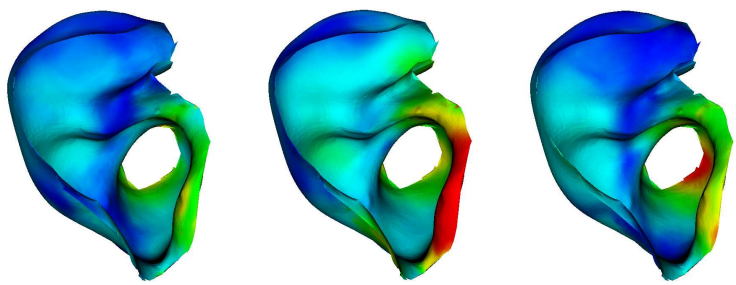

(j) Def. part of $-2\sigma PC_1$ (k) Def. part of $-2\sigma PC_2$ (l) Def. part of $-2\sigma PC_3$

Figure 7.12: The first 3 modes of variation with respect to normalized shape and deformation variation due to turning of the head, i.e. their covariations. 7.12(a)-7.12(f) are the deformation and below are the corresponding deformations. 7.12(a),7.12(d),7.12(g) and 7.12(j) are PC 1 and so forth.

(a) 1 block (b) 2 blocks (c) 3 blocks (d) 4 blocks

Figure 7.13: Pictures taken during impression making with 1-4 bite blocks.

their ear pieces was performed. The results can be seen in figure 7.16, where the ear pieces from different ears have been 'moved' with the registration to a reference ear. The pieces are so called micro molds (MM), and are supposed to sit very close to the second bend. The hypothesis is that the modelers, who make the MM place them in the same relative position in the ear of the different individuals. Therefor, when the ears are co-registered, the MM should end up at the same position in the reference ear. As depicted in figure 7.16, the MM's that are all placed close to the second bend, in fact they could probably be produced and used in the reference ear. Although, this does not quantify the registration error, it indicates that the registration results are reliable.

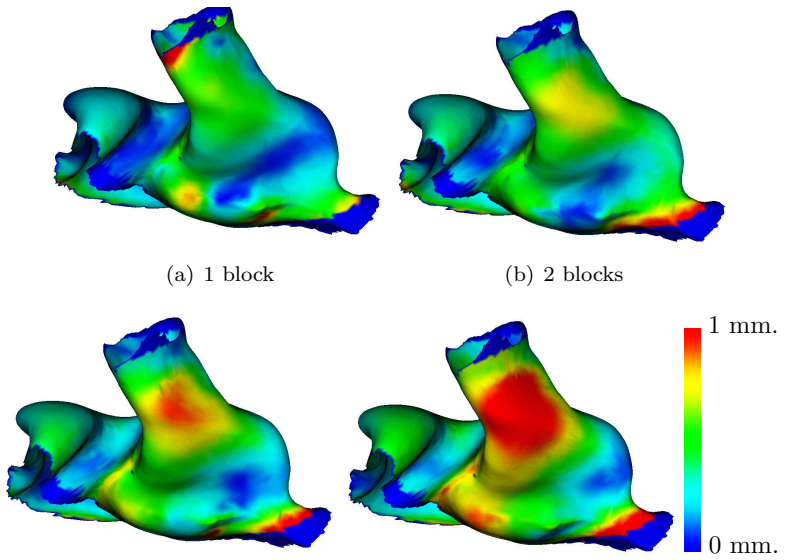

(a) 1 block (b) 2 blocks

(c) 3 blocks (d) 4 blocks

Figure 7.14: The magnitude of the deformation caused by opening of the jaw.

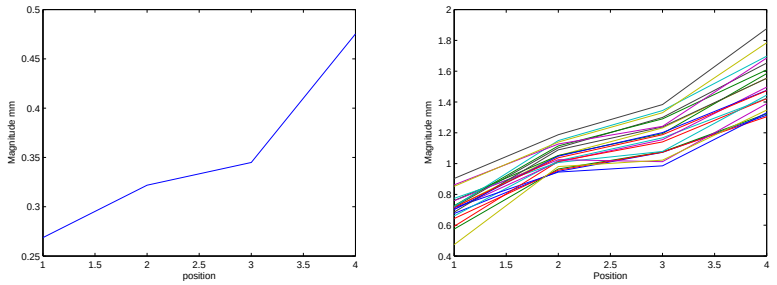

(a) Mean deformation (b) Max deformation

Figure 7.15: (a)The average magnitude of the deformation caused by opening of the jaw in the 4 positions and (b) the development of the deformation in the 10 points on the surface where the largest deformation occur.

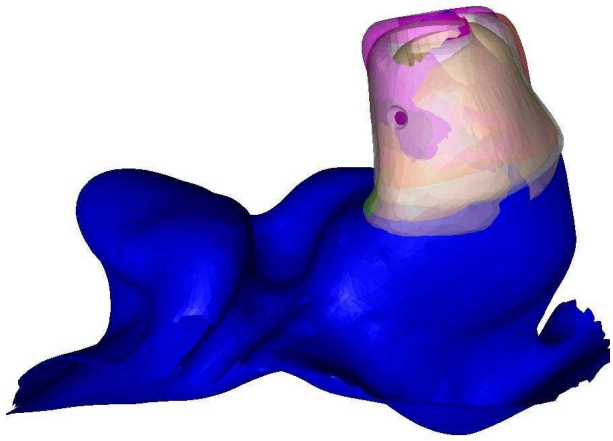

(a) Reference ear with 6 MM

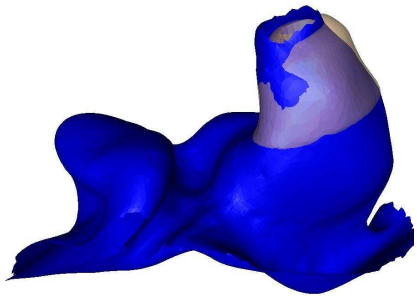

(b) Reference ear with 1 MM

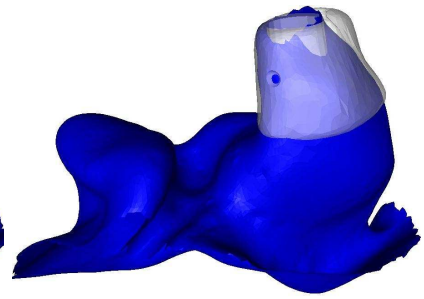

(c) Reference ear with 1 MM

Figure 7.16: (a) 6 Micro Molds inserted in the reference ear. (b & c) examples o a MM in the reference ear

Chapter 8

Discussion and Conclusion

The primary goal of this study was to investigate the deformation of the human ear canal due to jaw movement. The study was carried out using standard impression taking and scanning techniques. This has been challenging since it is quite time consuming and thus limits the number of impression from each individual in the data set. The outcome, however, is to the best of my knowledge the state of the art within shape analysis of the human ear and the results are groundbreaking within the field of deformation of the ear canal. The special type of data raised a demand for the development of specialized methods, in particular for registration [38, 43, 44], but also spawned some new ideas for regularization of methods based on the properties of the data, namely the orthogonally constrained SVM described in [23]. The registration is based on a distance map, which turns out to have a set of nice properties that makes approximations to derivatives very fast, which in turn makes the optimization very fast. The method has formed the basis of the shape analysis that has revealed a much more detailed and objective view on the deformation of the human ear.

The project has confirmed that the canal changes shape and revealed that the deformation is rather complex and not just a deformation of the canal in a particular direction. In fact, the entire soft part of the outer ear changes shape during movement of the jaw. Evidence that confirms that this deformation is related to feedback problems reported by the hearing aid users was published in [42], a relationship that to the best of my knowledge never previously has

been shown. In addition it has been shown that the deformation caused by jaw movement is present in all of the ears in the pilot study [40]. This is most likely also the case for main study, although this has not been investigated. Through the use of support vector machines it was possible to separate impressions taken with open mouth and closed mouth. The fact that such discrimination is possible, makes the directions for impression taking by Pirzanski and Berge [127] somewhat questionable since this indicate distinct differences between the impressions. Customized hearing aids such as the ITE (In The Ear) hearing aids should be made to fit the most common position, which is the normal relaxed position. This project has shown that the deformation varies greatly between individuals and the hearing aid should be customized to accommodate for the dynamic behavior of the individual ear.

The results in chapter 7, give clear indications of relations between specific shape features and particular kinds of shape deformation. This knowledge should be applied instead of the general assumption about the deformation field used today. Besides the deformation caused by jaw movement, the study has also shown that deformation has several other causes: turning of the head and leaning over. Although these causes have only been investigated superficially, they might also play a role in some of the comfort-related problems like retention (falling out of the ear) and perhaps acoustic feedback. The fact that these movements are not as frequent as jaw movement lowers the impact on the overall comfort level significantly. As an extra result a shape model of the human ear and canal was made that includes the entire concha. As a final remark the assumption of linearity between the two states the impressions were obtained in is reasonably close to the real deformation, as indicated in chapter 7.

It is my belief that the results from this study will enable audiologists to make better decisions when making impression, and thus take the necessary precautions to minimize the risk of acoustical feedback. In addition it is my hope that the development of hearing aids will benefit from the results presented in this thesis.

Part II

Contributions

Chapter 9

Analysis of Surfaces Using Constrained Regression Models

Sune Darkner, Mert R. Sabuncu , Polina Golland, Rasmus R. Paulsen , Rasmus Larsen

Abstract

We present a study of the relationship between the changes in the shape of the human ear due to jaw movement and acoustical feedback (AF) in hearing aids. In particular, we analyze the deformation field of the outer ear associated with the movement of the mandible (jaw bone) to understand its effect on AF and identify local regions that play a significant role. Our data contains ear impressions of 42 hearing aid users, in two different positions: open and closed mouth, and survey data including information about experienced discomfort due to AF. We use weighted support vector machines (WSVM) to investigate the separation between the presence and lack of AF and achieve classification accuracy of 80% based on the deformation field. To robustly localize the regions of the deformation field that significantly contribute to AF we employ logistic regression penalized with elastic net (EN). By visualizing the selected variables on the mean surface, we provide clinical interpretations of the results.

9.1 Introduction

One of the big challenges for hearing aid users is acoustical feedback (AF). When a customized hearing aid is produced, the ventilation size and gain are adjusted accordingly. However, when the ear changes shape due to movement of the mandible, false leaks and feedback can occur. Modern feedback cancellation algorithms exist, but they rely on the detection of feedback. The time lag between detection and cancellation causes a squeaking sound when a person talks or chews. Identifying and characterizing the main causes of AF can improve hearing aid designs to minimize AF risk. In this paper, we investigate the relationship between the deformation of the outer ear and AF. We are interested in localizing regions that play a significant role in this phenomenon. In our experiments, we work with surface scans of ear impressions from 42 subjects under two different conditions: open and closed mouth and questionnaire data that includes information about AF-related experience. The ear impressions are co-registered using a group-wise registration algorithm via a kernel-based nonlinear deformation model. We analyze the intra subject deformation fields using a classification method to illustrate the differences between the two groups: subjects who experience AF and subjects who do not. Using Weighted Support Vector Machines, we achieve 80% cross-validation accuracy on our data. Additionally, we employ logistic elastic net regression (logistic EN) to identify the surface points that consistently explain the difference between the two populations. Generalization performance and statistical significance of the fitted model are used to determine the parameters of the regression algorithm. We compute statistical significance based on a standard likelihood ratio test and the effective degrees of freedom for the model similar to Zou et al. [175]. The model is shown to be significant with $p < 0.001$ on the whole data set.

9.2 Prior Work

Previous studies investigated the deformation of the ear canal and concha using calipersOliviera et al. [115], and deformable shape models Darkner et al. [40], Paulsen et al. [123]. Yet, the relationship between deformations of the ear and clinical observations have so far not been explored. In other medical contexts, such as neuroimaging, the relationship between image-derived features and clinical data has been extensively studied Sjöstrand et al. [144]. A popular method used to explore differences between two groups in a population is Support Vector Machines (SVM) Boser et al. [17]. The discriminative direction of an SVM can be used to illustrate the differences between classes Golland [64]. However, an important challenge in such approaches, is the interpreta-

tion of discriminant features. Another problem commonly presented by medical data is its unbalanced nature: there are typically more negative samples than positive examples. To handle this, we use weighted SVMs Liu et al. [99]. Medical imaging provides further challenges: samples are high dimensional and few. Moreover, we expect that some of these dimensions exhibit significant correlations. Our goal is ideally to discover *all* these dimensions. Ridge regression Hoerl and Kennard [80] (or, in general Tikhonov ℓ_2 regularization Tikhonov [158]) takes this type of underlying structure into account. Additionally, we expect that only a small number of dimensions are related to the clinical outcome of interest. This prior knowledge can be formalized using a constraint on the ℓ_1 norm of the regression coefficients Tibshirani [156]. Elastic Net (EN) Zou and Hastie [173] combines these two approaches to achieve a sparse and correlated set of predictors. A Bayesian interpretation of this method yields an efficient implementation Zou and Hastie [173]. The method has been extended to fit the generalized linear model framework enabling various types of regressions through the canonical link functions including logistic regression. Analyzing multi-subject medical data requires spatial correspondence, usually determined via image registration. Motivated by group-wise registration methods Zollei et al. [172], we use a co-registration formulation that simultaneously aligns all surfaces. We employ a kernel-based nonlinear deformation model Rueckert et al. [135]Cootes et al. [36] to achieve a dense, diffeomorphic correspondence within and across subjects.

9.3 Data

The data consists of 84 impressions from 42 hearing aid users. Two impressions were obtained from each individual in different positions. (ı) Normal position, chosen as reference, (ıı) mouth opened. A spacer was used to ensure consistency with respect to the angle of the mouth opening. The impressions were all acquired from the subjects' right ear. Each impression consists of $\approx$ 5500 points in 3D i.e. vertices, corresponding to a 16500 dimensional feature vector. In addition to the shape data, the subjects filled out a questionnaire, including questions regarding acoustical feedback (AF). All subjects that experienced frequent AF problems (once a week or more) were grouped together if the annoyance was related to ear deformation, i.e. jaw movement and facial expressions. The latter is included because it often involves jaw movement. Thus, we obtained two groups: subjects who experience AF and subjects who do not.

9.4 Methods

9.4.1 Co-registration and Preprocessing

The ear impressions were scanned to obtain surfaces, which were then manually preprocessed to remove artifacts. We represent each surface as a triangular mesh S, with vertices denoted by $\vec{x}_S \in S \subset \mathbb{R}^3$. The registration framework is based on the method described in Darkner et al. [43], which uses the difference between signed distance maps of the two surfaces S_1 and S_2 to compute a similarity metric. For computational efficiency, the distance is only computed on a narrow band $Q \subset \mathbb{R}^3$ that covers both surfaces, i.e., $Q \supset S_1, S_2$. The distance between S_1 and S_2 is then defined as:

$$f(S_1, S_2) = \frac{1}{\|Q\|} \sum_{\vec{x} \in Q} (d_{S_1}(\vec{x}) - d_{S_2}(\vec{x}))^2, \tag{9.1}$$

where d_S denotes the signed distance map of the surface S and $\|Q\|$ denotes the volume of Q. The pairwise registration problem is formulated as the minimization of Eq. 9.1 and solved using Newton's method. We parameterize the deformations using a kernel-based approach Cootes et al. [36] defined on a control grid in a coarse-to-fine fashion, from $2^3 - 40^3$ control points. The gradient of the objective function with respect to this parametrization can be easily computed. We extend this approach to a multi-subject setting by defining a mean surface $S_\mu = \frac{1}{N} \sum_i S_i$, where N is the number of subjects. The mean surface is updated at every iteration and a set of transformation parameters is computed for each subject based on its distance to the mean surface. To anchor the deformations, we constrain the average deformation across all subjects to be identity. In other words, the mean of the deformation parameters is zero.

9.4.2 Classification and Regression

Our goal is to analyze the deformation fields obtained from the co-registration step to show differences between subjects who experience Acoustical Feedback (AF) and subjects who do not. Ground truth labels were based on the questionnaire data, as described in Section 3. The localized nature of the deformation parametrization allows us to identify regions that influence AF. We use the popular SVM method with no kernel to classify the data based on the whole deformation field. Since our data contained 18 positive samples and 24 negative samples, we investigated weighted SVM (WSVM) Liu et al. [99]. In contrast with SVM where the penalty of misclassification is universal, WSVM sets a different penalty for each class and the the ratio between class penalties are

inversely proportional to the class size ratio. In our experiments, this approach improves results by about 5% when compared with the uniform penalty on errors. Due to the challenges of interpreting the discriminant features, i.e., support vectors in the SVM experiment, we explored a logistic regression approach. Logistic regression models the probability P of a certain outcome, in our case subjects who experience AF and is estimated by the ratio of occurrences. This is accomplished through the canonical link $\log(\frac{p_i}{1-p_i})$, known as the log-odds or logit. Standard logistic regression can thus be formulated as:

$$\log\left(\frac{p_i}{1-p_i}\right) = \beta_0 + \boldsymbol{\beta}\mathbf{x_i}, \forall i \tag{9.2}$$

where β_0 is the intercept, $\boldsymbol{\beta}$ is the regression coefficients of size $1\times$ number of dimensions (16,500 in our case) and $\mathbf{x_i}$ is a column vector that represents an observation. Logistic elastic net extends standard logistic regression by penalizing the parameters $\boldsymbol{\beta}$ with the ℓ_1 and ℓ_2 penalty.

$$\log\left(\frac{p_i}{1-p_i}\right) = \beta_0 + \boldsymbol{\beta}\mathbf{x_i} + \epsilon_i, \quad \text{s.t. } \|\boldsymbol{\beta}\|^2 < \rho, |\boldsymbol{\beta}| < \xi \tag{9.3}$$

for some $\rho, \xi > 0$ and for all i. The solution can be found via a MAP approach where the following prior on the parameters is used:

$$P_{\lambda,\alpha}(\boldsymbol{\beta}) = C(\lambda,\alpha)e^{-\lambda(\alpha\|\boldsymbol{\beta}\|^2+(1-\alpha)\|\boldsymbol{\beta}\|)}, \tag{9.4}$$

where λ is the hyper-parameter that determines the total amount of regularization, α determines the trade-off between the two penalty terms and C is the normalization. Logistic EN has the properties of ridge regression and yields sparse solutions thanks to the ℓ_1 constraint. Thus the model takes covariations into account while only consisting of a small subset of significant regression coefficients. This yields dimensionality reduction conditioned on the information in the data set.

9.5 Model validation and selection

We use cross-validation to select the hyper-parameters α and λ. Furthermore, by using the likelihood ratio test, we can ensure that the selected parameters yield statistically significant models, i.e., explain the data well. The likelihood ratio computes $\Lambda = \frac{L(\boldsymbol{\beta}|\mathbf{X})}{L(\beta_0|\mathbf{X})}$, where the numerator $L(\boldsymbol{\beta})$ is the log-likelihood of the fitted model, defined as:

$$L(\boldsymbol{\beta}|\mathbf{X}) = \sum_{i=1}^{N}\left[y_i\boldsymbol{\beta}^t\mathbf{x_i} - \log(1+\exp(\boldsymbol{\beta}^t\mathbf{x_i}))\right], \tag{9.5}$$

where $y_i \in \{0, 1\}$ is the ground truth label, β_0 is included in $\boldsymbol{\beta}$ and $\mathbf{x_i}$ is the i'th observation in $\mathbf{X}$, the data to which the model is fitted. $L(\beta_0)$ is the null-hypothesis likelihood, computed with $\boldsymbol{\beta} = 0$. Note that $(-2 \log \Lambda)$ is approximately χ^2 distributed with a parameter equal to the effective degrees of freedom of the model minus 1. Following Malthouse [103], we can compute the effective degrees of freedom as $\sum_{j=1}^{P} \frac{\alpha_i}{\alpha_i + \lambda}$, where P is the number of dimensions and $\{\alpha_i\}$ are the eigenvalues of the data matrix $\mathbf{X}^T\mathbf{X}$.

9.6 Analysis

The analysis is divided into two parts, classification and regression. Performing classification demonstrates the difference between the two classes. To reveal how the deformation field relates to AF problem regression is performed. We fit a logistic regression model *to each variable i.e. vertex* independently and selects the significant models as determined by the likelihood test to identify *significant variables*. This approach does not take covariances into account since each variable is treated independently. We use logistic EN on all the data to perform variable selection while accounting for covariances. Logistic EN provides better and more robust localization, which yields interpretable results. Yet, SVM is typically superior with respect to classification accuracy.

9.6.1 Classification

To investigate if the data set size is sufficient for generalization, we use SVM to classify and perform cross validation (100 random trials) with an increasing number of samples included in the training set. The purpose is to investigate whether including further samples will improve the classification. The test error for each class vs. the number of samples included in the model is plotted in Fig. 9.1(c). From the figure it is clear that better results could be obtained with more data, however, the test error is around 22-25%, clearly showing separation in the data. Using WSVM reduces the error further to 20%. Fig. 9.2 illustrates the variable weights on a mean surface in four representative random trials. Comparing these four trials, one sees that even though the general patterns seem to be consistent, there is significant noise and the localization quality is not sufficient. Fig. 9.2(e)shows the frequency of each variable appearing in the top 20% quantile over all 100 trials. We notice that variables robustly (red regions) appearing in the top 20% quantile are sparse.

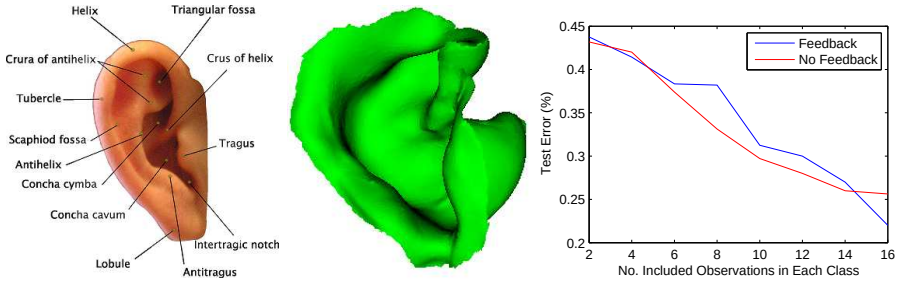

(a) (b) (c)

Figure 9.1: (a) An anatomical atlas of the ear. (b) A typical ear impression. (c) Number of parameters for each class included in the model vs. the test error.

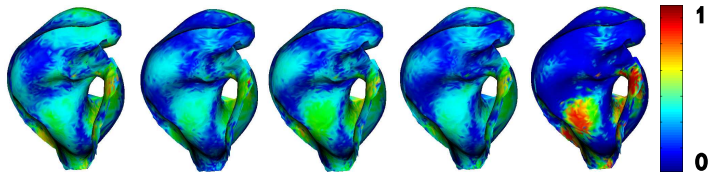

(a) (b) (c) (d) (e)

Figure 9.2: The normalized coefficients from the SVM solution for 4 random cross validation iterations mapped to the mean surface.(e) the frequency of each vertex appearing in the to 20% quantile.

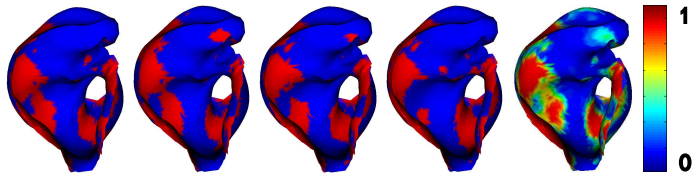

(a) (b) (c) (d) (e)

Figure 9.3: The selected coefficients from the penalized logistic regression solution for 4 different cross validation iterations mapped to the mean surface. Red indicate a selected variable.9.3(e) Is the cross-validated probability of a variable being selected

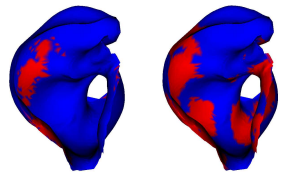

(a) (b)

Figure 9.4: (a) The significant logistic regression models on each variable mapped to the mean surface. (b) The selected variables of the full logistic EN regression model mapped to the mean surface. Red indicate a selected model/variable/vertex.

9.6.2 Regression

To get a base line, we perform a logistic regression of each parameter against the response variable. The significant variables are shown in Fig. 9.4(a), where red indicates a significant model. As can be seen significant variables cluster nicely. However, we expect significance in and around the canal as well, which is not present in this figure. This is due to the fact that each variable is treated independently. To recover from this, we use the Logistic EN with the hyper-parameters determined by cross validation and the likelihood ratio test. From the formula for effective degrees of freedom we can make an educated guess of the initial regularization parameter for the ℓ_2-penalty, which needs to be around 1000 for the model to be statistical significant. An interval around this value is searched to find a suitable combination where the likelihood ratio rejects the null hypothesis. This yields $\lambda = 1000$ and $\alpha = 0.997$. The resulting models contain between 2000-2500 variables but are heavily constrained with 2-3 free parameters. To validate the model, 10-fold cross validation is performed with an equal number of observations from each class used in training, which yields 73% accuracy for both classes. The regularization in the model increases test error to 5-10%. A representative selection of the resulting cross validation models can be seen in Fig. 9.3. We note that the models are consistent over different runs. Having estimated the regularization parameters we build a model on the full data set. The model is shown in Fig. 9.4(b). The estimated degrees of freedom for the model is 3.88, the model is significantly better than H_0 ($p < 0.001$). The resulting model is in very good correspondence with the individual models from the cross validation and includes far more of the surface in the model compared to the logistic regression in Fig. 9.4(a). Moreover, the logistic EN gives better and more consistent localization compared to the SVM, and the results are less noisy (Fig. 9.2 and Fig. 9.3). In addition the results are in good correspondence with clinical observations.

9.6.3 Clinical interpretation

The results are consistent with how hearing aids are situated in the ear. It is interesting that not only the entrance to the canal is important, but also the lower part of the outer ear, tragus and anti tragus (see Fig. 9.1(a)). The reason is that its often one or both of these that hold the hearing aid in place. The small In The Ear devices (ITE) are held in place by the opening of the canal and Tragus, where as Behind The Ear aids (BTE) are molded to the entire concha (most of the impression). Also the deformation, which we know occur deeper inside the canal seems to have little influence on the acoustical feedback. Only the bottom part of the inner canal seems to have a small influence, which

corresponds to clinical observations made during normal practice. The results in Fig. 9.4(b) lead to the possibility of improving the fit with respect to feedback.

9.7 Conclusion

By using constrained logistic regression, we find parts of the ear canal surface that explain the feedback problems experienced by users. The regression model gives good localization and the outcome is easy to interpret. Furthermore, by using an extended framework for estimation of the free parameters in the model, a cross validation scheme based on significant models can be used. We show that the final model is significant ($p < 0.001$). In addition, we show that a classifier based on the WSVM can achieve a classification accuracy of 80% for both classes, with the possibility of improvement if more data were available.

Chapter 10

Analysis of Deformation of the Human Ear and Canal Caused by Mandibular Movement

Sune Darkner, Rasmus Larsen, Rasmus R. Paulsen

Abstract

Many hearing aid users experience physical discomfort when wearing their device. The main contributor to this problem is believed to be deformation of the ear and ear canal caused by movement of the mandible. Physical discomfort results from added pressure on soft tissue areas in the ear. Identifying features that can predict potential deformation is therefore important for identifying problematic cases in advance. A study on the physical deformation of the human ear and canal due to movement of the mandible is presented. The study is based on laser scannings of 30 pairs of ear impressions from 9 female and 21 male subjects. Two impressions have been taken from each subject, one with open mouth, and one with the mouth closed. All impressions are registered using non-rigid surface registration and a shape model is built. From each pair of impressions a deformation

field is generated and propagated to the shape model, enabling the building of a deformation model in the reference frame of the shape model. A relationship between the two models is established, showing that the shape variation can explain approximately 50% of the variation in the deformation model. An hypothesis test for significance of the deformations for each deformation field reveals that all subjects have significant deformation at Tragus and in the canal. Furthermore, a relation between the magnitude of the deformation and the gender of the subject is demonstrated. The results are successfully validated by comparing the outcome to the anatomy by using a single set of high resolution histological sectioning of the region of interest.

10.1 Introduction

A recent survey has shown that physical comfort and acoustical feedback are among the ten most important issues for hearing aid user satisfaction Kochkin [93]. It is well known among hearing-aid manufacturers that physical deformation of the human ear canal is connected to problems with both comfort and acoustical feedback. Furthermore, it is known that deformation of the ear canal is closely linked to speaking, chewing, yawning, and movement of the mandible in general. The human ear canal consists of a soft and a bony part. The bony part is embedded in the mastoid and, thus, not subject to deformation. However, the soft part of the canal is situated between the mandible and the mastoid surrounded by skin, cartilage, and fat; all tissues that are highly deformable. Fig. 10.1(a) shows an anatomical labelling of the human ear. From fig. 10.1(b) and (c) it is obvious that movement of the mandible will cause deformation of the tissue around it, hence, changing the shape of ear canal. Very little is known about the nature of this deformation seen from a hearing-aid perspective. We believe that systematic knowledge of the shape change of the ear canal can be used in future hearing-aid production, thus, creating better and more comfortable hearing aids. In this study, a set of 3D scanned ear impressions (see fig. 12.2(a)) is used in a non-rigid registration framework to create a shape model and a deformation model. In the following analysis, we try to establish an understanding of where in the ear and canal the significant shape changes occur and if these changes are related to the shape of the ear and canal. Furthermore, it is examined if there is any gender-related differences in ear-canal dynamics. All such relations will be beneficial in discovering problematic cases.

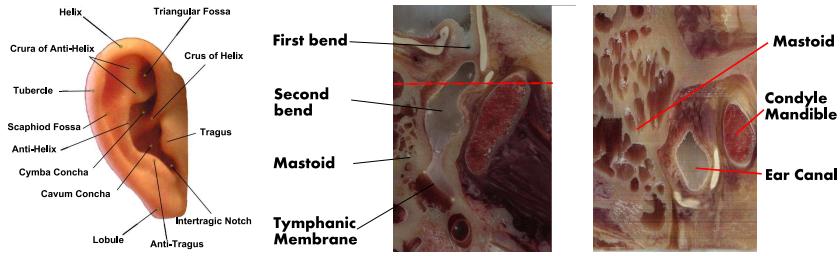

(a) (b) (c)

Figure 10.1: (*a*) Map of the anatomy of the human ear. (*b*&*c*) Histological sectioning of the human ear from Sorensen et al. [145]. (*b*) A transversal cut containing the canal. As can be seen, the canal is situated between the mastoid and the mandible before entering the mastoid itself. Furthermore, there are two bends of the canal. The outer bend is called the first bend and the inner, just before the canal enters the mastoid, is called the second bend. (*c*) A cut in the sagittal plane at the dashed red line of *b* showing the soft tissue around the ear canal between the mandible and the mastoid.

10.2 Previous Work

It is only recently that 3D scanners have been introduced in the production of hearing aids. Therefore, most prior work on ear canal shape was done directly on ear impressions using calipers etc. Oliviera et al. Oliviera et al. [115, 116] have analyzed the changes that occur in the ear canal due to movement of the mandible and concluded that there is a deformation and also a change in volume. They claim that the deformation only occurs in the coronal plane. However, Grenness et al. Grenness et al. [69] have shown that the deformation is more complex, assuming that the Concha is stable during movement of the mandible. This claim remains to be proven. Finally, Pirzanski Pirzanski [126] has analyzed the dynamics of the ear canal with the goal of increasing hearing aid users acceptance rates. However, all of the above is based on manual measurements and manual registration, which is prone to error. A statistical shape model of the static ear canal based on scanned ear impressions and automated registration have been presented by Paulsen et al. Paulsen et al. [123].

10.3 Data

The data consists of 60 scannings of ear impression taken from 30 individuals, 21 males and 9 females, ranging from 25 to 65 years of age. Two impressions

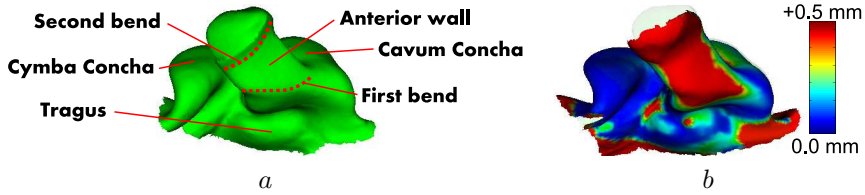

Figure 10.2: (a) A typical scanning of an impression taken from the production. The scanning has been opened at the top, and the lower part has had most artifacts removed manually. Some of the anatomical features have been labelled. (b) The magnitude of the deformation field projected onto the open mouth impression.

were taken from each, one with open mouth using a mouth prop to create a similar opening angle for all subjects and one with closed mouth. To ensure consistency, all impressions were made by the same audiologist and scanned on a 3D laser scanner by the same operator.

10.4 Inspection of the Anatomy

The images seen in fig. 10.1(a) and (b) are a part of a high-resolution histological sectioning study by Sørensen et al. Sorensen et al. [145]. The data set includes the outer ear, making it possible to investigate the physiology of the human ear and canal. As mentioned, the mandible is situated in front of the ear canal between the first and the second bend. It is known that the tissue surrounding the canal is not directly attached to the mandible. When the mandible moves forward a small void is created, which is filled by the surrounding tissue. It is expected that this will cause a deformation of the wall of the ear canal on the anterior side between the first and the second bend. As fig. 10.1(c) shows, the posterior and top side of the canal are situated very close to the mastoid, thus, limiting the amount of deformation on this side of the canal. Tragus and Cavum Concha is situated on the soft tissue surrounding the Mandible. In fact, careful examination reveals that the whole outer ear is situated on soft deformable tissue, especially the part below Crus of Helix. Hence, Grenness' assumption of a stable Concha seems to be wrong and the ear below Crus of Helix can be expected to move inwards perpendicular to the sagittal plane as the mouth opens. Inspection of the histological data reveals that the best reference for the data in this study is the Cymba Concha. This part of the ear might also be subject to deformation. However, since it is situated on the outside of the mastoid, contrary to the Cavum Concha which is situated just beneath, it is not as likely as other parts of the outer ear to displace and deform.

10.5 Model Generation

To make a consistent data analysis a frame of reference must be established. A fully automatic rigid registration algorithm by Darkner et al. Darkner et al. [38], evaluated by Darkner et al. [41], is used to register the Cymba Concha of all impression pairs. A highly constrained non-rigid surface registration is then applied to create the deformation field, see fig. 12.2 (b). Secondly, to establish dense point to point correspondence across the population the non-rigid surface registration algorithm is applied to all closed mouth impression. Dense point to point correspondence is generated from the resulting registration using the angle weighted normal method by Bærentzen and Aanæs Bærentzen and Aanæs [9] and ray tracing Whitted [169]. The result is then propagated to the deformation field for correspondence between the deformations and shapes. The non-rigid registration is based on the diffeomorphic warp presented by Cootes and Twining Cootes et al. [35], extended to 3D by Vester-Christensen et al. Vester-Christensen et al. [164], using the distance and cost functions of Darkner et al. [38]. A steepest descent algorithm implemented as the inverse compositional algorithm by Baker and Matthews Baker and Matthews [10] reduces the registration time to 4-8 minutes per shape registered on a 1.7 GHz laptop PC. From the Procrustes Dryden and Mardia [49], registered shapes a shape model and a deformation model are created. Generally, the impressions do not depict the exact same part of the ear, only an overlapping region; hence, the models are cropped to their common subset.

10.6 Analysis and Results

Visual inspection of the data reveals that almost all of the subjects have a clear visible deformation of their ear canal due to movement of the mandible. It is evident that a deformation occurs in the canal that has its maximum on the anterior side of the wall between the first and the second bend. As seen from fig. 10.3 the mean deformation is exactly that. This confirms our observations from the histological sectioning. Additionally, a deformation of Tragus, Anti-Tragus and Cavum Concha can be observed in the deformation model, which again corresponds well with the observations from the histological sectioning. The magnitude of the deformation varies among individuals from ≈ 0.2 mm. to 2.3 mm. Using the mean shape as reference the average, minimum and maximum deformation over all sets of impressions can be calculated as $average = 0.4349$ mm.,$min \approx 0.0$ mm. and $max \approx 2.3$ mm..

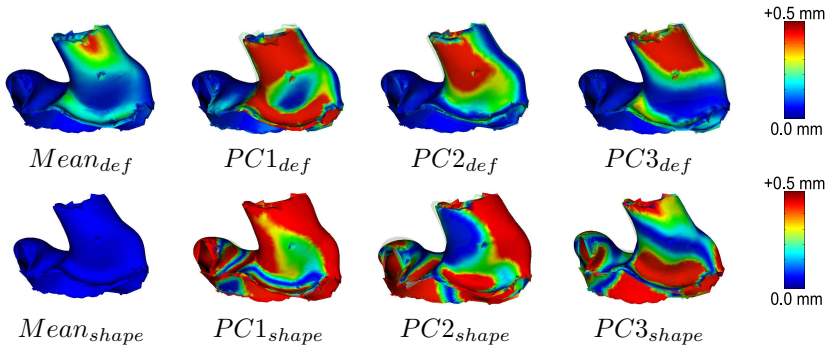

Figure 10.3: The mean deformation and the first 3 modes of deformation variation and the mean shape and the first 3 modes of shape variation. All +2 standard deviations.

It is a well known fact that ear size and gender are related Paulsen et al. [123]. It is observed that the first mode of variation ($PC1_{shape}$) of our shape model is related to size (fig. 10.3). This is confirmed by using a logistic regression model to predict gender from this variable. Let p be the posterior probability of a male. Then the model $logit(p) = \alpha + \beta PC1_{shape}$ is significant with significance levels less than 7%. Visual inspection of the deformation fields has led us to suspect that males tend to have larger deformations than females. Hence, a logistic regression was performed with the mean amount of deformation over the entire shape as predictor of the gender. A model without intercept was chosen since no deformation should model odds 50/50 between genders. The resulting model is significant at a 4% level, confirming the hypothesis. The modelled difference between genders in deformation is most likely related to the differences in the male and female mandible. Such discrimination has been reported by Giles Giles [63] and Graw Graw [68] using the size and strength of the mandible.

10.6.1 Shape Related to Deformation

To investigate if shape and deformation are related, the deformation and the shape models are investigated (see fig. 10.3). Comparison of the first 5 modes explaining 82% of the total variation of the deformation model and the first 7 modes explaining 80% of the total variation of the shape model are made. The number of modes are found using parallel analysis by Horn Horn [81]. The first mode of deformation variation, containing primarily size of the deformation, cannot be explained by any of the 7 modes from the shape model. However, the next 3 modes of variation can. The second mode of deformation can be

interpreted as change in angle of the canal in the plane bisecting the coronal-transversal angle in relation to Concha. This mode can be modelled by the second and third mode from the shape model. These two modes represents the vertical length of the Concha and the angle of the canal in the transversal plane. The third mode of deformation is the angle of the canal in relation to Concha in the transversal plane and the shape of the canal; round or oval. This mode of deformation can be modelled by the 6th mode of shape variation. Both these models $PC2_{def} = \alpha + \beta_1 PC2_{shape} + \beta_2 PC2_{shape}$, and $PC3_{def} = \alpha + \beta_1 PC6_{shape}$ are significant at the 1% level. The 4th deformation mode is the bending of the canal in the transversal plane and the deformation of the Intertragic notch and can be related to the roundness of Concha and the angle of the canal in the coronal plane. The model has the form, $PC4_{def} = \alpha + \beta_1 PC4_{shape}$ and is significant at the 1% level. The first mode of shape variation mode can explain the 5th mode of deformation variation with significance $p < 0.08$. Combined with the 6th mode the significance becomes $p < 0.06$.

10.6.2 Analysis of the Deformation Field

Now we will examine the deformation field for an individual ear in more detail, i.e. at every vertex of the triangulated surface representing the ear we will test if a significant deformation occurs as a function of opening the mouth. This involves simultaneous testing of ≈ 10000 hypotheses. In order to do this we will employ Efrons Efron [52] procedure for estimating the empirical null hypothesis for each individual. Using a i.i.d. normal assumption for the deformation vector elements under the null hypothesis - H_i - we have that the magnitude of the deformation vector for the ith vertex Y_i follow a $\sigma\chi(3)$ distribution. For each vertex we can transform the Y_i's to z-values (Φ is the standard normal cumulative distribution), where

$$z_i = \Phi^{-1}(\text{prob}\{Y_i > y_i\}, \qquad z_i | H_i \in N(0,1) \tag{10.1}$$

The latter part is the theoretical null hypothesis. In Fig. 10.4(a) we show as a bar plot the histogram of z's from an experiment where two impressions have been taken from the same ear with closed mouth. The heavy right tail was expected due to shifting of ear wax, hair etc. We approximate the histogram with a smoothing spline and extract the maximum point and the full width half maximum of the (first) major top. This provides us with robust estimates of the mean and standard deviation under the null hypothesis. The empirical null is $z_i | H_i \in N(-0.40, 0.60)$. The reasons for the difference between the theoretical and empirical nulls may be hidden correlations or the presence of genuine but uninteresting small effects.

Assuming that for each ear a large proportion of the vertices will exhibit no

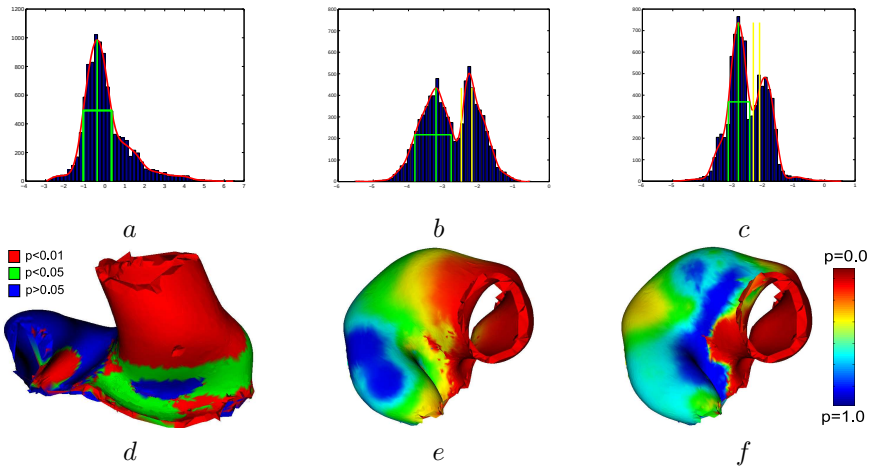

Figure 10.4: (a) Histogram of the z-values under the null hypothesis and robust estimation of the normal parameters using a smoothing spline. (b-c) Histograms of $z-values$, robust null estimation and 95% and 99% quantiles for two ears.(d) the 95% and 99% quantiles of the ear in b. (e-f) p-value maps of b and c respectively.

change due to mouth opening we can use a similar procedure to identify those vertices where significant change occur. In Fig. 10.4(b-c) the null is estimated from the first major peak and 95% and 99% quantiles are determined. The corresponding vertices where significant changes occur are shown in Fig. 10.4(d-f). We see that significant changes occur in Cavum Concha, at Tragus and Anti-Tragus and in the canal; in full correspondence with our expectations and precisely where most hearing aids are situated in the ear. This confirms that movement of the mandible causes discomfort for some hearing-aid users.

10.7 Conclusion

We have shown that it is possible to consistently locate regions of significant deformation caused by movement of the mandible in all subjects. The occurrence of the deformations corresponds well to the physiology of the human ear, in terms of soft tissue and bony structures. The locations that are deforming the most are exactly where hearing aids normally are situated in the ear. Hence, we can confirm that movement of the mandible can cause discomfort in the ear when wearing a hearing aid. Furthermore, we have shown that males in general are more prone to deformation of the ear and canal and that the common as-

sumption of men having larger ears than women seems to hold. Finally we have shown several significant relations between the shape of the ear and canal and the deformation occurring during movement of the mandible. We can explain 50% of the variation of the deformation using the first 6 modes of variation from the shape model. Our findings are very significant, even when considering the limited size of the data set. The features described by the modes of variation in the shape model can be used as guidelines to detect potentially problematic cases. They point to a problem caused by a specific kind of deformation, thus enabling the dispenser or hearing-aid manufacturer to take appropriate actions to eliminate the problem.

Chapter 11

Non-rigid Registration of 2D Manifolds in 3D Euclidian Space

Sune Darkner, Martin Vester-Christensen,
Rasmus R. Paulsen, Rasmus Larsen

Abstract

This work describes a non-rigid registration method for open 2D manifold embedded in 3D Euclidian space. The method is based on difference of distance maps and grid based warps interpolated by splines constrained in such a way that the deformation field is diffeomorphic. We then create a dense surface to surface correspondence using angle weighted normals and ray tracing. The implementation using a derivation of the inverse compositional algorithm for optimization of computational speed is described. The results are evaluated as a shape model showing the principal modes of variation.

11.1 Introduction

Building generative model is a common way of analyzing variation across a population. However, these models require correspondence and are very sensitive to the registration of the observations. The methods were originally intended to analyze rather sparse data, but as data acquisition techniques has improved the number of parameters in each observation have increased. Today it is not unusual to have 10000+ parameters in an observation. These parameters are often sampled from a continuous domain but very seldom with correspondence to the next observation hence registration is needed. Often, this task is done manually, but automatic and semi automatic methods such as ICP exist. The manually and the semi automatic often involves some kind of annotation which are often quite labor intensive and very prone to bias or error.

11.2 Previous work

The registration problem i.e. creating correspondence between observations is one of the most researched topics within image analysis and a lot of both semi automatic and automatic methods exist. Most methods consists of a rigid and a non-rigid registration and the most difficult part of this is the nonrigid part. A lot of automatic and semi automatic methods exist for this problem such as ICP Besl and McKay [15] based methods and TPS Bookstein [16] based methods like Andreasen Andresen and Nielsen [6], Paulsen and Hilger Paulsen and Hilger [121]. Recent publications within this field focussed on dffeomorphic warps see Cootes et al. [35]. The diffeomorphism ensures a one to one smooth mapping which is a very desirable property for registration between shapes since standard statistical methods can be applied. Several algorithms have recently been developed for both 2D and 3D images based on non rigid deformations some including diffeomorphisms, Cootes Cootes et al. [36],Rueckert Rueckert et al. [135] Rueckert et al. [136] and Moderzitski Modersitski [104]. Some of these methods also propose to build a 'warp' model rather than a shape model. This paper focuses on a point distribution model (PDM) as in Cootes and Taylor [30] since this is the parametrization of a triangulated surface. Most of the diffeomorphic warp methods have primarily been developed for images and not 2D manifolds embedded in 3D Euclidian space. By taking some of the concepts and adapting them to surface to surface correspondence and assuming that the rigid registration problem has been solved, see Darkner et al. Darkner et al. [38], this paper presents a non-rigid registration algorithm for 2D manifolds embedded in a 3D euclidian space.

11.3 Measuring the Error

The non-rigid registration problem is an optimization problem where an error measure has to be defined. As proposed by Tsai et al. [160] and formulated specifically for 2D manifolds in 3D euclidian space by Darkner et al. [38] we choose difference of distance maps as our error measure. Let A some volume in euclidian space and let S_a and S_b be to surfaces fully embedded and contained in A and let $F(x)$ be a function describing the distance maps of some surface x. We can then write the cost of the given configuration of S_a and S_b wrt. A as the following

$$f_{\text{cost}}(S_a, S_b) = \frac{1}{A} \int_A F(S_a) - F(S_b)\ d\Omega \tag{11.1}$$

giving a normalized difference for the distance maps of S_a and S_b over A. Integrating the difference of the two distance maps over the entire space results in either infinity or zero (for a perfect match) and A should therefor be finite making the integral finite. It is the value of this integral that we want to minimize. The discrete equivalent of $F(x)$ can be generated using various algorithms (e.g. fast marching Sethian [139], implicit surfaces Dinh et al. [47]) or other functions. We propose to sample the distance map at a finite number of locations in a box (the volume A) containing the zero levels sets of the two surfaces to be registered. A cost function based on this can then be formulated as follows. Let p_i be a point in a Euclidian space $p_i \in Q$ and let S be a surface embedded in Q so that $S \subset Q$. Let p_s be a point on the surface S hence $p_s \in S$. We then define the distance between p_i and S, $f_{\text{dist}}(p_i, S)$ as,

$$f_{\text{dist}}(p_i, S) = min(||p_i - p_s||^2)\ \forall p_s \in S. \tag{11.2}$$

The distance between two shapes S_1 and S_2 is then defined by the following. Given N points $P = p_1 \dots p_N$ the cost function $f_{\text{cost}}(S_1, S_2)$ is

$$f_{\text{cost}}(S_1, S_2) = \frac{1}{N} \sum_{i=1}^{N} ||f_{\text{dist}}(p_i, S_1) - f_{\text{dist}}(p_i, S_2)||^2. \tag{11.3}$$

In practice the N points are organized in a cubic grid with the same center as one of the shapes. We emphasize that other distances i.e. $|p_i - p_s|$ and $\sqrt{|(p_i - p_s)|}$ can be used in Eq.11.2 and other norms in Eq.11.3 such as:

$$f_{\text{cost}}(S_1, S_2) = \frac{1}{N} \sum_{i=1}^{N} sign \cdot \log(1 + |f_{\text{dist}}(p_i, S_1)|) - \log(1 + |f_{\text{dist}}(p_i, S_2)|). \tag{11.4}$$

where *sign* is the sign of $f_{\text{dist}}(p_i, S_1) - f_{\text{dist}}(p_i, S_2)$ which can be omitted if signed distances is not utilized. The *log* is a weighting of the coefficients in the

sense that if p_i is close to both surfaces the weight is normal, if it's close to only one surface the weight will be significant, but if p_i is far from both surfaces the weight will be very small. Further this weight emphasizes movement in the direction of the surface normals and hence minimizes the aperture problem.

11.4 Diffeomorphic Warp

The reason for using diffeomorphic warps is that the diffeomophic constraint ensures certain desirable properties. First of all it is a one to one mapping and the derivative of the mapping is also one to one. This ensures a smooth warp and that the space we warp does not fold onto itself. Furthermore, the composition of diffeomorphisms is a diffeomorphism it self. However, other types of warps could easily be applied such as thin plate splines or b-splines. Let $f(x|\phi_i)$ be a diffeomorphic mapping controlled by ϕ_i. Complex diffeomorphisms can then be constructed as a composition of simple diffeomorphisms. Complex diffemorphism consisting of several simple ones $f_1 f_2(x) == f_1(f_2(x))$ can then be written as:

$$f(x|\Phi) = f_1 f_2 \dots f_{n-1} f_n(x) \tag{11.5}$$

Shapes from different individuals are most likely not diffeomorphic to each other, but to avoid singularities we impose this criteria and assume that a one-to-one mapping does indeed exist.

11.4.1 The Warp

The warps used in this paper are splines i.e. a grid warp where all points between control points are interpolated using some basis function. By moving grid nodes (in this case control points) the warp displacement in the surrounding space is defined. The basis described by Cootes is formulated for use in 2D Cootes et al. [36], however, it is easily extended to 3D and for simplicity we will describe the 2D version here. For a point p with coordinates x, y within a grid cell with the corners a, b, c and d (see Fig. 11.1) where a has coordinates (i, j), b $(i, j+1)$, c $(i+1, j+1)$ and d $(i+1, j)$ the warp function yielding p' is defined as follows in 2D.

$$\begin{aligned} p'(x,y) = {} & k(x-i)k(y-j)a' + k(x-i)k(1+j-y)b' + \\ & k(1+i-x)k(y-j)d' + k(1+i-x)k(1+j-y)c' \end{aligned} \tag{11.6}$$

where $k(r)$ is a kernel function that describes the displacement of the surrounding space in relation to the 4 corners:

$$k(r) = (1 - r^2)^2 \tag{11.7}$$

$$k(r) = \frac{1 + \cos(\pi r)}{2} \tag{11.8}$$

where $0 < r < 1$ Cootes et al. [35]. For eq. 11.8 $r < \frac{1}{\pi}$ ensures diffeomorphism. The kernel in Eq. 11.8 has been used in the implementation for this paper.
It is straight forward to see the reason for the constraint imposed on the movement of the nodes since the constraint ensures that the cosine only maps to one value and satisfy the diffeomorphic property.

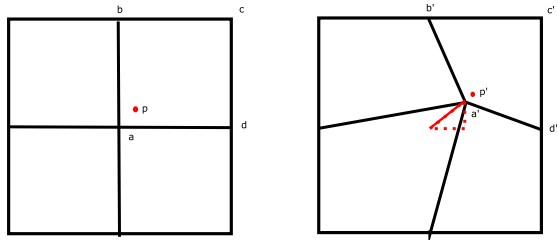

Figure 11.1: The principles of warp in 2D using Cootes framework .

11.5 Optimization

Having defined the warp we need some optimization and some cost to minimize. The cost function chosen is Eq.11.4 and the open surface tactic described in Darkner et al. [38]. By starting out with a coarse warp grid optimizing on this an d then using a progressively finer grid, a significant increase in computational speed is obtained.

11.5.1 Using The Inverse Compositional Algorithm

Moving one node at the time is a very time consuming and since we are minimizing under the ℓ_2-norm it is obvious to use a Gauss-Newton scheme. We propose to use the inverse compositional algorithm Baker and Matthews [10] but without the use of the estimate of the Hessian i.e setting it to the identity. The algorithm then becomes a simple gradient descend. The reason for leaving

out the Hessian is that the estimate is inaccurate and the inversion becomes unstable and the result unreliable. The basic idea behind the inverse compositional algorithm is to minimize:

$$\sum_x ||S_t(W(x;p)) - S_s(x)||^2 \tag{11.9}$$

where S_s is the source shape, S_t is the target shape and $S_t(W(x;p))$ is S_t warped with the parameters p. The algorithm we originally proposed by Lukas and Kanade Lucas and Kanade [101]. Say we have an estimate of p the new warp can then be written as

$$\sum_x ||S_t(W(x;p+\Delta p)) - S_s(x)||^2 \tag{11.10}$$

by doing a first order Taylor expansion of $S_t(W(x;p+\Delta p))$ we get

$$\sum_x ||S_t(W(x;p)) + \Delta S_t \frac{\partial W}{\partial p}\Delta p - S_s(x)||^2 \tag{11.11}$$

The partial derivative wrt. Δp is given by

$$\sum_x [\Delta S_t \frac{\partial W}{\partial p}]^t [S_t(W(x;p)) + \Delta S_t \frac{\partial W}{\partial p}\Delta p - S_s(x)] \tag{11.12}$$

Setting this equation to zero and solving for Δp gives

$$\Delta p = [[\Delta S_t \frac{\partial W}{\partial p}]^t [\Delta S_t \frac{\partial W}{\partial p}]]^{-1} \sum_x [\Delta S_t \frac{\partial W}{\partial p}]^t [S_s(x) - S_t(W(x;p))] \tag{11.13}$$

However, as it is obvious from Eq. 11.13 that both $\frac{\partial W}{\partial p}$ and ΔS_t has to be re-calculated for each iteration. A simple way of re-writing equation 11.10 is introduced by Baker And Matthews Baker and Matthews [10] . Since the warp we use is diffeomorphic every warp has an inverse and since the warp is just movements of control points. Then $W_1(\cdot, p_1) \circ W_2(\cdot, p_2)$ can be approximated by addition of the control points position of $W(\cdot, p_1 + p_2)$ for small values of p_1 and p_2. Eq. 11.10 now becomes:

$$\sum_x ||S_t(W(x;p)) - S_s(W(x;\Delta p))||^2 \tag{11.14}$$

giving us

$$\Delta p = [[\Delta S_s \frac{\partial W}{\partial p}]^t [\Delta S_s \frac{\partial W}{\partial p}]]^{-1} \sum_x [\Delta S_s \frac{\partial W}{\partial p}]^t [S_t(W(x;0)) - S_s(x)] \tag{11.15}$$

Using this approach one estimates the warp for the source but applies the inverse to the target. This way the Jacobian and the gradient become constant and can therefor be precalculated see (Baker and Matthews [10] for details). Let us set

$$H = [\Delta S_s \frac{\partial W}{\partial p}]^t [\Delta S_s \frac{\partial W}{\partial p}] \tag{11.16}$$

which is the Gauss-Newton estimate of the hessian. In our case this estimate is singular and since it only adjusts the length and direction of a step along the gradient we set H to be the identity matrix. This gives us the following gradient descend:

$$\Delta p = \mathbf{I} \sum_x [\Delta S_s \frac{\partial W}{\partial p}]^t [S_t(W(x;0)) - S_s(x)] \tag{11.17}$$

11.5.2 Properties of the Formulation

The chosen formulation of the cost function holds certain valuable properties which can rapidly increase the speed of the registration. By utilizing standard computer graphics algorithms and making some approximations, a very fast implementation can be made. The most important property of the distance map is the fact that the gradient of the distance map everywhere in space (where defined) is equal to minus the surface normal at the closest point on the surface. The best way to convince yourself is to imagine a sphere with center in the given point and then expanding it until it exactly touches the surface. In the point where the two meet the surface is exactly the tangent plane and hence the gradient of the distance map is exactly the normal of this tangent plane as illustrated in fig.11.2. Having realized this, the gradient of the entire space can be computed on the surface exactly and the accuracy does not depend on the spatial resolution but on the surface resolution only. Furthermore, the distance for any given point to the surface can be calculated on the fly. This is a very desirable property when using non linear deformations. When deforming the space, the distance map immediately becomes invalid and needs to be recalculated. Since this can be done on the fly, both the use of memory and computational power becomes highly optimized. Furthermore, the same argument is valid for the deformation. Since the only part of the deformation that is of interest is the one on the surface, only grid points or deformations in general that affects the surface, needs to be considered in the optimization scheme. These properties in practice reduces the problem from a 3D to a 2D (which is the dimension of the manifold). The information of the surface is then extrapolated into 3D space without adding significantly to the computational complexity of the registration. To limit the extrapolation a narrow band approach is used limiting the number of evaluation of the distance map etc. Normal registration uses around 1-2000 points but still, due to the basis

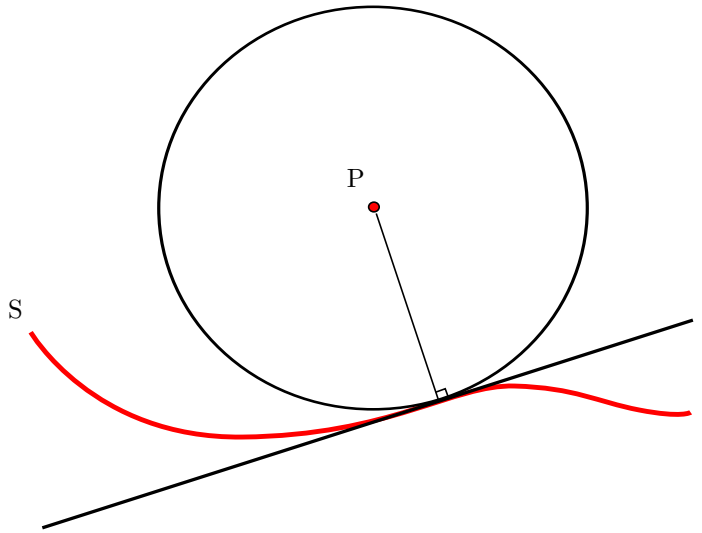

Figure 11.2: A 2D illustration of the properties of the distance map. As can be seen the distance map at point P has the same gradient as the closest point on the surface S. $\frac{\partial W}{\partial p}$ at P is how the deformation changes at P, but since only the surface is of interest we choose to keep the distances intact, hence the $\frac{\partial W}{\partial p}$ in P becomes the same as in the closes point on the surface.

functions of the transformation gives excellent results. Finally, this formulation detaches the cost function from the sampling of the surface allowing arbitrarily sampling of the distance map without any loss of performance. The performance is only dependent on the number of samples and the degrees of freedom of the deformation, thus, one can easily abandon the grid like sampling structure and choose any structure desired.

Evaluating the Jacobian and the Gradient So to sum it up: Working with surfaces the evaluation of the Jacobian of the warp wrt. the parameters i.e. $\frac{\partial W}{\partial p}$ and the gradient becomes very simple and sparse. In order to evaluate the Jacobian for a point q find the closest point on the surface and evaluate the Jacobian there. The same is valid for the gradient of the distance map. A good approximation of this is to use a KD-tree, a binary search tree to find the closest vertex and calculate the needed information there.

11.5.3 Computational Speedup

The most important reason for using the inverse compositional algorithm is to gain computational speed. The improvement is approx. a factor of 1.5 from compared to standard gradient descend with line search. The average registration time is around 1 min. pr shape depending on the number of vertices and faces in the shape. However, due to the fact that the hessian does not have to be formed the difference is rather small, and the only gain from the inverse compositional is that you only have to calculate the Jacobian of the warp and the gradient once at each level.

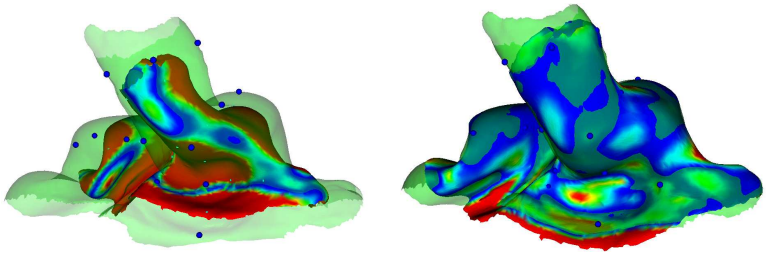

a *b*

Figure 11.3: a) The rigid registration b) The non-rigid registration

11.6 Computing the Correspondence

To compute the final registration it is assumed that the warp has brought the two surfaces on top of each other ($f_{cost} \approx 0$). By calculating the angle weighted normals Bærentzen and Aanæs [9] for all vertices of the shape not warped a direction of point to surface registration can be made. A dense point to surface correspondence can be obtained using standard ray tracing Whitted [169] and pruning. These algorithms execute in less than one second without approximations.

11.7 Results

The data set consists of 30 scannings of ear impressions taken from 21 male and 9 female subject. All impressions have been opened at the top and the

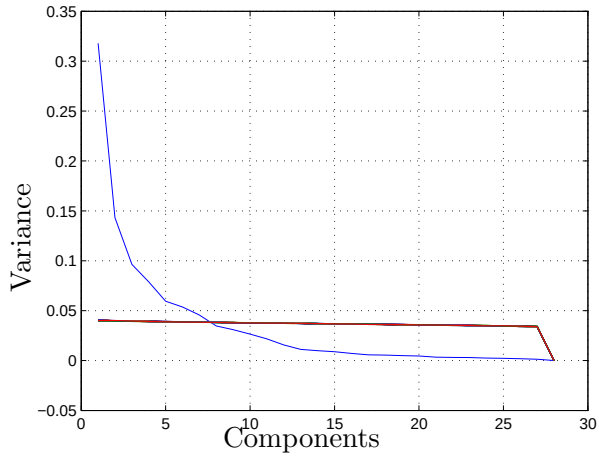

Figure 11.4: The outcome of Horns parallel analysis. The eigenvectors are sorted according to their normalized eigenvalues so that they sum to one. As can be seen the noise model (red line) and the eigenvalues intersect around the 8th eigenvalue.

bottom to remove artifacts that is not a part of the anatomy. The impressions are a part of a larger study in which the the dynamic behavior of the human ear canal is investigated. Several impressions have been taken from the same individual in different positions. However, in this paper we are only interested in the registration method itself so only the base line from the study is considered. To evaluate the registration algorithm we have build a shape model. Horns parallel analysis is employed to select the number of significant parameters of the PCA which turn out to be 8. Studying the eigenvalues also reveals that they rapidly decrease. Furthermore, the mean shape is smooth as well as the principal components which can be related to the observed variation. This can be seen in Fig. 11.5

The algorithm is very fast and executes as stated in around 1 min. for each pair of shapes on a laptop with 1.6 GHz intel centrino. Using a multicore PC it is expected that the registration of 100 surfaces will take less than 30 min.

11.8 Conclusion

A fast algorithm for 3D non-rigid surface registration has been presented. It offers a way of registering surfaces to each other and is independent of the sampling of the surface. The results of the registration show that the algorithm

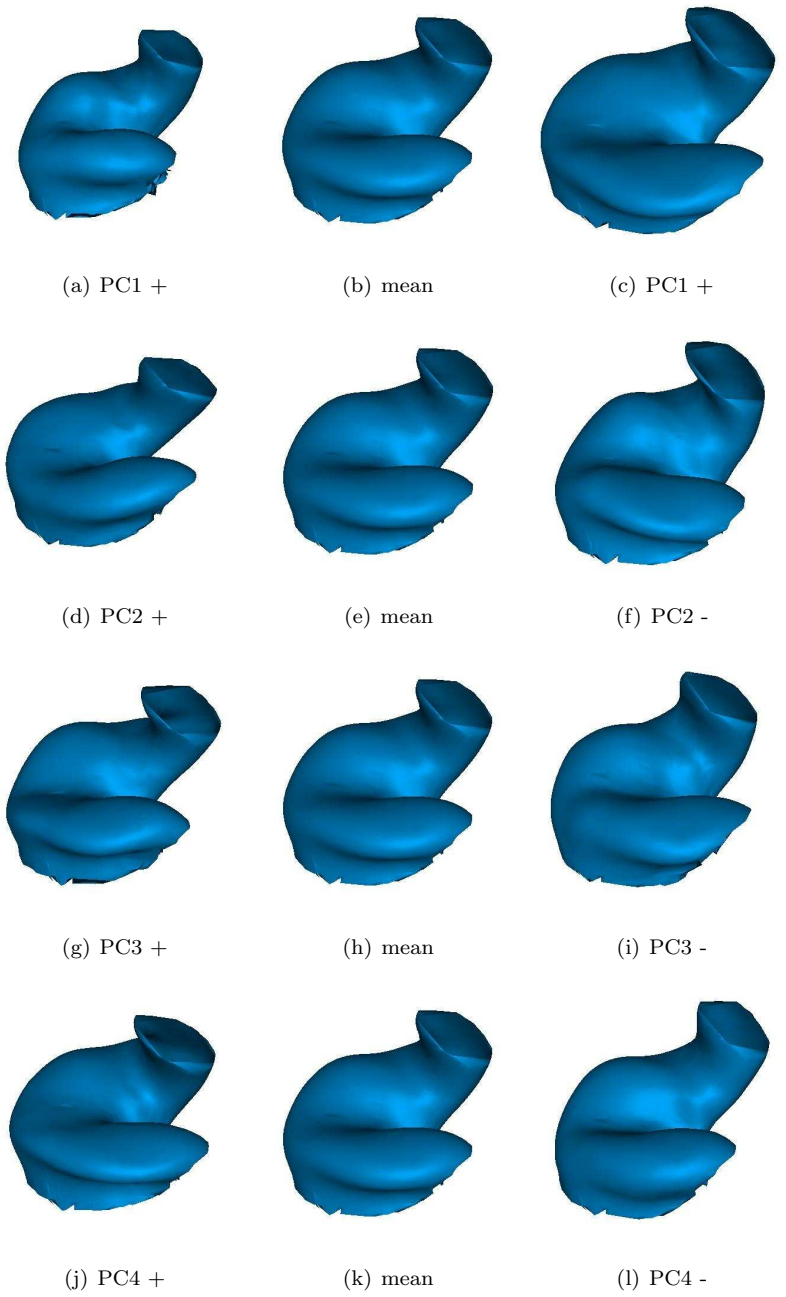

(a) PC1 + (b) mean (c) PC1 +

(d) PC2 + (e) mean (f) PC2 -

(g) PC3 + (h) mean (i) PC3 -

(j) PC4 + (k) mean (l) PC4 -

Figure 11.5: The Mean shape of the model and the first 4 eigenshapes.

is reliable. The usage of the inverse compositional algorithm gives some speedup, but one could easily use a standard gradient descend or Newton-scheme without significant loss in performance. The formulation of the cost function opens the door to computer graphics algorithms that within the past 20 years continuously has been improved wrt. speed and are well tested. This in combination creates the foundation for algorithms that reduces the memory usage and the amount of calculations needed.

Chapter 12

Robust Registration for Change Detection

Sune Darkner, Dan Witzner Hansen, Rasmus R. Paulsen, Rasmus Larsen

Abstract

We address the problem of intra-subject registration for change detection. The goal is to separate stationary and changing subsets to be able to robustly perform rigid registration on the stationary subsets and thus improve the subsequent change detection. An iterative approach using a hybrid of parametric and non-parametric statistics is presented. The method uses non-parametric clustering and large scale hypothesis testing with estimation of the empirical null hypothesis. The method is successfully applied to 3D surface scans of human ear impressions containing true changes as well as data with synthesized changes. It is shown that the method improves registration and is capable of reducing the difference between registration using different norms.

12.1 Introduction

Registration is the problem of determining the optimal geometric mapping of corresponding sets. Intra-subject registration includes time studies such as growth and pathology developments. These problems are characterized by examining differences between observations from the same subject where both changing and stationary regions may be present. Using rigid methods for intra-subject registration may cause misalignments as the norm is imposed simultaneously on both changing and stationary subsets. Consequently, the overall registration is influenced by the magnitudes of the local changes and vice versa, causing false change detection. A correct separation of changing and stationary subsets is crucial for correct change detection. The chosen norm influences the optimization procedure and is often dictated by computational efficiency, however, the distribution of registration vectors may reveal trends (exemplars) in the registration, which can be used for minimizing the influence of the norm and reveal the changes. This distribution is a priori unknown, but properties of particular local trends may be known. Exemplars indicate subsets of registrations under the same transformations and are located at local peaks in the registration density.

A method for separating changing and stationary regions is presented. The method incorporates knowledge of the local distribution using both parametric and non-parametric robust statistics to reduce the influence of the chosen norm. The method is detailed in section 12.3 and in section 12.4 the effectiveness of the method is demonstrated on 3D surface registration of ear impressions scannings with both true deformation caused by jaw movement and synthesized (with known) deformations. Finally, it is shown that the method provides an estimate of the nonrigid registration error with confidence bounds for the stationary regions.

12.2 Previous Work

Registration is an important research topics within image analysis, medical applications and geoinformatics Andresen and Nielsen [6], Fisher et al. [57], Modersitski [104], Paulsen and Hilger [121], Tolt et al. [159] and forms the foundation for for further analysis. Registration is an ill posed problem and as a consequence several semi-automatic and fully-automatic methods aimed at specific problems have been proposed (see Moderzitski Modersitski [104] for an overview). A variety of methods consists of a rigid and a non-rigid registration letting the rigid registration form the basis for non-rigid registration Rueckert et al. [135].

Diffeomorphic warps have gained some interest and have been applied to both 2D and 3D images as well as surfaces Cootes et al. [35, 36], Modersitski [104]. A combined approach for rigid and non rigid registration has been suggested based on the level set formulation Overgaard and Solem [118]. Registration for change detection is a well known issue within geoinformatics Tolt et al. [159] where changes in satellite images are tracked. Application to medical images as well as the issue of outlier detection in image registration have been proposed by Fisher et al. [57].

12.3 Method

This section presents an overview of the proposed method. Registration of point configurations C_1 and C_2 is a mapping T, which in turn, is defined as the concatenation of a rigid and a non-rigid registration functions T_1 and T_2 respectively. An overall optimized registration is obtained at the expense of exact registration of the stationary regions. A registration induces a distribution of displacements vectors. The underlying distribution function of displacements is a priori unknown and multi modal and it is through this we seek to separate changing and stationary regions. It is assumed that only measurement noise influences the registration on stationary regions. A fair assumption is therefore to assume identically independent distributed (i.i.d.) registration vectors for the stationary regions.

Non-parametric methods are useful when little information about the distribution is available, alas less obvious is how to incorporate local information in these methods. We employ non-parametric mean shift clustering (section 12.3.1) for exemplar localization. With the above assumptions the exemplar representing the registration of the stationary regions follows a well known distribution, however, the cluster of interest may contain outliers. The remaining outliers can be removed using the null hypothesis of the underlying distribution of inliers and considering the empirical distribution. Parametric methods require knowledge of the underlying model (such as the number of Gaussians in Gaussian mixture models). Using the assumption of a locally Gaussian distributed stationary subset, a parametric method is employed which additionally provides an estimate registration error and confidence bounds. Even though a theoretical distribution is assumed, the empirical data may deviate from this. Large scale hypothesis tests (section 12.3.2) are used to account for such cases and to separate inliers from outliers as well as providing error estimates and confidence boundsEfron [52]. In the experiments a distance map-based rigid registration and a diffeomorphic grid warping applied to distance maps for non-rigid registration Darkner et al. [40] is employed. Notice, the framework is not specific to

any particular registration method.

12.3.1 Mean Shift Clustering

Mean shift is a non-parametric kernel density estimation method proposed by Fukunaga and Hostetler [61] and for feature space analysis and tracking Comaniciu et al. [24, 25]. Given n observations in a d-dimensional space $x_i, i = 1 \dots n$, the multivariate kernel density estimator with kernel K is defined as:

$$\hat{f}(x) = \frac{1}{nh^2} \sum_{i=1}^{n} K(\frac{x - x_i}{h}) \tag{12.1}$$

The mean shift vector:

$$m_{h,g}(x) = \left[\frac{\sum_{i=1}^{n} x_i g\left(\left\| \frac{x-x_i}{h} \right\|^2 \right)}{\sum_{i=1}^{n} g\left(\left\| \frac{x-x_i}{h} \right\|^2 \right)} - x \right] \tag{12.2}$$

where g is the negative derivative of K and the kernel size h, describing the gradient of the kernel density and thus the modes of the distribution can be found iteratively through the mean shift vector.

Clustering in the distribution correspond to the $m < n$ basins of attraction when initializing mean shift at each observation. The method is very attractive since it requires no prior information of the number of clusters or any assumptions of the underlying density distribution. We use mean shift clustering on deformation vectors (3D - direction and length) to detect outliers and find trends in the distribution. Assuming the initial registration is a reasonably good approximation of the true registration, the deformation vectors of the stationary points will be close to the origin and thus easily identifiable. Clusters with insignificant support are disregarded.

12.3.2 Large Scale Hypothesis Testing

The usual point of large-scale testing is to identify a small percentage of interesting cases that deserve further investigation using parametric modelling. The problem is that a part of the interesting cases may be extracted, but if

more are wanted then also an unacceptably many false discoveries Efron [52]. A major point of employing large-scale estimation methods is that they facilitate the estimation of the empirical null density rather than using the theoretical density. The empirical null may be considerably more dispersed than the usual theoretical null distribution. Besides from the selection of the non-null cases (the selection problem) large-scale testing also provides information of measuring the effectiveness of the test procedure (estimation problem). In this paper we employ both measures to improve registration.

Simultaneous hypothesis testing is founded on a set of N null hypotheses $\{H_i\}_{i=1}^N$ and test statistics which are possibly not independent. $\{Y_i\}_{i=1}^N$ and their associated p -values $\{P_i\}_{i=1}^N$ defining how strongly the observed value of Y_i contradicts H_i.

In this paper we assume the N cases are divided into two classes, Null (stationary) and non-null (changing) occurring with prior probabilities p_0 and $p_1 = 1 - p_0$. Denote the density of the test statistics given its class $f_0(z)$ and $f_1(z)$ (null or non-null respectively). False discovery rate methods are central to some large scale method and is employed here. It is typical to consider the actual distribution as a mixture of outcomes under the null and alternative hypotheses. Assumptions about the alternative hypothesis may be required. The sub-densities $f_0^+(z) = p_0 f_0(z), f_1^+(z) = p_1 f_1(z)$ and mixture density $f(z) = f_0^+(z) + f_1^+(z)$ leads directly to the local false discovery rate: $fdr(z) \equiv P(null|z_i = z) = p_0 f_0(z)/f(z) = f_0^+(z)/f(z)$. The false discovery rate describes the expected proportion of false positive results among all rejected null hypotheses and guarantees that the fraction of the number of false positives over the number of tests in which the null hypothesis was rejected Efron [52]. Figure 12.1 illustrates the fundamentals of the approach.

For registration purposes the hypothesis test is used to find variables of the observations that deviates significantly from the average registration. We use large-scale testing to estimate the empirical null hypothesis for a given subject. We use the deformation field of length and orientation vectors to perform the hypothesis test of the assumed stationary exemplar obtained through mean shift. The vertices to be included in the rigid registration in the subsequent iteration are determined through the fdr. The distribution of squared lengths follow a $\sigma\chi(3)$ distribution, assuming i.i.d. normal distributions of the elements of the deformation vector as mentioned for the stationary regions. Impressions of the stationary regions only change up to measurements noise and thus a fair assumption is that the distribution of registration lengths in the stationary part is as such i.e. if H_i is exactly true and thus it is convenient to consider $z_i = \Phi^{-1}(P_i), \quad i = 1 \ldots N$ where Φ is the standard normal c.d.f and $z_i|h_i \sim N(0,1)$. Estimates of the non-rigid registration error and confidence bounds can be mapped back to the distribution of deformation vectors through Φ

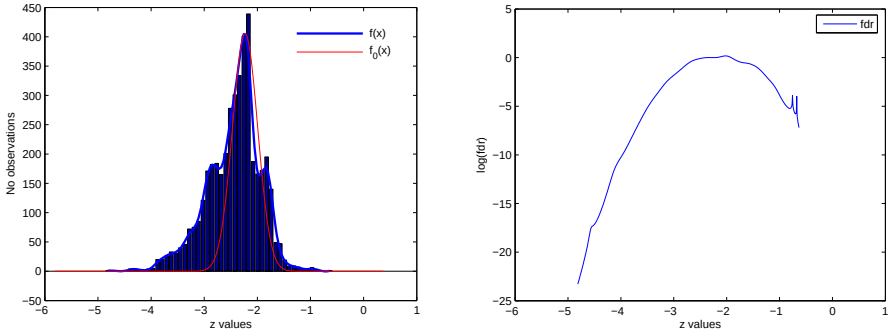

(a) mapped histogram (b) false discovery rate

Figure 12.1: a) The distribution of registration vector lengths with the mixture density (red) and empirical null distribution (blue). b) The false discovery rate. Inliers can be selected based on the desired probability of selecting false discoveries without overly modelling the null distribution.

12.4 Experiments

In the following, the experiments of applying the method on both synthesized and real data are presented. In addition we test with both L_1 and L_2 norms on the synthetic data to show how the difference of using different norms i minimized. The error measure is the point-to-surface distance in the normal direction. Synthesized data is used to validate the method on known deformations.

Data set The data set consists of 50 ear impression scans of 25 individuals. Two impressions are taken from each subject, one with open mouth (using a mouth prop) and one with closed mouth. To ensure consistency, all impressions are made by the same audiologist and scanned on a 3D laser scanner by the same operator. Each scan consists of 8,000-12,000 points depending on the size of the impression.Fig. 12.2 labels the prominent features of the ear. The outer ear is primarily situated upon soft tissue that deforms with jaw motion. However, the concha cymba is situated on a bony part of the skull called the mastoid. This part of the ear is much less prone to deformations and displacements than the rest of the ear. The part of the impression around and between the first and the second bend is expected to change the most. It is observed that the change occurring in this region varies significantly (0.2 - 2.3 mm.) among individuals Darkner et al. [40]. The synthetic data is a surface scanning where the surface

has been manually deformed. This why there is full control over which part of the data differs and and which part does not and how much of the surface is deformed.

Figure 12.2: (Left) A typical scanning of an ear impression with anatomical features labelled. (Right) Registration errors projected onto the surface. The color indicates the magnitude.

Experiments on Clinical Data Fig. 12.3 shows a typical progress of the method. The colors on the surface depicts the magnitude of the error, showing a clear improvement over a few iterations. The registration error of the Cymba Concha is significantly reduced leaving a more correct analysis of the true deformations confirming recent observations Darkner et al. [40]. The difference in errors between registration using L_1 and L_2 norms is reduced by 1/4 after one iteration of the method. Similar results are found on synthetic data (Fig. 12.5).

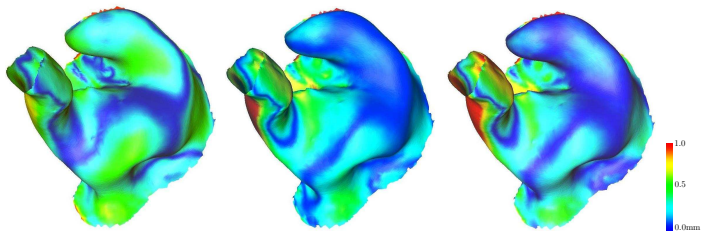

(a) 1 iteration (b) 2nd iteration (c) 5th iteration

Figure 12.3: (*a*) The initial registration. The result after the first iteration (b) and after 5 iterations (c) .

The changes in the registration seen in Fig .12.3 and in Fig. 12.4 corresponds well to what is expected after careful studies of the anatomy. The deformation that

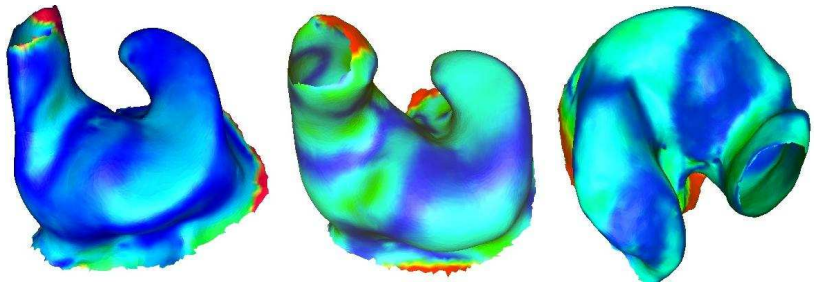

(a) (b) (c)

First initial registration

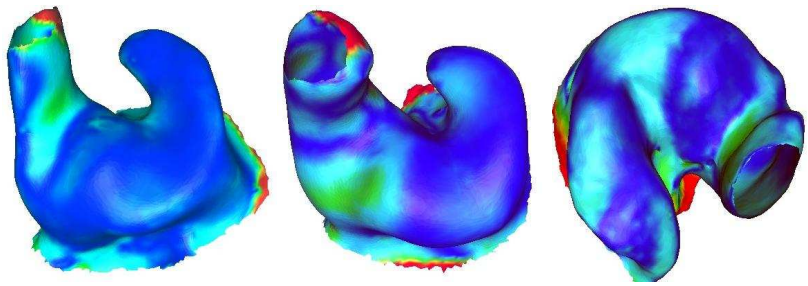

(d) (e) (f)

After application of the proposed method

Figure 12.4: The top row is after normal rigid registration. The bottom row is after 1-2 iterations with the proposed method. The observations are paired column wise.

occur in the canal is emphasized and the concha itself is fitted more precise. This is expected due to the fact that the first part of the canal is surrounded by soft tissue and is located very close to the mandible, the source of the deformation. The concha itself is made from cartilage and is partially situated on bone and should therefore only deform slightly. However, what can also be seen is that the concha do deform and this will, in most cases, cause the hypothesis of stationary regions to be an approximation, but one we believe holds. In general, the changes are emphasized and the stationary regions are registered better. This of cause comes at a cost. In the case where everything changes ie. no stationary subset is present, this method will emphasize large deformation an suppress small changes. The method should therefor be used with care. In the case of the ear impressions, we are mostly interested in the relative changes in the canal with Concha as a reference and the method is well suited for this purpose.

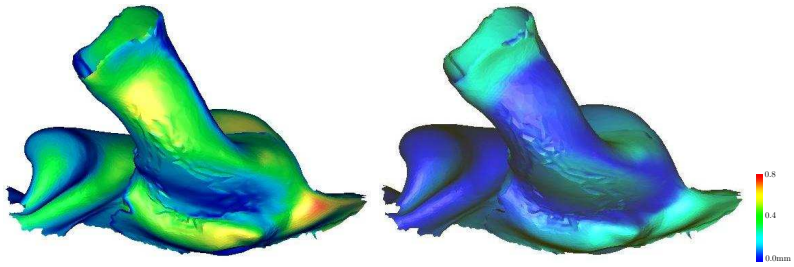

Figure 12.5: (Left) The difference on synthetic data applying L_1 and L_2 norms. The maximal difference is 0.78 mm and the average is 0.24 mm. (Right) The difference on synthetic data applying L_1 and L_2 using the proposed method using 4 iterations. The average distance is 0.06 mm and the largest is 0.27 mm - an 3-4 times improvement with the proposed method.

Experiments on Synthesized data The method is tested on 3 impression pairs with synthesized changes to know ground truth. Synthetic data is created by taking an impression scan and deforming it locally on one or two locations. A total of 35% of the vertices are changed and may be deformed as much as has 3 mm, corresponding to highly deformed impressions. One scan deforms the ear canal 1 mm in the area of the first and second bend. The same impression is used for the second case, but additionally the Cavum Concha is deformed 1 mm. In the third test case, the Tragus and Canal is deformed non-linearly up to 3 mm. Fig. 12.6 shows the error of the registration on the synthesized data (case 3). The results show a significant improvement regardless of the minimization norm. In both cases the registration is close to ground truth. The error prior to applying our method using the L_1 norm is on average 0.12 mm and maximally is 0.52 mm. Using the L_2 norm the error is 0.37 mm on average and 1.31 mm maximally. After the first iteration the L_1 norm is reduced to 0.01 mm on average and maximally 0.04 mm. The results with the L_2-norm yields an error of 0.23 mm maximally and on average 0.05 mm.

Experiments with both L_1 and $L2$ norms in test cases 1 and 2, yield a maximum error less than 0.004 mm. Thus the proposed method reduces the effects of the chosen norm significantly (Fig. 12.5). The cause of their difference is that the L_2 norm heavily weights outliers even though the methods employed should discard these. Both the mean shift and the hypothesis test (c.f. fdr) will allow some outliers to be classified as inliers. Convergence with the L_1 norm is usually faster and usually produce a better initial guess.

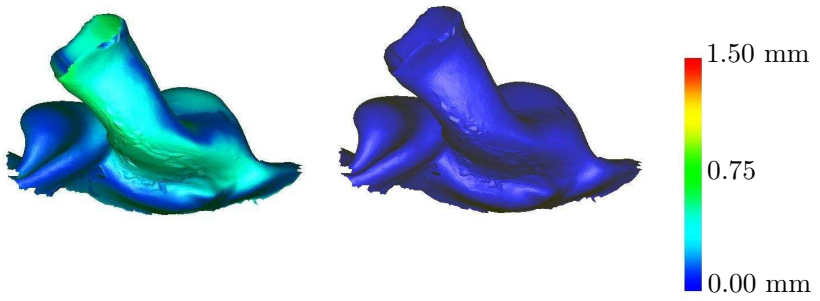

(a) ℓ_1 initial (b) ℓ_1 after 4 iterations

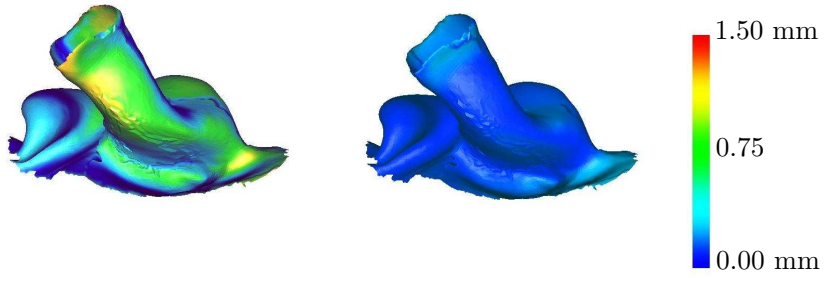

(d) ℓ_1 initial (e) ℓ_2 after 4 iterations

Figure 12.6: Validation on synthetic data. From the left the initial registration using L_1 compared to the truth. The result after 4 iterations (L_1). The initial registration using L_2 compared to the truth. The result after 4 iterations (L_2)

Discussion Computational speed is an issue when dealing with registration and since the method is dependent on several iterations registration speed is essential. The full surface registration used here takes 2-3 minutes and it is shown that a similar speedup can be achieved for 3D volume data Vester-Christensen et al. [164]. Since the outer ear is primary cartilage, local deformation will to some extend affect the rest of the outer ear. Consequently, points considered stationary may in fact be slightly deformed. We therefore believe that the method is applicable to other change studies. Finally, we mention that for impressions with small changes this method will have little or no additional effect.

12.5 Conclusion

We have proposed a method for robust intra-subject registration using a hybrid of parametric and non-parametric density models. Mean shift and large scale hypothesis testing are employed for locating stationary regions. The method is in principle independent of the registration method and modality.

We have successfully applied the method on both synthesized and clinical ear impression data and have shown that the method improves registration for change detection significantly. The method reduces the sensitivity to the choice of minimization norm. The results on clinical data are in full correspondence with anatomical observations and use the Cymba Concha for rigid registration. This lead us to conclude that the method is capable of finding stationary parts and let these parts guide the rigid registration. Other methods for clustering and hypothesis testing (one-class classification) may produces similar results and could be of interest for other applications. Since the method can locate stationary areas, we have reduced the need for manual guidance of the registration for change detection.

Chapter 13

Classification in Longitudinal Studies

Data Driven Constraints for the Support Vector Machine

Line Clemmensen, Sune Darkner

Abstract

Motivated by knowledge embedded in the structure of data, extensions of the well known support vector machine (SVM) are presented. Classification in longitudinal studies holds knowledge of the pairing of observations, which is not always exploited when modelling the development of a specific condition. This paper examines change in the shape of the ear canal caused by movement of the mandible. A classification method for paired observations in high dimensions is developed. The method imposes a constraint, demanding orthogonality of the vectors between paired observations and the estimated hyper plane in order to obtain more robust solutions. This is useful in a variety of medical studies where the same patient is observed at several stages, such as before and after treatment. The knowledge is embedded directly in the SVM model which gives additional information about the difference from one stage to another. The primal and dual optimization problems are derived and extended to kernel space for the general

case of adding data specific constraints to the SVM, and the usage of kernels under the ℓ_1-norm approximation is discussed. It is shown that the constrained SVM under the ℓ_2-norm generalizes to a linear kernel. Imposing the constraint of orthogonality on the paired data is more robust, compared to the standard SVM, as the results have highly reduced variance and the misclassification rates are slightly improved. The effects of applying the constraint of orthogonality are illustrated on simulated data as well as a high-dimensional paired data set of ear canal surfaces.

13.1 Introduction

In some cases the data to be analyzed have more information than what seems apparent. The structure of the data or the way the data is collected often contains information of covariances in feature space or a more direct linkage between observations. An additional constraint to the SVM can be used to obtain a solution that takes such prior knowledge into account. A general framework for adding constraints based directly on the data to the SVM in the primal formulation is presented. The dual formulation is derived from the generalized primal formulation with constraints and hereby both classification and regression is extended to a non-linear kernel space. It is shown for a general constraint based directly on data that selecting the appropriate formulation the constraint can be formulated as inner products, and therefore the kernel trick M. Aizerman and Rozonoer [102] can be applied to its dual. Specifically, for paired observations a constraint is presented that enforces orthogonality of the vectors spanned by paired observations and the estimated hyperplane.

This paper examines shape differences of ear canals. Ear canals deform slightly with the movement of the mandible. This deformation occurs when chewing or making similar movements and in some cases leads to discomfort when the individual wears hearing aids. It is therefore of interest to characterize such deformations in general. Additionally, it is not always known if an impression taken from an ear comes from an individual with open or closed mouth and it is therefore also desirable to be able classify the shapes into open and closed mouth.

The SVM is a well known method for classification within pattern recognition and is widely used for classification and regression. The method is closely related to Tikhonov regularization Tikhonov [158] for regression and offers a vast general regularization of the solution. However, knowledge embedded in feature space or in the data, such as pairing, is not included in the model. It is proposed to include such constraints for specific data structures such as paired data. The additional constraints are introduced to the quadratic programming (QP)

problem in order to use information from the physical properties of the data to regularize in particular high dimensional problems and thereby exploit crucial a priori information and reduce effects due to the curse of dimensionality in $p \gg n$ problems [1] Hastie et al. [76].

Recently, the SVM was extended to use an ℓ_1-norm instead of an ℓ_2-norm Li et al. [98], and to include both norms as in the elastic net formulation Wang et al. [165]. The additional constraints added here are based directly on data and therefore introduces additional information to the previous methods and on top of that the kernel trick is straightforward to apply. In particular, when observations are paired as e.g. in several medical studies it is considered adding a constraint that enforces orthogonality between the separating hyperplane and the vectors spanned by the paired observations in two groups. Adding this constraint reduces the variance of the model by introducing a bias. It will be shown that when such a pairing of data exists the bias/variance trade off ensures more robust results while the classification error is statistically comparable or slightly better compared to that of ordinary SVM.

In addition to classification into two groups it is also of interest, in particular with paired data, to find the direction which describes the difference between the two classes. This direction is given implicitly by the SVM framework as the normal vector to the separating hyperplane, and has been described in detail in Golland [64].

In the following some of the previous work on the support vector machine will briefly summarized, the addition of the data driven constraints to the SVM will be described, its performance on simulated data as well as real data for the orthogonality constraint on paired data will be illustrated. Finally, the paper is summed up with a discussion.

13.2 Summary of Previous Work on the SVM

The SVM was introduced in Boser et al. [17]. The SVM builds on theory for the optimal separating hyperplane developed by Vapnik and Chervonenkis in 1965 Vapnik [163] but constructs the hyperplane in a kernel feature space, and therefore the feature space does not have to be in explicit form. SVMs are most known for their use in classification problems but other uses such as regression has been proposed Hastie et al. [76], Shawe-Taylor and Cristianini [140]. The

[1] p is the number of features and n the number of variables

SVM is in its simplest form defined as the separating hyperplane given by:

$$\boldsymbol{y} = \boldsymbol{\beta}^t \mathbf{x} + \boldsymbol{\beta}_0 \tag{13.1}$$

where t denotes the transpose and y_i is coded according to the class of $\mathbf{x}_i$: $\{-1, 1\}$. The SVM maximizes the distance between the observations defining the boundary of the two classes. Since the groups are not always separable, slack variables ξ_i are introduced to allow for misclassification. Figure 13.1 illustrates the SVM. We use the following formulation of the minimization problem

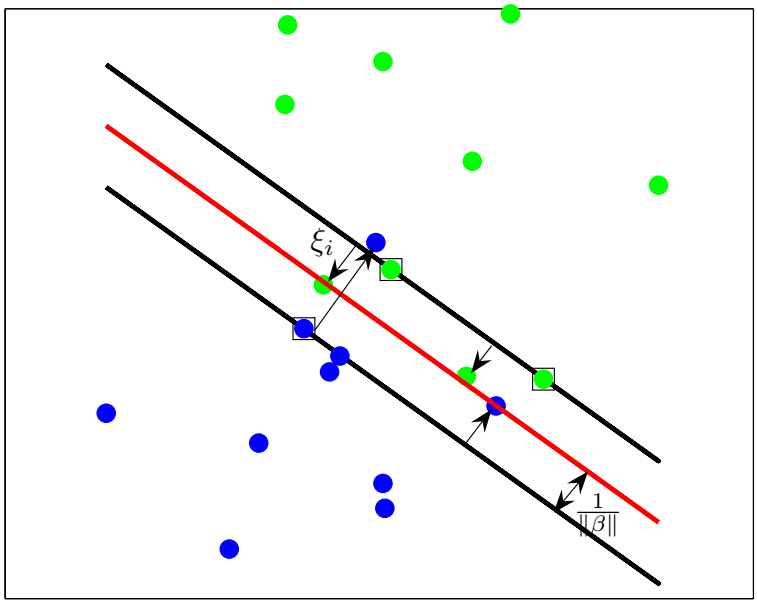

Figure 13.1: Geometry of the SVM. The decision boundary separates the two classes and the margin of total width $\frac{2}{\|\beta\|}$ is created. Each point inside the margin is associated with a slack variable ξ_i, the single arrows illustrates the slack variables. The margin is maximized while keeping the sum of the slack variables under some constant. The points marked with squares are support vectors which lie on the margin.

$$\begin{aligned} &\min \|\boldsymbol{\beta}\|^2 + \gamma \sum_{i=1}^{n} \xi_i \\ &\text{subject} \quad \text{to}: \quad y_i(\mathbf{x}_i^t \boldsymbol{\beta} + \beta_0) \geq 1 - \xi_i, \quad \xi_i \geq 0 \quad \forall i \quad , \end{aligned} \tag{13.2}$$

where γ is a constant. In the case where the number of variables p is the same or larger than the number of observations n the SVM suffers from instability issues due to the curse of dimensionality Hastie et al. [76]. However, by reformulating the problem to its Lagrange dual Vapnik [163] the solution can be found in the

n-dimensional space like in ridge regression Hoerl and Kennard [80] to which the regression problem easily can be reformulated Hastie et al. [76], Shawe-Taylor and Cristianini [140]. The SVM for regression has been modified earlier to embrace the LASSO constraint for regression Li et al. [98] but has in this form not been generalized to classification, different loss functions of the residual Hastie et al. [76], or the doubly SVM as a classification version of the elastic net regression Wang et al. [165], Zou and Hastie [173].

Finally, Golland [64] originally defined a discriminative direction to be the direction which moves a point towards the other class while introducing as little irrelevant change as possible with respect to the classifier function. This idea is used to visualize the discriminative direction in the original space of the shape models and additionally use the physical properties of data to obtain a variance reduction in the classifier function.

13.3 Methodology

First a general framework for adding data driven constraints to the SVM will be derive both with ℓ_1-norm and ℓ_2-norm penalty. The ℓ_2-norm gives more weight to outliers than the ℓ_1-norm. Section 13.3.1 and 13.3.2 add a regularization term to the formulation for the ℓ_1-norm approximation and ℓ_2-norm, respectively including the derivation of the dual formulation of the minimization problem to show how and when the kernel trick can be applied in the formulations. The third section discusses the added constraint in general whereas section 13.4 introduces the constraint of orthogonality added for data with paired observations.

13.3.1 ℓ_1-norm Constraint

The ℓ_1-norm does not punish outliers as heavily as the ℓ_2-norm and in many cases when the constraint depends on data and we want to regularize according to the trend and not according to outliers it is a more appropriate choice than the ℓ_2-norm. The SVM is formulated with an ℓ_1-norm of $\boldsymbol{\beta}\mathbf{A}$ added $\|\boldsymbol{\beta}^t\mathbf{A}\|_1$, where $\mathbf{A}$ is a $p \times m$ matrix. However, since the ℓ_1-norm is not differentiable at zero the problem must be modified to avoid this singularity. Here, the ℓ_1 is approximated by letting $\boldsymbol{\delta} \geq \boldsymbol{\beta}\mathbf{A} \geq -\boldsymbol{\delta}$ and then minimizing with respect to δ. This approximation furthermore gives a suitable formulation of the dual problem and ensures, as we see later, that the kernel trick can be applied. The

primal SVM problem with added constraint is

$$\min \frac{1}{2}\|\boldsymbol{\beta}\|^2 + \gamma \sum_{i=1}^{n} \xi_i + \lambda \sum_{k=1}^{m} \delta_k \tag{13.3}$$
$$\text{s.t.} \left\{ \begin{array}{l} -\delta_k \leq \boldsymbol{\beta}^t \mathbf{a}_k, \quad \delta_k \geq \boldsymbol{\beta}^t \mathbf{a}_k \quad \forall k \\ y_i(\mathbf{x}_i^t \boldsymbol{\beta} + \beta_0) \geq 1 - \xi_i, \quad \xi_i \geq 0 \quad \forall i \end{array} \right.$$

The Lagrange primal can then be written as

$$\begin{aligned} L_P &= \frac{1}{2}\|\boldsymbol{\beta}\|^2 + \gamma \sum_{i=1}^{n} \xi_i + \lambda \sum_{k=1}^{m} \delta_k - \sum_{k=1}^{m} \rho_k(\boldsymbol{\beta}^t \mathbf{a}_k + \delta_k) + \sum_{k=1}^{m} \rho'_k(\boldsymbol{\beta}^t \mathbf{a}_k - \delta_k) \\ &\quad - \sum_{i=1}^{n} \alpha_i[y_i(\mathbf{x}_i^t \boldsymbol{\beta} + \beta_0) - (1 - \xi_i)] - \sum_{i=1}^{n} \mu_i \xi_i \end{aligned} \tag{13.4}$$

Differentiating L_P with respect to $\boldsymbol{\beta}$, β_0, ξ_i, δ_k and δ'_k and equating to zero, the following is obtained

$$\boldsymbol{\beta} = \sum_{i=1}^{n} \alpha_i y_i \mathbf{x}_i + \sum_{k=1}^{m} \rho_k \mathbf{a}_k - \sum_{k=1}^{m} \rho'_k \mathbf{a}_k \tag{13.5}$$
$$0 = \sum_{i=1}^{n} \alpha_i y_i \tag{13.6}$$
$$\alpha_i = \gamma - \mu_i \tag{13.7}$$
$$0 = \lambda - \rho_k - \rho'_k \tag{13.8}$$

as well as the positive constraints $\alpha_i, \mu_i, \xi_i \geq 0 \ \forall i$ and $\rho_k, \rho'_k, \delta_k \geq 0 \ \forall k$. By insertion of by (13.6),(13.7) and (13.8) in (13.4) we get the dual objective function

$$\begin{aligned} L_D &= \sum_{i=1}^{n} \alpha_i - \frac{1}{2} \sum_{i=1}^{n} \sum_{j=1}^{n} \alpha_i \alpha_j y_i y_j \mathbf{x}_i^t \mathbf{x}_j - \sum_{k=1}^{m} \sum_{i=1}^{n} \alpha_i y_i (\rho'_k - \rho_k) \mathbf{x}_i^t \mathbf{a}_k \\ &\quad - \frac{1}{2} \sum_{k=1}^{m} \sum_{l=1}^{m} (\rho'_k - \rho_k)(\rho'_l - \rho_l) \mathbf{a}_k^t \mathbf{a}_l \end{aligned} \tag{13.9}$$

Maximizing L_D subject to $0 \leq \alpha_i \leq \gamma$, $\sum_{i=1}^{n} \alpha_i y_i = 0$ and $\rho'_k + \rho_k = \lambda$ yield the desired result. Additional to (13.5)-(13.8) the Karush-Kuhn-Tucker (KKT) conditions Karush [91] are given as:

$$\rho_k(\boldsymbol{\beta}^t \mathbf{a}_k + \delta_k) = 0, \quad \rho'_k(\boldsymbol{\beta}^t \mathbf{a}_k - \delta_k) = 0 \quad \forall k \quad . \tag{13.10}$$

The hyper plane is written as

$$f(\mathbf{x}) = \sum_{i=1}^{n} \alpha_i y_i \mathbf{x}^t \mathbf{x}_i + \sum_{k=1}^{m} (\rho'_k - \rho_k) \mathbf{x}^t \mathbf{a}_k \quad . \tag{13.11}$$

Since kernels are applicable to all inner products of the input space $\mathbf{x}$, the feature space of the kernel $\phi(\mathbf{x})$ must be explicitly known or $\mathbf{A}$ must be defined as a function of the input space $\mathbf{x}$, $\mathbf{A} = \mathbf{XB}$, where $\mathbf{X}$ is a matrix representing all observations. When the constraint on $\boldsymbol{\beta}$ is not a function of $\mathbf{x}$ it is desirable to know the feature space explicitly in order to add a meaningful constraint. The the choice of $\mathbf{A}$ will be addressed in the following sections.

A special case is when $\mathbf{A} = \mathbf{I}$; this corresponds to an elastic net formulation Wang et al. [165], Zou and Hastie [173] where both the Ridge (ℓ_2-norm Hoerl and Kennard [80]) and the LASSO (ℓ_1-norm Tibshirani [156]) constraints are added.

13.3.2 ℓ_2-norm Constraint

The addition of the constraint on $\boldsymbol{\beta}$ under the ℓ_2-norm $\|\boldsymbol{\beta}^t\mathbf{A}\|_2^2$ is derived. This can is formulated as the following minimization problem

$$\begin{aligned} &\min \frac{1}{2}\|\boldsymbol{\beta}\|^2 + \gamma\sum_{i=1}^{n}\xi_i + \frac{\lambda}{2}\|\boldsymbol{\beta}^t\mathbf{A}\|_2^2 \\ &\text{s.t.} \quad y_i(\mathbf{x}_i^t\boldsymbol{\beta} + \beta_0) \geq 1 - \xi_i, \quad \xi_i \geq 0 \quad \forall i \end{aligned} \tag{13.12}$$

where γ is a constant weight on the slack variables and λ is a weight on the introduced constraint. The primal Lagrange function can then be stated as

$$L_P = \frac{1}{2}\|\boldsymbol{\beta}\|^2 + \gamma\sum_{i=1}^{n}\xi_i - \sum_{i=1}^{n}\alpha_i[y_i(\mathbf{x}_i^t\boldsymbol{\beta} + \beta_0) - (1 - \xi_i)] - \sum_{i=1}^{n}\mu_i\xi_i + \frac{\lambda}{2}\|\boldsymbol{\beta}^t\mathbf{A}\|_2^2 \tag{13.13}$$

By differentiating with respect to $\boldsymbol{\beta}$, β_0 and ξ_i the following expressions are obtained.

$$\boldsymbol{\beta} = \sum_{i=1}^{n}\alpha_i y_i(\mathbf{I} + \lambda\mathbf{A}^t\mathbf{A})^{-1}\mathbf{x}_i \tag{13.14}$$

$$0 = \sum_{i=1}^{n}\alpha_i\mu_i \tag{13.15}$$

$$\alpha_i = \gamma - \mu_i \tag{13.16}$$

as well as the positive constraints $\alpha_i, \mu_i, \xi_i \geq 0 \forall i$. By insertion in (13.13) we get the dual objective function (c.f. App. 13.8)

$$L_D = \sum_{i=1}^{n}\alpha_i - \frac{1}{2}\sum_{i=1}^{n}\sum_{j=1}^{n}\alpha_i\alpha_j y_i y_j \mathbf{x}_i^t(\mathbf{I} + \lambda\mathbf{A}^t\mathbf{A})^{-1}\mathbf{x}_j \tag{13.17}$$

which we maximize subject to $0 < \alpha_i < \gamma$ and $\sum_{i=1}^{n} \alpha_i y_i = 0$, and the KKT conditions include the constraints

$$\begin{aligned} \alpha_i[y_i(\mathbf{x}_i^t\boldsymbol{\beta} + \beta_0) - (1 - \xi_i)] &= 0 && (13.18) \\ \mu_i\xi_i &= 0 && (13.19) \\ y_i(\mathbf{x}_i^t\boldsymbol{\beta}) - (1 - \xi_i) &\geq 0 && (13.20) \end{aligned}$$

We see that the matrix $(\mathbf{I}+\lambda\mathbf{A}^t\mathbf{A})^{-1}$ in (13.17) simply is a linear kernel applied to the input space x. It is possible to apply another kernel if this kernel is linear since it then holds that $< \phi(\Phi(x_i)), \phi(\Phi(x_j)) >=< \Phi(\phi(x_i)), \Phi(\phi(x_j)) >$, where $\Phi(.)$ and $\phi(.)$ are some linear kernels, thus (13.17) can then be formulated as

$$L_D = \sum_{i=1}^{n} \alpha_i - \frac{1}{2}\sum_{i=1}^{n}\sum_{j=1}^{n} \alpha_i\alpha_j y_i y_j K((\mathbf{I} + \lambda\mathbf{A}^t\mathbf{A})^{-1/2}\mathbf{x}_i, (\mathbf{I} + \lambda\mathbf{A}^t\mathbf{A})^{-1/2}\mathbf{x}_j) \quad . \tag{13.21}$$

A Taylor expansion of a nonlinear kernel can be used obtain linearity.

13.4 General Constraints

In general the matrix $\mathbf{A}$ can be any matrix, it can form the derivatives of $\boldsymbol{\beta}$ like in Fused Lasso Tibshirani et al. [157], it can perform feature selection with $\mathbf{A} = \mathbf{I}$ under the ℓ_1-norm Zou and Hastie [173] or it can be dependent on data. However, when $\mathbf{A}$ is independent of data the kernel trick can not be applied.

When the matrix $\mathbf{A}$ is dependent on the data x then $\mathbf{A}^t\mathbf{A}$ can be written as purely inner products of the data and therefore the kernel trick is in principle applicable, i.e. $\mathbf{A} = \mathbf{XB}$, where $\mathbf{B}$ is some $n \times m$ matrix. However, it is important to consider whether the introduced constraint is meaningful in kernel space. In the next section we will look at the constraint of orthogonality for paired observations.

13.5 Constraints for Paired Observations

Consider data with two classes of paired observations also called matched points, i.e. an observation in one class has a natural pairing with an observation in the second class and they are therefore not independent. This is for example the case when the same individual is observed at two stages or when subjects are matched according to some criterion such as age or family background. If we want to

separate the two classes with a traditional clustering method or classifier Duda et al. [50], Hastie et al. [76] the information about the pairing is not exploited. In particular, in sparse feature spaces, e.g. few observations are present in relation to dimensions of the feature space, exploiting such information is crucial in order to avoid the curse of dimensionality Hastie et al. [76]. Specifically for the orthogonality constraint (OC) we set $\mathbf{A} = (\mathbf{X_1} - \mathbf{X_2})$, where $\mathbf{X_1}$ and $\mathbf{X_2}$ are matched points sets the following is obtained for the ℓ_2-norm

$$\mathbf{A}^t\mathbf{A} = (\mathbf{X_1} - \mathbf{X_2})^t(\mathbf{X_1} - \mathbf{X_2}) = \mathbf{X_1}^t\mathbf{X_1} + \mathbf{X_2}^t\mathbf{X_2} - \mathbf{X_1}^t\mathbf{X_2} - \mathbf{X_2}^t\mathbf{X_1} \quad (13.22)$$

where $\mathbf{X_1}$ contains observations belonging to group 1 and $\mathbf{X_2}$ contains the ordered counterpart belonging to group 2, i.e. $\mathbf{a}_k = \mathbf{x_1}_k - \mathbf{x_2}_k$.

The hyper plane for the OC-SVM under the ℓ_1-norm is given by

$$f(\mathbf{x}) = \sum_{i=1}^{n} \alpha_i y_i \mathbf{x}^t\mathbf{x}_i + \sum_{k=1}^{n/2} (\rho'_k - \rho_k)\mathbf{x}^t(\mathbf{x_1}_k - \mathbf{x_2}_k) \quad . \quad (13.23)$$

The optimization problem and the hyperplane equation is given by inner products in the input space, and therefore, in principle, the kernel trick can be applied.

The cosine of the standard inner product emphasizes large angles in this setting and thereby gives weight to outliers, i.e. directions which are far from orthogonal to the separating hyperplane. It is not of interest to emphasize outliers further by using the ℓ_2-norm. It is of interest to get a more general picture of the difference and therefore the ℓ_1-norm is preferable. Another factor is the length of $\mathbf{a}$. Since $|\boldsymbol{\beta}|$, is constant the length of $\mathbf{a}$ acts like a weight where large differences in terms of distance between observations are weighted proportionally to this distance. To circumvent this, the directional vectors of $\mathbf{A}$ could be normalized. However, we consider large differences to be more trustworthy than small so here this weighting is desirable.

As the constraint penalizes angles (in normalized form) it is reasonable to, at least, constrain the basis transformation to be conformal, i.e. angle preserving. Conformal transformations include functions such as radial basis, power, exponential, logarithmic, and elliptic functions, for an extended list see e.g. Moon and Spencer [105]. However, in the case of paired observations for shape models we are in general interested in orthogonality in the original space and therefore kernel transformations should be used with care.

Additionally, the dual problem can be useful to consider even without use of kernels as the dual problem is solved in the observation space. Hence, for problems with $p \gg n$ the dual problem has much smaller dimensions than the corresponding primal problem.

13.6 Experiments

The performance of the OC-SVM is tested on synthetic as well as real data and compared to the performance of the standard SVM. The synthetic data serves to visualize the performance of OC-SVM as well as to test the performance for various numbers of observations and dimensions. Finally the methods are tested on real high dimensional data in terms of 60 ear canal impression scannings from 30 individuals.

13.6.1 Synthetic Data

The synthetic data is generated from a normal distribution with standard deviation one (group one). To simulate the coherence between the two groups all points in group one are translated by $\sqrt{p}$, where p is the dimension of the space, along each axis in the positive direction. White noise with standard deviation, $\sigma_\epsilon = 0.1$, 0.3 and 0.5 is added to each of the translated data points (group two). This ensures that the two distributions are non-separable and have approx. 70% overlap (depending on σ and σ_ϵ). Using this procedure 1000 paired samples are generated from which the training and test sets are drawn. To properly test the method the regularization parameters are changed in such a way that the standard SVM estimates the optimal separating hyperplane including all samples. The purpose is to show that the added constraint actually influences the result. The OC-SVM regularization parameter is fixed at 10% of the SVM regularization, which from our experience is a good heuristic. Samples are generated in 2, 5, 10, 100, 500, 1000 and 10000 dimensions and the models are for each dimension build on 2, 5, 10, 50 and 100 paired samples. For each combination the experiment is repeated 100 times where the SVM and the OC-SVM is build on the same samples. The training error and the test error are measured for each method and a hypothesis of the test error being equal for the two methods is tested. Figure 13.2 shows the distribution of the two generated classes in 2D for 1000 data points in each class.

Figure 13.3 illustrates the separating lines for SVM and OC-SVM in two dimensions. From Figure 13.4 it is clearly seen that the OC-SVM perfoms marginally better on the simulated data than the the standard SVM. However, more interestingly the solutions of the OC-SVM has far less variance than the normal SVM, thus the variance over 100 solution is as little as 40% of the solutions of the variations from the SVM. The plots show that the added information gives much more stability to the OC-SVM compared to the SVM. By increasing the distance between the two distributions it is possible to observe the behavior of variance in the method as the two classes become more and more separable.

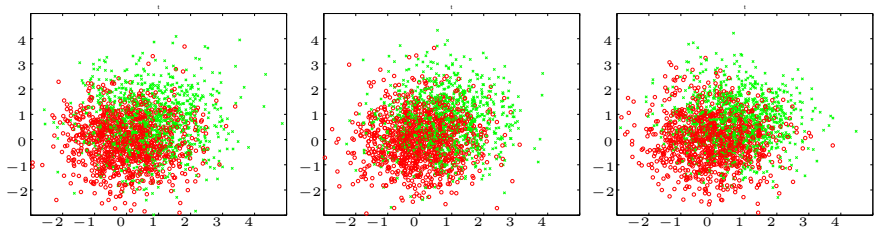

(a) $\sigma_\epsilon = 0.5$ (b) $\sigma_\epsilon = 0.3$ (c) $\sigma_\epsilon = 0.1$

Figure 13.2: The synthetic data with added noise $N(0, 0.5)$, $N(0, 0.3)$ and $N(0, 0.1)$.

Figure 13.5 show how the above measures evolve as the distance between the two classes changes. As can be seen from figure 13.5 the variance ratio is decreasing for higher dimensions and fewer observations as the classes becomes more and more separable. The extra bias introduced marginally improves performance in some cases and does not decrease performance in general. In addition to this it is obvious that the OC-SVM significantly reduces the amount of variation between solutions build from the same distribution. In the next section this variance reduction effect becomes even more pronounced as we study the ear experiment.

13.6.2 Ear Data

This data is part of a larger study of how the ear canal changes shape mainly due to the movement of the mandible. The purpose is to investigate to what extent the changes appear and what influences on hearing aid wearer comfort they might have. Some individuals experience changes to the shape of the ear canal when the mouth is opened. For some hearing aid users this causes discomfort either as direct physical discomfort or in the form of acoustical feedback. In the hearing aid industry the hearing aids are sold to the consumer through an audiologist. Their practice with respect to impressions acquisition influences the shape and thus the comfort level of the individual hearing aid. Since there is no standard way of obtaining impressions, different audiologist have different practices: Some are using open ear impressions and some closed. If a hearing aid is rejected by the user the hearing aid manufacturer has to take the loss of the returned hearing aid. Therefore it is desirable for the manufacturer to be able to classify a given impression as being taken with open or closed mouth as this information is not passed along with the impression. The hope is that this eventually will enable analysis of the shape and lead to guidelines for best practice in this respect. The data analyzed consists of 30 pairs of impressions

from 21 male individuals and 9 female, a total of 60 impressions. Two impressions were obtained from each individual; one with closed mouth and one with open mouth. The impressions were made by the same audiologist to ensure consistency and scanned by the same operator on a 3D-laser scanner. Figure 13.6 shows the resulting surface scanning of an ear impression.

All impressions have been registered to create a common frame of reference, see Darkner et al. [40], resulting in 8191 points in 3D with full correspondence. Each individual ear is then represented as a 24573 dimensional vector. Since $p \gg n$ the two classes are in practice 100% separable. By permuting the order of the observations 100 times and each time training on the first half of the data and testing on the last half, measures of classification, variance in the model and significance of improvement are obtained. For this experiment, the classification of both methods have a training and test error of 0%. The variation of $\boldsymbol{\beta}$ over the 100 permutations can be seen in Figure 13.7. Since the method regularizes the model and thereby increases the bias, the variance should be reduced and a more generalizable result obtained. Comparing the average variance of the results obtained with the OC-SVM and SVM respectively shows that the additional constraint reduces the variance of the normalized result with a factor of 50.

Figure 13.8 show the discriminative direction of a solution for OC-SVM. The general areas which change when the mouth is opened are the ear canal and the concha cymba. As the figure shows the discriminant areas are around the canal (left side of figure), however also the shape of Concha Cymba (left part) seems to have importance in the classification.

13.7 Conclusion

A classification model based on the SVM with additional constraints based on knowledge of data has been derived. For the constraint of orthogonality on paired data the variance of the separating hyperplane was reduced by up to 50 times leading to more robust solutions. This is of great importance, in particular when few observations are available where the variance in general is known to be high due to the curse of dimensionality. Furthermore, the classification rates for the OC-SVM proved to be significantly better or comparable to those of the ordinary SVM. Thanks to Golland Golland [64], we can from the OC-SVM derive a direction, which illustrates the difference between two classes. For the OC-SVM the paired observations are automatically weighted according to the euclidian length of the difference vector between the paired observations. That is, paired observations with large differences have a higher weight in the constraint of orthogonality than paired observations with subtle differences. In

extension to that, a general framework for adding data specific constraints to the SVM was derived in this paper. The framework makes it easy to use underlying a priori knowledge of data to obtain robust solutions for classification problems. On top of that the framework may also be used to obtain certain desired properties for the solutions such as sparseness or correlation between variables.

13.8 Appendix

In this section we give details on the derivation of the Lagrange dual, L_D for the ℓ_2-norm constraint. Differentiating (13.13) with respect to $\boldsymbol{\beta}$ and equating to zero gives

$$\begin{aligned} \boldsymbol{\beta} &= \sum_{i=1}^{n} \alpha_i y_i \mathbf{x}_i - \lambda \mathbf{A}^t \mathbf{A} \boldsymbol{\beta} \Leftrightarrow (\mathbf{I} + \lambda \mathbf{A}^t \mathbf{A}) \boldsymbol{\beta} = \sum_{i=1}^{n} \alpha_i y_i \mathbf{x}_i \Leftrightarrow \\ \boldsymbol{\beta} &= (\mathbf{I} + \lambda \mathbf{A}^t \mathbf{A})^{-1} \sum_{i=1}^{n} \alpha_i y_i \mathbf{x}_i \end{aligned} \tag{13.24}$$

By insertion of (13.14)-(13.16) in (13.13) and setting $X = \sum_{i=1}^{n} \alpha_i y_i \mathbf{x}_i$ we get the dual objective function

$$\begin{aligned} L_D &= \frac{1}{2} \|(\mathbf{I} + \lambda \mathbf{A}^t \mathbf{A})^{-1} X\|^2 + \sum_{i=1}^{n} \alpha_i + \frac{\lambda}{2} \|(\mathbf{I} + \lambda \mathbf{A}^t \mathbf{A})^{-1} X)^t \mathbf{A}\|^2 \\ &\quad - X^t (\mathbf{I} + \lambda \mathbf{A}^t \mathbf{A})^{-1} X \\ &= \sum_{i=1}^{n} \alpha_i + \frac{1}{2} X^t (\mathbf{I} + \lambda \mathbf{A}^t \mathbf{A})^{-t} (\mathbf{I} + \lambda \mathbf{A}^t \mathbf{A})^{-1} X \\ &\quad + \frac{\lambda}{2} X^t (\mathbf{I} + \lambda \mathbf{A}^t \mathbf{A})^{-t} \mathbf{A}^t \mathbf{A} (\mathbf{I} + \lambda \mathbf{A}^t \mathbf{A})^{-1} X - X^t (\mathbf{I} + \lambda \mathbf{A}^t \mathbf{A})^{-1} X \\ &= \sum_{i=1}^{n} \alpha_i + \frac{1}{2} X^t (\mathbf{I} + \lambda \mathbf{A}^t \mathbf{A})^{-1} (\mathbf{I} + \lambda \mathbf{A}^t \mathbf{A}) (\mathbf{I} + \lambda \mathbf{A}^t \mathbf{A})^{-1} X \\ &\quad - X^t (\mathbf{I} + \lambda \mathbf{A}^t \mathbf{A})^{-1} X \\ &= \sum_{i=1}^{n} \alpha_i - \frac{1}{2} X^t (\mathbf{I} + \lambda \mathbf{A}^t \mathbf{A})^{-1} X \end{aligned} \tag{13.25}$$

since the matrix $(\mathbf{I} + \lambda \mathbf{A}^t \mathbf{A})$ is symmetric.

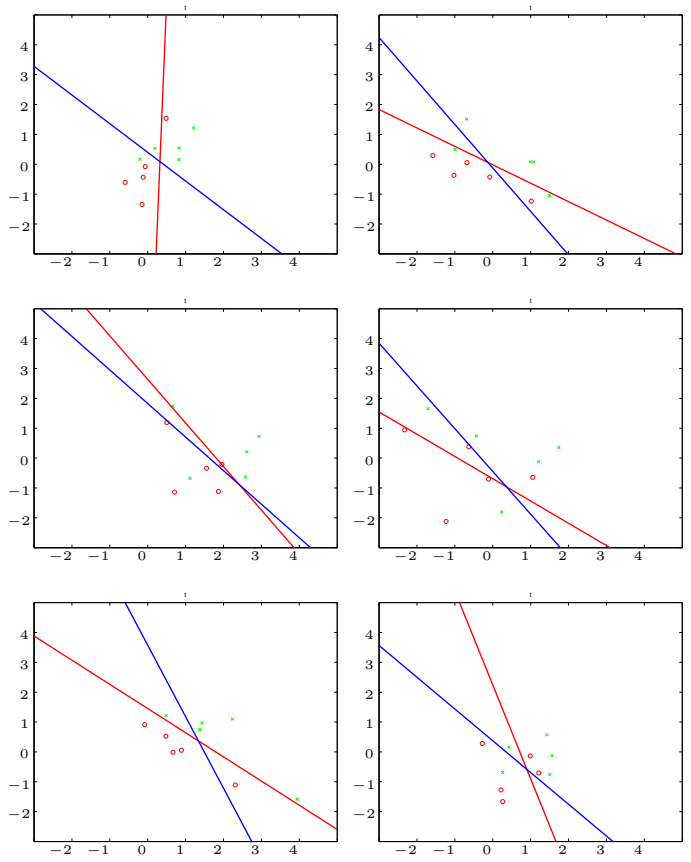

Figure 13.3: A visualization of the difference between OC-SVM and SVM on simulated data build from sets of 5 points with added noise $N(0, 0.5)$. The blue line is the OC-SVM and the read is the SVM.

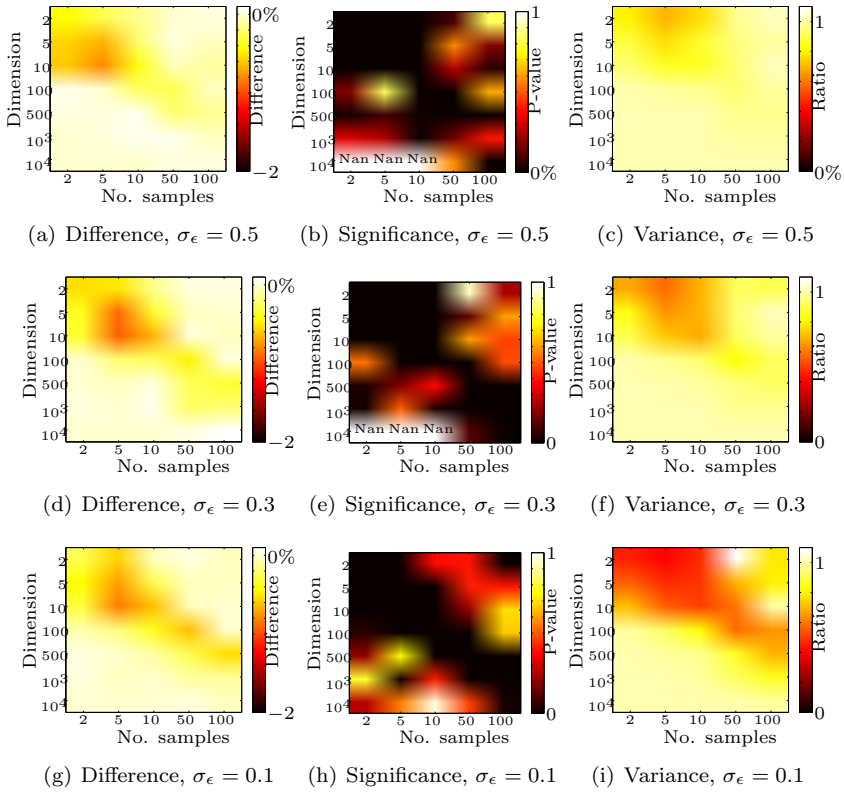

(a) Difference, $\sigma_\epsilon = 0.5$ (b) Significance, $\sigma_\epsilon = 0.5$ (c) Variance, $\sigma_\epsilon = 0.5$

(d) Difference, $\sigma_\epsilon = 0.3$ (e) Significance, $\sigma_\epsilon = 0.3$ (f) Variance, $\sigma_\epsilon = 0.3$

(g) Difference, $\sigma_\epsilon = 0.1$ (h) Significance, $\sigma_\epsilon = 0.1$ (i) Variance, $\sigma_\epsilon = 0.1$

Figure 13.4: The difference of the misclassification rates between OC-SVM and SVM from simulated data with added noise $N(0, 0.5)$, $N(0, 0.3)$ and $N(0, 0.1)$, respectively in the three rows. Negative values indicate that OC-SVM performs better than SVM. The significance (p-values) of this difference using a paired t-test (H_0 = no difference) are illustrated in the second column. The last column is the ration of the average variance of the 100 solutions $\frac{Var(OC-SVM)}{Var(SVM)}$.

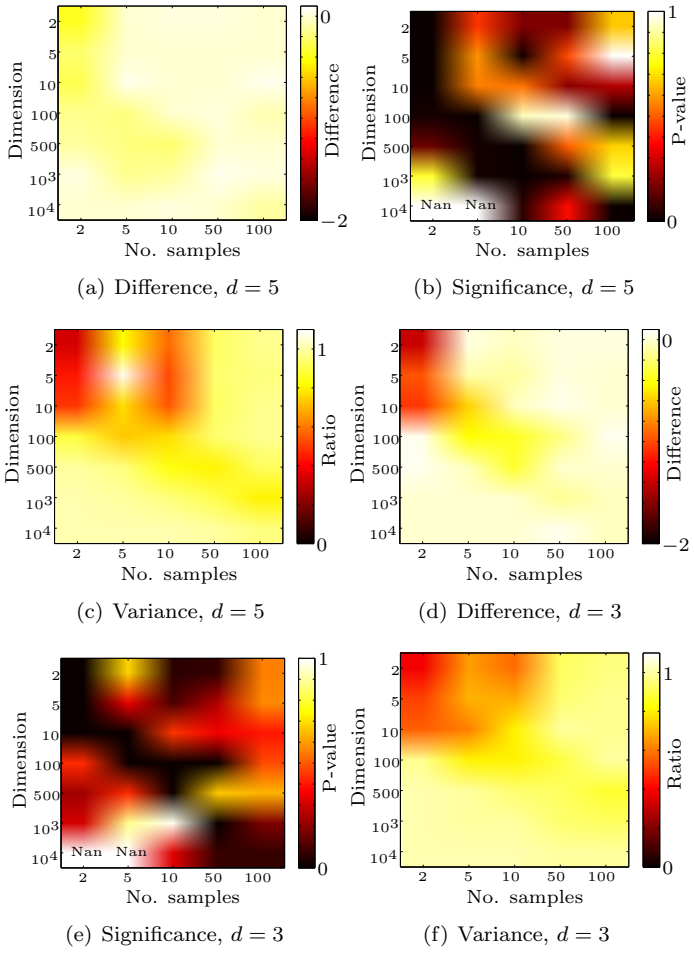

(a) Difference, $d = 5$ (b) Significance, $d = 5$

(c) Variance, $d = 5$ (d) Difference, $d = 3$

(e) Significance, $d = 3$ (f) Variance, $d = 3$

Figure 13.5: The difference of the misclassification rates between OC-SVM and SVM are illustrated in the first column. The synthetic data is with has noise with $\sigma_\epsilon = 0.5$, and the distances $d = 5$ and $d = 3$ between the classes, respectively for the two rows. Negative values indicate that OC-SVM performs better than SVM. The second column is the significance (p-values) of this difference using a paired t-test (H_0 = no difference). The last column is the ratio of the average variance of the 100 solutions $\frac{Var(OC-SVM)}{Var(SVM)}$.

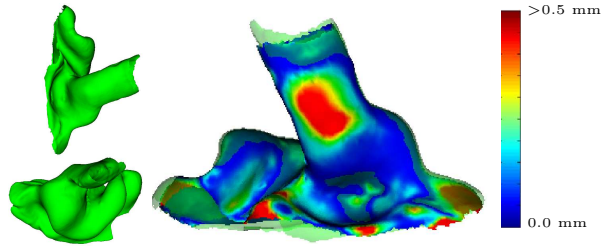

(a) Ear from 2 perspectives

(b) Difference

Figure 13.6: Typical example of an ear impression from two perspectives and an example of the difference map between an open and a closed mouth impression.

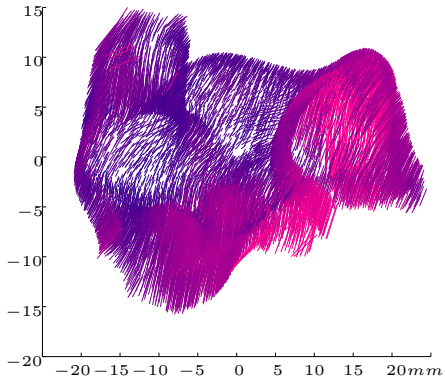

(a) SVM

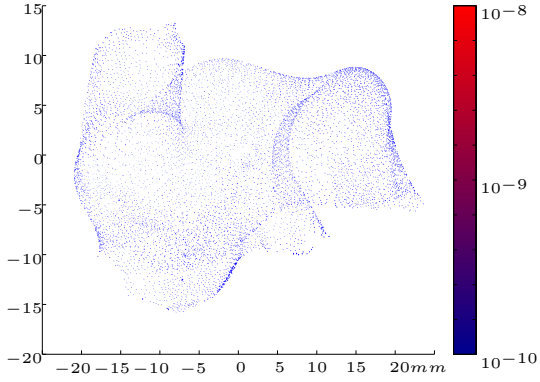

(b) OC-SVM

Figure 13.7: The variance of the solutions, β projected onto the ear canal shape model. Results are shown for 100 SVM and OC-SVM solutions of the ear canal problem. The more red and the longer the vector, the higher is the variation of the parameters in $\boldsymbol{\beta}$.

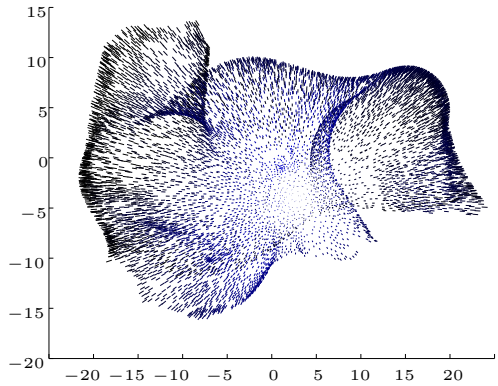

Figure 13.8: A random solution of the OC-SVM projected onto the mean shape of the ears. The darker the color is and the longer the vector, the more important the direction is.

Chapter 14

Estimation of Shape Model Parameters for 3D Surfaces

Søren G. H. Erbou, Sune Darkner, Jurgen Fripp,
Sébastien Ourselin, Bjarne K. Ersbøll

Abstract

Statistical shape models are widely used as a compact way of representing shape variation. Fitting a shape model to unseen data enables characterizing the data in terms of the model parameters. In this paper a Gauss-Newton optimization scheme is proposed to estimate shape model parameters of 3D surfaces using distance maps, which enables the estimation of model parameters without the requirement of point correspondence. For applications with acquisition limitations such as speed and cost, this formulation enables the fitting of a statistical shape model to arbitrarily sampled data. The method is applied to a database of 3D surfaces from a section of the porcine pelvic bone extracted from 33 CT scans. A leave-one-out validation shows that the parameters of the first 3 modes of the shape model can be predicted with a mean difference within [-0.01,0.02] from the true mean, with a standard deviation less than 0.34.

14.1 Introduction

Statistical shape models (SSM) [28] are often used to characterize unseen shapes in terms of model parameters which can be used for classification or regression. In order to estimate the shape model parameters of an unseen shape, full point correspondence is usually needed to be able to project the shape into the parameter space. Obtaining full point correspondence might not be possible in some applications due to restrictions such as acquisition and computation time, dosage (CT) and cost. In such applications there is a need for registration of dense models to incomplete data and for parameter estimation of the unseen shape.

In [162] van Assen *et al.* proposed a method for fitting a dense model to sparse data. Model points near sparse data points are propagated onto void areas using a Gaussian kernel in order to achieve (pseudo-) correspondence making it possible to estimate model parameters. The framework is applied to segmentation of cardiac MRI data and different sparsity schemes are tested. Rajamani *et al.* [133] formulated an algorithm for matching a SSM to sparse digitized points to create patient specific models for pre-operative planning. A linear system of equations is solved to obtain a least squares fit of the model to the digitized points. A Mahalanobis distance based regularization term and M-estimator based weighting of the digitized points are included in the matching algorithm. Due to the nature of their applications both papers focus on the reconstruction error but not on how well the actual model parameters are estimated.

In this paper the focus is on how accurate the model parameters can be estimated. For applications where the parameters are used for classification or regression it is important to quantify how trustworthy this estimate is. An iterative Gauss-Newton optimization algorithm is proposed for fitting a SSM to unseen data using sampled distance maps. It is investigated on dense data, without requiring point correspondence and in future papers the effect of reducing the amount of data, i.e. increasing sparsity, will be investigated. Several authors, e.g. Golland *et al.* [65], have proposed representing shapes using distance maps. This results in a more dense model which would not be feasible in the present application.

The proposed method is applied to a SSM of a porcine bone structure which will be used in a slaughterhouse robotic tool. In this specific application the model parameters are interesting as they can be used to obtain a relation with specific quality measures of the carcasses. The method is also applicable in a range of biomedical applications.

14.2 Methods

14.2.1 Statistical shape models

SSM's were proposed by Cootes *et al.* as a compact way of describing shape variation in a data set [28]. Let the n shapes, or in our case 3D surfaces, be represented by k corresponding 3D points, each arranged in a $3k$ vector $\mathbf{s}$. The idea is to formulate a parameterized model of the form $\mathbf{s} = M(\mathbf{b})$ describing the variation seen in the data, where $\mathbf{b}$ is a vector of shape parameters of the model M. To exclude the effects of translation, rotation and scaling, a generalized Procrustes alignment is performed before constructing the shape model [66]. The sample mean ($\bar{\mathbf{s}} = 1/n \sum_{i=1}^{n} \mathbf{s}_i$) and sample covariance matrix ($\mathbf{C} = 1/(n-1) \sum_{i=1}^{n} (\mathbf{s}_i - \bar{\mathbf{s}})(\mathbf{s}_i - \bar{\mathbf{s}})^T$) are then computed. Since the original parameter space is usually much larger than the number of observations ($3k >> n$) applying principal components analysis (PCA) on the covariance matrix is an obvious choice for dimensionality reduction. The PCA determines the main axes (eigenvectors ϕ_i) of variation of the data and sorts them according to the amount of variation they describe (eigenvalues λ_i). The model can then be formulated as a perturbation of the mean shape:

$$\mathbf{s} = \bar{\mathbf{s}} + \Phi \mathbf{b} \tag{14.1}$$

where Φ is the matrix composed of the eigenvectors ϕ_i.

The model parameters of a new aligned shape s' can be obtained by projecting it into the parameter space,

$$\mathbf{b}' = \Phi^T (\mathbf{s}' - \bar{\mathbf{s}}). \tag{14.2}$$

This is only possible if all the k points of the aligned shape are available.

14.2.2 Optimization Algorithm

The Lucas-Kanade algorithm for image registration was originally formulated using image intensities [10, 101] and was typically applied within fields such as stereo vision and motion analysis. It is an iterative Gauss-Newton optimization algorithm. In the following the parameter estimation of the SSM is considered as a constrained registration problem, thus the Lukas-Kanade approach can be applied. This allows parameter estimation without all the points being available.

Let I be the signed distance map of the input surface and T the signed distance map of the template surface, with regions of the template surface that are within

the input surface having negative distance. Furthermore let $\mathbf{x} = (x, y, z)^T$ be a vector of sample points in the distance maps, $\mathbf{p}$ be a set of parameters and $\mathbf{W}(\mathbf{x}; \mathbf{p})$ a warp of $\mathbf{x}$ with $\mathbf{p}$. The objective function to be minimized is the sum of squared differences between the warped I, and T,

$$\sum_{\mathbf{x}} [I(\mathbf{W}(\mathbf{x}; \mathbf{p})) - T(\mathbf{x})]^2. \tag{14.3}$$

This can be formulated iteratively with incremental updates of $\mathbf{p}$ using a Gauss-Newton scheme [101],

$$\sum_{\mathbf{x}} [I(W(\mathbf{x}; \mathbf{p} + \Delta\mathbf{p})) - T(\mathbf{x})]^2. \tag{14.4}$$

For each step the parameters are updated,

$$\mathbf{p} \leftarrow \mathbf{p} + \Delta\mathbf{p}, \tag{14.5}$$

and this procedure is repeated until convergence. Linearizing by performing a first order Taylor expansion of eq. (14.4) results in,

$$\sum_{\mathbf{x}} [I(\mathbf{W}(\mathbf{x}; \mathbf{p})) + \nabla I \frac{\partial \mathbf{W}(\mathbf{x}; \mathbf{p})}{\partial \mathbf{p}} \Delta\mathbf{p} - T(\mathbf{x})]^2. \tag{14.6}$$

where ∇I is the gradient of I evaluated at $\mathbf{W}(\mathbf{x}; \mathbf{p})$ and $\frac{\partial \mathbf{W}(\mathbf{x}; \mathbf{p})}{\partial \mathbf{p}}$ is the Jacobian of the warp. Solving for $\Delta\mathbf{p}$ reveals,

$$\Delta\mathbf{p} = \mathbf{H}^{-1} \sum_{\mathbf{x}} \left[\nabla I \frac{\partial \mathbf{W}(\mathbf{x}; \mathbf{p})}{\partial \mathbf{p}} \right]^T [T(\mathbf{x}) - I(\mathbf{W}(\mathbf{x}; \mathbf{p}))] \tag{14.7}$$

where H is the Gauss-Newton approximation to the Hessian,

$$\mathbf{H} = \sum_{\mathbf{x}} \left[\nabla I \frac{\partial \mathbf{W}(\mathbf{x}; \mathbf{p})}{\partial \mathbf{p}} \right]^T \left[\nabla I \frac{\partial \mathbf{W}(\mathbf{x}; \mathbf{p})}{\partial \mathbf{p}} \right]. \tag{14.8}$$

Since I consists of distances to the surface to be registered, the gradient (∇I) corresponds to inward pointed normals of the surface evaluated at $\mathbf{W}(\mathbf{x}; \mathbf{p})$. If the surface is moved along the inward pointed normal (away from the sample $\mathbf{x}$) the distance I increases.

The warp $\mathbf{W}(\mathbf{x}; \mathbf{p})$ can be any type, e.g. rigid, affine or nonrigid transformation with corresponding parameters $\mathbf{p}$ [10, 164]. In our case the warp is $\mathbf{W}(\mathbf{x}; \mathbf{p}) = \mathcal{C}(\mathbf{x}, \mathbf{s})$. $\mathcal{C}(\mathbf{x}, \mathbf{s})$ is the set of points in the warped surface $\mathbf{s}$, eq. (14.1), that are closest point to each sample in $\mathbf{x}$. These are obtained using a kd-tree. The parameters $\mathbf{p}$ are the first t shape model parameters weighted by the square

root of their corresponding eigenvalues, normalizing $\mathbf{p}$ to standard deviations ($\mathbf{p} = (b_1/\sqrt{\lambda_1}, ..., b_t/\sqrt{\lambda_t})^T$) off the mean in model parameter space.

∇I is computed as the negative mean of the normals of the faces connected to each point in $\mathbf{W}(\mathbf{x}; \mathbf{p})$.

$$\nabla I_i = -\frac{1}{f_i} \sum_{k=1}^{f_i} \mathbf{v}_k, \tag{14.9}$$

where f_i is the number of faces connected to the i^{th} vertex/point and $\mathbf{v}_k$ is the outwards normal of the k^{th} connected face. Using the angle weighted normals would likely give a better estimate of the mean curvature at the vertices, but it would be computationally more expensive. The Jacobian of the warp for the i^{th} sample in $\mathbf{x}$ is composed from the respective counterparts in the eigenvectors of the model.

$$\frac{\partial \mathbf{W}(\mathbf{x}_i; \mathbf{p})}{\partial \mathbf{p}} = \begin{pmatrix} \phi_{x_i,1}\sqrt{\lambda_1} & \dots & \phi_{x_i,t}\sqrt{\lambda_t} \\ \phi_{y_i,1}\sqrt{\lambda_1} & \dots & \phi_{y_i,t}\sqrt{\lambda_t} \\ \phi_{z_i,1}\sqrt{\lambda_1} & \dots & \phi_{z_i,t}\sqrt{\lambda_t} \end{pmatrix} \tag{14.10}$$

In the above formulation the sample vector $\mathbf{x}$ can be constructed arbitrarily, (within a sensible range from the surface) and the optimization algorithm will seek to minimize the rms error between the distance maps. It is therefore possible to estimate the model parameters without having full point correspondence.

To estimate $\mathbf{p}$ requires an initial estimate, which in this case is $\mathbf{p} = \mathbf{0}$ which corresponds to the mean shape of the shape model. By applying equations (14.7, 14.9, 14.10, 14.8 & 14.5) we obtain a new estimate of $\Delta\mathbf{p}$ that minimize a first order estimate of a quadratic surface to the parameter space. If this is far from the global optimum, the estimate will be inaccurate. To rectify this a line search is applied at each iteration if the full step did not reduce the cost function. This is initialized with a small step size, which doubles until one step before the cost function starts to increase, which ensures a reasonable tradeoff between computations and optimum step size.

To improve speed several papers, e.g. [10, 164], propose to formulate the Lukas-Kanade algorithm in the inverse compositional way making it possible to precompute several steps, especially the Hessian in eq. (14.8). This is beneficial if the sample vector $\mathbf{x}$ is very large, which it is not in the present application. Furthermore applying the inverse compositional algorithm would require the use of surface information from the template image, which may not be feasible to acquire.

14.2.3 Validation

The validation is performed in a leave-one-out scheme (LOO), where the model parameters for each surface i are estimated using a SSM constructed using all but the i^{th} surface. The true set of parameters are found by projecting the aligned surface into the parameter space of the model using eq. (14.2). The actual parameter estimates and the rms errors (point-to-point) are then compared. Only absolute distances less than 5 mm are included when computing the rms error in order to reduce the effect of outliers which can occur due to missing and non-corresponding regions.

14.3 Data

The method is applied to a data set consisting of 33 cases of 3D surfaces from a section of the porcine pelvic bone. Implicit surfaces are extracted from CT scans using radial basis functions [47] from which the surfaces are reconstructed as triangular meshes. The surfaces of the bone of interest are disconnected from the skeleton by planes and therefore have two open ends. Furthermore they would have genus 1 topology, i.e. topological similar to a torus, if the ends were closed.

Correspondence is obtained using the iterative closest point (ICP) algorithm [15] using a similarity transform (translation, rotation and scaling) extended with a point-to-surface step determined by a search along the direction of the estimated vertex normal to the other surface. A reference shape is constructed by initially performing registration of a specific shape to the other shapes, then computing a new reference shape as the mean, performing registration of this to all shapes until convergence of the mean shape. The reference shape consists of 3815 vertices and 7397 faces.

Choosing the number of modes (t) to include in the model is a tradeoff between including the general intrinsic variation of the data and excluding noise. Applying parallel analysis (PA) as suggested by Horn [81], results in 7-9 modes of variation to be included for the different LOO models. PA only includes modes that contain more variation than can be explained by noise, i.e. modes with intrinsic variation less than the noise level are excluded.

Since we investigate the parameter estimation ability of the algorithm for this specific data set, the sample vector $\mathbf{x}$ is composed of the full point set of the surface to register the model to. $T(\mathbf{x})$ is $\mathbf{0}$.

14.4 Results

Figure 14.1 shows the first 3 modes of variation (rows) in one of the LOO models, perturbed -3 std. (left column) and +3 std. (right column). The middle column is the mean shape, with the first 3 and 7 modes containing 45% and 65% of the variation in the data, respectively.

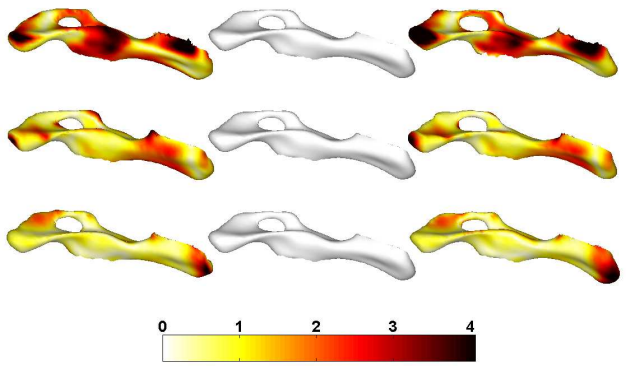

Figure 14.1: Three principal modes of variation (rows) cover 25%, 12% and 8% respectively of the total variation in the data. Left and right columns denote -3 and +3 std. from the mean shape (middle column). The color coding indicates the absolute distance in mm to the mean shape.

When estimating shape model parameters errors accumulate through modes and it might not be possible to estimate more than the first few of modes. If the estimate of the first mode is incorrect, the other modes try to compensate in terms of reducing the rms error of the point-to-point distance. With that in mind 3 schemes are reported, one where all the model parameters are estimated in a combined optimization (comb.) and 2 sequential schemes where only the last mode is estimated, fixing the previous modes to the estimated value (seq-est), and to the true value (seq-true). The latter scheme is included for comparison even though the true parameters would not be accessible in an application. Still it gives an indication of the error levels that should be expected.

In the 3 schemes the true pose is used as initialization and parameter estimates and rms errors compared when including from 1 to 7 modes. The true pose is defined as the pose obtained from the ICP registration, applying the similarity transform. The effect of not having the true pose will be investigated in future work.

Figure 14.2 and table 14.1 show the mean and std. of the difference between the estimated and true values of the parameter estimates in the LOO validation. For

the majority of cases the mean is within ±0.1 std. from the true value, which seems reasonable. The std. of the difference is more interesting, since it gives an idea of how far off most of the estimates are. When estimating 1 or 2 modes the three schemes approximately have the same std. of the difference, less than 0.35. When estimating 3-6 modes the two sequential schemes have a std. within 0.53, while the std. of the combined scheme only is within 0.76 when estimating 3-5 modes. This shows that the parameter estimates for the combined scheme try to balance each other out, resulting in less reliable estimates.

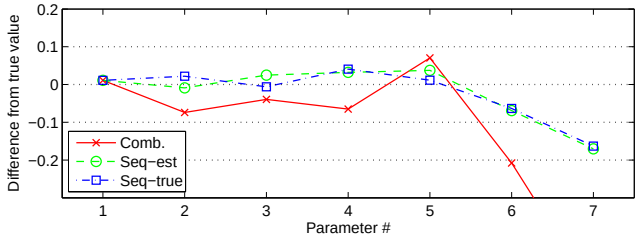

(a) Mean.

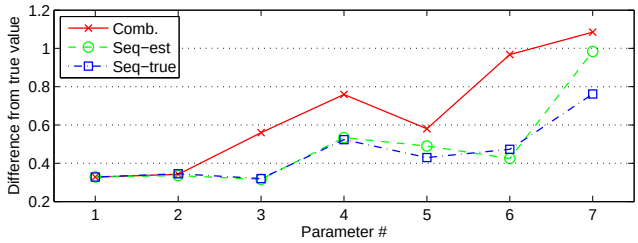

(b) Std.

Figure 14.2: Difference between estimated and true parameter values for the three optimization schemes.

Figure 14.3 shows the mean rms errors for the three parameter estimation schemes and for the true set of parameters. For the initial set of parameters, the mean rms error is 1.85 mm. It shows that the more parameters that are estimated in the combined scheme, the more likely the optimization is to converge to a local minima, where the rms error is significantly higher than for the true set of parameters. For the seq-est scheme the difference is within 0.01 mm for 1-5 modes. This indicates that the seq-est scheme is preferable to the combined scheme, revealing similar rms values as for the true parameter values when using 1-5 modes. The std. of modes higher than the third mode are substantially higher than for the first three modes, so including more than 3 modes should depend on the acceptable level for the std. of the difference. For the present application it is suggested to include 3 modes.

Modes	Comb.	Seq-est	Seq-true
1	0.01 (0.33)	0.01 (0.33)	0.01 (0.33)
2	-0.07 (0.34)	-0.01 (0.34)	0.02 (0.35)
3	-0.04 (0.56)	0.02 (0.32)	-0.01 (0.32)
4	-0.07 (0.76)	0.03 (0.53)	0.04 (0.52)
5	0.07 (0.58)	0.04 (0.49)	0.01 (0.43)
6	-0.21 (0.97)	-0.07 (0.42)	-0.06 (0.47)
7	-0.55 (1.08)	-0.17 (0.98)	-0.16 (0.76)

Table 14.1: Difference between estimated and true parameter values for the three schemes when estimating 1 through 7 modes. Mean and (std.) are reported.

Figure 14.4 shows the mean and std. of the rms error for each surface point plotted on the mean surface, when 3 modes of variation are used. The error is nicely distributed over the central parts of the shape, with the main errors located at either end and along the edge of the top right part of the hole. The mean rms error is 1.50 mm and the mean std. is 0.59 mm.

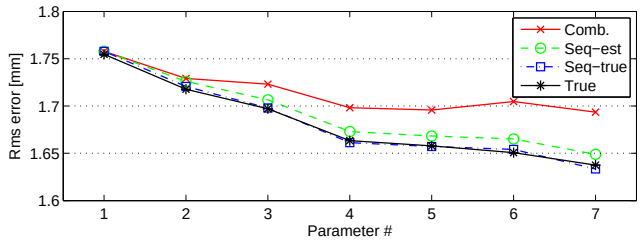

Figure 14.3: Mean rms error of leave-one-out validation for different number of modes included, the std. is 0.12 mm. The mean value of the initial rms error is 1.85 mm.

14.5 Conclusion

An iterative Gauss-Newton algorithm is applied to estimate statistical shape model parameters for unseen data. The optimization is driven by sampling in distance maps, which can be done arbitrarily. This enables the estimation of model parameters without the need of full point correspondence, which would be needed if the aligned shape were to be projected into the parameter space.

For applications where it is of interest to fit a dense model to sparse data in order to estimate model parameters e.g. for classification or regression purposes this

(a) Mean [mm]. (b) Std. [mm].

Figure 14.4: Mean (a) and std. (b) of rms error, in mm, for each point plotted on the mean shape and reconstructed using 3 modes. The mean rms error on the surface is 1.50 mm. and the mean of the std. is 0.59 mm.

method can be applied. This is important in applications where time, dosage, cost etc. are issues.

Leave-one-out validation of parameter estimates for a data set of 3D surfaces of a specific porcine bone shows that the three primary modes of the statistical shape model can be estimated with a mean difference between [-0.01,0.02] std. and with a std. of the difference within 0.34. This is done using a sequential estimation scheme where each parameter is estimated sequentially with previous parameters fixed. If 6 modes are estimated the upper limit of the std. of the difference increases to 0.53 and the mean difference is between [-0.07,0.04] std. The difference between the true and the estimated rms error is below 0.01 mm. The rms error decreases when increasing the number of modes, but the parameter estimates are only reliable enough for the first 3 modes in the present application.

The sample vector that drives the optimization can be arbitrarily defined, which is a topic for future work, along with the introduction of weights on the cost function. Other topics to investigate include applying more localized models, i.e. ICA-models, varimax rotation or sparse PCA.

The statistical shape model will be used in a slaughterhouse robotic tool and the parameters are of interest as they can be used to obtain a relation with specific quality measures of the carcasses.

14.6 Acknowledgements

The CT data was provided by the Danish Meat Research Institute as a part of the project "The Virtual Butcher" funded by the Danish Pig Levy Fund and the Directorate for Food, Fisheries and Agri Business.

Appendix A

Application to research ethical committee

A.1 Etiske aspekter for forskningsprojektet: Opmåling af ydre øre og øregangsdynamik

A.1.1 Indledning

Forsøgene er beskrevet i Protokol for Opmåling af ydre øre og øregangsdynamik (herefter benævnt Protokollen). I Deltagerinformation om forskningsprojektet: Opmåling af ydre øre og øregangsdynamik findes desuden en beskrivelse af de bivirkninger, risici, komplikationer eller ulemper, som det for testpersonerne er forbundet med at deltage i forskningsprojektet. Nærværende dokument samler de etiske overvejelser vedrørende forsøgene.

A.1.2 Bivirkninger og ulemper

Forsøget indebærer, at testpersonerne ved besøget vil blive udsat for, at der laves øreaftryk i fire forskellige ansigts-, hoved- og kropsstillinger. Det er almindelig klinisk praksis at lave øreaftryk i siddende positur. Det forventes ikke, at

testpersonen vil blive påvirket af bivirkninger som følge af dette. Aftryk fortaget med åbenstående mund gennemføres ved hjælp af en bideklods, en såkaldt spacer, kendt fra tandlægers kliniske praksis. Spaceren anvendes dels for at sikre, at alle testpersoner holder munden åben under selve aftryksprocessen og dels for at sikre, at alle testpersoner åbner munder lige meget. Der vil kunne forekomme lettere ømhed i kæbeleddene efter dette aftryk. Denne ømhed vil normalt fortage sig efter en dags tid. Øreaftryk foretaget med hovedet drejet ca. 60 grader forventes ikke at give anledning til bivirkninger. Aftryk foretaget i foroverbøjet positur giver i sig selv ikke anledning til bivirkninger. Det er almindelig kendt, at specielt ældre personer, kan blive svimle eller i enkelte tilfælde besvime, hvis de skal stå foroverbøjet i kortere eller længere tid. Testpersonen vil blive placeret på en stol eller bænk, hvor kroppen kan støttes i foroverbøjet positur for at forhindre fald ved evt. besvimelse. Der vil under processen med at tage dette øreaftryk være ekstra opmærksomhed for om muligt at undgå ubehageligheder. Der vil skulle tages fire øreaftryk af testpersonens ene øre ved det første besøg. Den anvendte øreaftryksmetode er svarende til den metode, som anvendes ved almindelig daglig klinisk praksis. Under hvert øreaftryk påvirkes øregangen af aftryksmaterialet med et mindre tryk, der hos enkelte personer giver anledning til en let hævelse. Selve hævelsen er ikke ubehagelig. Det kan ikke afvises, at øret vil hæve ekstra, specielt efter det sidst tagne øreaftryk. Erfaringer fra tidligere forsøg har i praksis vist, at en hævelse i øret i værste fald vil betyde, at testpersonen ikke vil kunne anvende høreapparat i nogle timer. Hævelsen vil normalt være væk dagen efter. Denne type hævelse kan bedst sammenlignes med den hævelse, der kan forekomme efter at en person har fået fjernet ørevoks mekanisk ved en øre-næse-halslæge. Ud over nævnte forhold er der ingen bivirkninger, risici, komplikationer eller ulemper forbundet med at deltage i forskningsprojektet.

A.1.3 Nytte ved forsøget

Høreapparatbrugere udtrykker ofte utilfredshed med komfort eller hyl fra høreapparatet. En stor del af disse problemer skyldes de dynamiske forhold i ydre øre og øregang, ved ansigts, hoved og kropsbevægelser. Det er således af stor almen interesse dels at kortlægge disse problemer - med henblik på en bedre forståelse - og i særdeleshed at undersøge mulige tiltag til at afhjælpe disse problemer, hvilket er formålet med forsøget. For den enkelte deltager kan deltagelse i forsøgene føre til en dokumentation af personens egen øredynamik. Denne viden vil kunne anvendes, når personen senere skal have tilpasset høreapparat, ved at tilpasningen med stor sansynlighed vil kunne gøres mere komfortabel fysisk og ved at reducere høreapparatets eventuelle akustiske feedback/hyl. Ved deltagelse i forsøget bidrager testpersonerne med data, der fremadrettet vil kunne forbedre den mekaniske konstruktion af både individuelle og seriefremstillede

høreapparater.

A.1.4 Forsikringsforhold og sikkerhedsforanstaltninger

Forsøgene gennemføres i forskningslaboratorium med højt kvalificeret teknisk- og audiologisk personale, som har stor erfaring med brug af eksperimentelt udstyr og afvikling af forsøg. Såfremt forsøgsledelsen mod forventning skulle pådrage sig et erstatningsansvar er projektgruppen økonomisk dækket af Oticons erstatningsansvarsforsikring. Adgang til elektroniske data kan kun ske ved brug af autoriseret adgangsnavn og password. Fysiske data opbevares i aflåste skabe eller i aflåste arkivrum og under ikke åbne adgangsforhold.

A.1.5 Konklusion

Ulemper og risici ved at deltage som testperson i de forsøg, der er beskrevet i dokumentet, Protokol for Opmåling af ydre øre og øregangsdynamik er i grove træk sammenlignelige med de ulemper, som hørehæmmede oplever i forbindelse med modtagelse af almindelig privat eller offentlig høreforsorg. Med hensyn til transportomkostninger kompenseres testpersonerne efter faste km-satser. Det synes hermed godtgjort, at de forventede gavnlige virkninger for høreapparatforskningen og de deltagende testpersoner opvejer de forudsigelige ulemper, risici og komplikationer, som der for testpersonerne kan være forbundet med at deltage i forsøgene. Claus Nielsen

A.2 Lægmans protokol for Opmåling af ydre øre og øregangsdynamik

A.2.1 Formål

Formålet med forskningsprojektet 'Opmåling af ydre øre og øregangsdynamik' er ved tredimensionel opmåling at indsamle data for at undersøge, hvorledes det ydre øre og øregang ændrer form, når en person bevæger munden/kæben, ved ansigtsmimik, hoveddrejning og ændring af kropsstillingen eks. ved foroverbøjning. Ydre øre og øregangens dynamiske forhold volder i større eller mindre grad besvær for høreapparatbrugere i deres dagligdag. Der er mindst to problemer, som er fremtrædende: 1. Komfortproblemer da den del af høreapparatet, som

er placeret i øret, typisk er lavet af et hårdt materiale og dermed kun i meget ringe omfang kan følge øret og øregangens bevægelser. Specielt høreapparater, der er placeret dybt i øregangen, kan volde problemer med komfort. 2. Akustisk feedback, dvs. hyl fra høreapparatet, som skyldes at apparatet ikke slutter tæt i øregangen. Høreapparatet er ofte udstyret med et anti-hyle kredsløb, der er i stand til at reducere hyl. Dette betyder, at høreapparatet ikke vil hyle konstant, men kan hyle kortvarigt, når apparatet ikke slutter helt tæt i øret. Tidligere undersøgelser har indikeret, at der sker en ændring af øregangens diameter, når munden åbnes, og at det ydre øre ikke ændrer nævneværdig form. Det er derfor interessant at undersøge, hvorvidt der er hold i disse antagelser eller om der er tale om en mere kompleks sammenhæng. Vi opstiller to påstande, der ønskes efterprøvet i projektet. Dynamikken i ydre øre og øregang er en kompleks størrelse, der ikke kun omfatter en ændring af øregangens tværsnitsareal forårsaget af mund/kæbebevægelser.

A.2.2 Forsøgsmetodik

Den overordnede metodik er baseret på, at en gruppe personer vil få lavet øreaftryk af deres ydre øre og øregang under forskellige mund/kæbe, hoved og kropspositioner. Testpersonerne vil blive bedt om at besvare et spørgeskema, hvor forskellige fysiske forhold omkring deres høreapparat vil blive belyst. Der laves et antal traditionelle øreaftryk i forskellige mund/kæbe, hoved og kropspositioner. Det forventes, at der vil indgå ca. 50 testpersoner i forsøgene.

A.2.3 Tidsforløb

Forskningsprojektet består af to delforsøg. For testpersonen betyder det, at de skal aflægge to besøg på Oticons Forskningscenter Eriksholm. Ved det første besøg tages der fire øreaftryk af højre øre. De fire aftryk omfatter: normal opretsiddende, med åben mund, foroverbøjet og med hovedet drejet til siden. Endvidere besvares et spørgeskema vedrørende komfort ved brug af høreapparat. Ved andet besøg gentages forsøget, denne gang med den eksperimentelle øreskanner. Dvs. at der laves 4 skanninger i samme positurer som ved første besøg.

A.3 Protokol for Opmåling af ydre øre og øregangsdynamik

A.3.1 baggrund

Ydre øre og øregangens dynamiske egenskaber volder i større eller mindre grad besvær for høreapparatbrugere i deres dagligdag. Der er mindst to problemer, som er fremtrædende: 1. Komfortproblemer, da høreapparatet typisk er lavet af hård acryl og dermed kun i begrænset omfang kan følge ørets og øregangens bevægelser. Specielt høreapparater, der er placeret dybt i øregangen kan volde problemer med komfort. 2. Akustisk feedback, hyl fra høreapparatet på grund af lækage. Hvis forstærkningen er stor nok til at den forstærkede lyd i øregangen kan finde vej tilbage til høreapparatets mikrofon vil dette resultere i hyl fra apparatet. Ydre øre og øregangens dynamik vil for nogle personer betyde, at der periodevis vil være lækager, der er så store, at høreapparatet vil hyle. Nutidens mest avancerede høreapparater er udstyret med anti-hyle kredsløb, der er i stand til at reducere hyl. Dette betyder, at høreapparatet ikke vil hyle konstant, men kortvarigt, når ørets dynamik forårsager lækage. Der er kun publiceret lidt om ørets dynamik, primært af Oliveria,[1][2][3][4] der har lavet et par studier, hvor han har undersøgt øregangens dynamik som funktion af åben og lukket mund. Disse studier er dog langt fra fyldestgørende, da de anvendte målemetoder må betegnes som metoder, der har en stor risiko for at være behæftet med fejl, idet målingerne er foretaget manuelt bl.a. med en skydelære, og at der derfor kan drages tvivl om konsistensen af målepunkterne og nøjagtigheden. Hertil kommer at størrelsen af datasættet er meget begrænset (ca. 14 observationer) og derfor mangler 'statistisk kraft' til at kunne drage endelige konklusioner, men kun giver et fingerpeg om, hvad der sker. Weller et. al. [5] har gennemført en undersøgelse, hvor man også har undersøgt ørets dynamik. Målingerne er foretaget manuelt på et relativt lille datasæt, hvilket kun giver et fingerpeg om ændringerne og ikke mere nøjagtige mål, som i dag er muligt med laserscannere. Endvidere har han nogle tvivlsomme antagelser, der giver gennemslag i hele undersøgelsen bl.a. at den centrale del af øremuslingen, concha ikke bevæger sig, hvilket vi i et pilot forsøg har observeret at den gør, både ved kæbebevægelser samt ved ændring af hovedets position. Herudover er der lavet et forsøg med fremstilling af et blødt apparat som en mulig løsning på de problemer, der opstår som følge af ørets dynamiske egenskaber[6] samt et par observationer på kadavere[7], der af åbenlyse grunde ikke fortæller noget om dynamik. Det er derfor vigtigt for forståelsen af den kontinuerte bevægelse i øregangen, der foregår hos mennesker, at lave et fyldestgørende studie på en betydelig gruppe af testpersoner.

A.3.2 Formål

Formålet med dette forskningsprojekt er ved geometrisk tredimensionel opmåling at indsamle data for at undersøge dynamikken i ydre øre og øregang, når personen bevæger munden/kæben, ved ansigtsmimik, hoveddrejning og ændring af hovedstillingen eks. ved foroverbøjning. Aftryk af ydre øre og øregang har indtil nu været den mest udbredte måde at aftaste ørets geometri på. Dertil udviklet siliconebaseret materiale og en gennemprøvet metode anvendes ved øreaftryk. Øreaftrykket anvendes til fremstilling af individuelle øreproppper eller høreapparater. Udover generel indsamling af data af ydre øre og øregangens dynamik opstilles der følgende hovedhypotese, der ønskes efterprøvet i projektet. Dynamikken i ydre øre og øregang er en kompleks størrelse, der ikke kun omfatter en ændring af øregangens tværsnitsareal forårsaget af mund/kæbebevægelser.

A.3.3 Forsøgsmetodik

De opstillede hovedhypoteser efterprøves i en række delforsøg, der beskrives i detaljer nedenfor. Den overordnede metodik er baseret på, at en gruppe personer vil få lavet øreaftryk og opmålt deres ydre øre og øregang under forskellige mund/kæbe, hoved og kropspositioner. Testpersonerne vil blive bedt om at besvare et spørgeskema (er vedlagt i kopi), hvor forskellige fysiske forhold omkring deres høreapparat vil blive belyst. Der laves et antal traditionelle øreaftryk i forskellige mund/kæbe, hoved og kropspositioner. Det forventes, at der kommer til at indgå ca. 50 testpersoner i forsøgene. Forsøgenes hjemsted er Oticons forskningscenter, "Eriksholm". Forsøgene gennemføres således i forbindelse med forskningslaboratorium med højt kvalificeret teknisk- og kliniskaudiologisk personale, som har stor erfaring i både almindelig og dyb øreaftrykstagning og i almindelig afvikling af forsøg.

A.3.4 Testpersoner

Testpersonerne skal være fysisk og intellektuelt i stand til både at medvirke i aftrykstagningen og øreskanningerne samt at besvare spørgeskema om de fysiske forhold omkring deres høreapparater. Testpersonerne skal være erfarne høreapparatbrugere. Personer, der har oplevet problemer med enten komfort eller umotiveret hyl fra deres høreapparater, og personer som ikke har oplevet disse problemer vil indgå i delforsøgene. Testpersonerne oplyses skriftligt om forsøgets formål, personlige fordele og ulemper (beskrevet i dokumentet om etiske aspekter ved forskningsprojektet) ved deltagelse samt at de er berettigede

til at udtræde af forsøget uden varsel til enhver tid. Hver testperson skal afgive en skriftlig samtykkeerklæring før forsøgets start, jf. bekendtgørelsen af 12. oktober 2000 om information og samtykke i biomedicinske forskningsprojekter.

A.3.5 Rekruttering

Erfarne høreapparatbrugere rekrutteres fra testpersondatabasen på forskningscenter Eriksholm. Testpersondatabasen er en database over voksne frivillige testpersoner med høretab, som er kommet i kontakt med forskningscenteret med et ønske om at medvirke som testperson ved centerets løbende arbejde. Kandiderende testpersoner vil blive inviteret til deltagelse i forsøgene og få udleveret materialet, Deltagerinformation om forskningsprojektet: Opmåling af ydre øre og øregangsdynamik.

A.3.6 Teknisk udstyr

Øreaftryk laves ved hjælp af almindeligt udstyr til øreaftrykstagning, såsom sprøjte, lyspen til isætning af ørebeskyttelsesvat i øregangen og siliconebaseret øreaftryksmateriale. Til inspektion af øregangen anvendes et standard videootoskop, der er sammensat af en lyskilde, et ccd-kamera og en monitor. Videootoskopet er forbundet til en PC via en framegrabber, der er i stand til at fastfryse og gemme billeder fra videokameraet. Øreskanningerne gennemføres ved hjælp af en prototype øreskanner der består af en måleprobe, der bedst kan beskrives som en blanding af en lyspen og et endoskop. Proben er få millimeter i diameter og næsten rigid. Måleproben udsender synligt lys, som anvendes til opmålingen af ørets geometri. Ved isætning af måleproben, er det muligt samtidig at se, hvor dybt måleproben er placeret i øregangen. Måleproben udsender også et magnetfelt under skanningen. Testpersonen bærer et headset med ni spoler, hvis funktion er at måle magnetfeltet udsendt af måleproben. Magnetfeltsdata og optiske data processeres i en ekstern enhed og sendes til PC'en, hvor der genereres en 3D repræsentation af ydre øre og øregang.

A.3.7 Elektrisk sikring

Elektrisk sikring af testpersonerne opnås ved brug af ægte jording af de instrumenter, der har forbindelse til lysnettet.

A.3.8 Kontakt med egen ørelæge

Som en del af projektet anmodes testpersonen om at opsøge en ørelæge for at sikre, at personen ikke har behandlingskrævende sygdomme i ydre øre, øregang eller trommehinde. Testpersonen vil kun kunne rekrutteres til projektet, hvis ørelægen finder normale forhold ved sin undersøgelse.

A.3.9 Kontakt med Forskningscenter Eriksholm

Alle testpersoner deltager i et informationsmøde, hvor folderen, Deltagerinformation om forskningsprojektet: Opmåling af ydre øre og øredynamik,udleveres og gennemgås. Testpersoner der giver samtykke til deltagelse i et forsøg, der omfatter instruktion, øreaftryk og/eller øreskanninger og eventuelt et afsluttende interview - forløbet beskrives nedenfor i detaljer.

A.3.10 Dokumentation

Testpersonernes anonymitet sikres ved at holde deres identitet skjult bag et chifreret monogram (f.eks. TPnnn). Alle data med relevans for forsøgene rapporteres. Speciel opmærksomhed skal rettes mod følgende,

. Beskrivelse af forsøgspersoner; alder, køn, civil status, profession.

. Beskrivelse af alle målemetoder og resultater.

. Testpersonernes spontane reaktioner vil blive rapporteret.

. Testpersoner, der forlader projektet samt data, der ikke medregnes og grunden herfor.

. Identificerede ulemper eller tekniske problemer vil blive rapporteret, såfremt de opstår.

Adgang til elektroniske data kan kun ske ved brug af autoriseret adgangsnavn og password. Fysiske data opbevares i aflåste kartoteksskabe eller i aflåste arkivrum og under ikke åbne adgangsforhold. Der henvises i øvrigt til vor anmeldelse til Datatilsynet Journal nr. 2002-42-0398.

A.3.10.1 Den statistiske analyse og beskrivelse af resultaterne

Studiet består af longitudinale delforsøg, hvor testpersonerne fungerer som deres egen kontrol. Der vil dels blive lavet en principal komponent analyse på differencerne mellem aftryk for hvert individ for at anskueliggøre den variation, der findes på tværs af populationen. Dette betyder, at den variation, vi finder hos de enkelte personer, sammenholdes og analyseres, således at der vil kunne siges noget generelt om variationer for hele populationen. Samtidigt vil vi lave en regression af de indsamlede spørgeskemadata på de principale komponenter for at undersøge for eventuelle sammenhænge mellem svar og øregeometri. Endvidere vil vi anvende en ANOVA (varians analyse) på aftryksdata alene for på den måde at analysere hvorledes variationen i observationerne forholder sig. Vi forventer at kunne drage en række konklusioner om, hvorledes et ydre øre ændrer form under normal daglig færden. Vi vil sammenholde de to dataindsamlingsmetoder og vurdere deres kvaliteter ved at holde dem op imod hinanden og lave tests af statistiske hypoteser udført med traditionel parametrisk eller ikke-parametrisk statistik, test for samme middelværdi, og varians etc. Hvis en forsøgsperson beslutter sig for at trække sig ud af projektet, eller hvis det af andre grunde viser sig umuligt at opnå den nødvendige mængde data, udelades den pågældende forsøgspersons resultater fra de videre analyser. Sådanne resultater vurderes og rapporteres imidlertid.

A.3.11 Etiske aspekter

Nærværende forsøgsprotokol skal godkendes af den Videnskabsetiske Komite i Frederiksborg Amt.

A.3.12 Ejerskab af resultater

Oticon A/S ejer alle rettigheder vedrørende forsøgets data. Der udarbejdes en rapport over forsøgets resultater, og denne rapport vil være tilgængelig inden for Oticon A/S. Muligvis vil visse dele af data blive anvendt til publikation i et fagtidsskrift eller ved en faglig kongres. I alle tilfælde vil alle data optræde i anonymiseret form.

A.3.13 Finansiering

Alle udgifter i forbindelse med forsøgene afholdes af Oticon A/S. Testpersonerne godtgøres udgifter til transport efter standardtakster.

A.3.14 Opsamling af data ved hjælp af øreaftryk

Der tages aftryk for at estimere de yderpunkter af variation i form, som vi mener at øret antager i dagligdagen. Det er således muligt at udspænde et rum af ændringer, som øret udviser under normale omstændigheder. Aftrykstagningen vil blive foretaget af en og samme audiolog, der er erfaren i aftrykstagning. Dette er for at sikre testpersonen mod ubehageligheder og samtidigt sikre en ensartethed i de aftryk, der bliver taget. I forbindelse med besøget vil testpersonen blive stillet en række spørgsmål vedrørende fysisk komfort af deres nuværende høreapparat med henblik på sammenholdning med analysen af afstøbningerne.

A.3.14.1 Aftrykstagning

Der tages derfor fire aftryk af øret med hovedet i forskellige positioner. De fire positioner er følgende:

1. Normal positur. Personen sidder med lukket mund, helt afslappet og kigger lige ud mens aftrykket tages.
2. Med åben mund. Personen sidder med åben mund, hvor afstanden sikres ved brug af en bideskinne af ca. 3. cm tykkelse, som testpersonen bider sammen om, imens aftrykket tages.
3. Bukke sig ned. Testpersonen sidder og kigger direkte ned i gulvet i foroverbøjet positur imens aftrykket tages. Hovedet kan evt. hvile og støttes ved placering på en pude el. lignende på kanten af et bord.
4. Dreje hovedet. Testpersonen sidder almindeligt opret med hovedet drejet ca. 60 grader mod den modsatte skulder af den side hvor aftrykket tages.

A.3.14.2 Risici

Det er et almindeligt kendt fænomen, at enkelte, specielt ældre personer, meget kortvarigt kan blive svimle og i meget sjældne tilfælde miste bevidstheden i

foroverbøjet position. For at sikre at personen ikke kommer til skade, vil vi sikre personen med et blødt underlag eventuelt støtte personens krop ved at anvende en bænk af samme type som anvendes i motionscentre. Audiologen har gennemført et certificeret førstehjælpskursus og vil være i stand til at tage de nødvendige forholdsregler, hvis det skulle vise sig at være påkrævet.

A.3.14.3 Spørgeskema

Testpersonen vil blive stillet en række spørgsmål, om hvorledes personen opfatter komforten af sit høreapparat, om vedkommende oplever hyl, gnaven i øret/øregangen eller andre gener af fysisk karakter ved almindeligt brug af apparaterne. Alle spørgeskemaer vil blive administreret af en interviewer i et lukket interview for at sikre kvaliteten af de indsamlede data.

Appendix B

Questionnaire

Introduction: This questionnaire is a part of an investigation of the dynamics of the human ear canal carried Eriksholm Research Center. The purpose is to investigate how the human ear canal behaves under normal circumstances. The dynamics has a huge impact on how well a hearing aid fits it 31s user.

(To be filled in by audiologist)

TP NR _____ Age _____

Age of Hearing aid _____

Sex — Male ☐ Female ☐

Type of hearing aid — ITE ☐ BTE ☐

Has the subject been diagnosed with TMJD (Temporo Mandibular Joint Disfunction) — Yes ☐ No ☐ Suspected ☐

New User (first hearing aid) — Yes ☐ No ☐

If your hearing aid howls, how often does this howling occur?

	Almost all the time	Several time every day	Dayly	Weekly	Very seldom or never
Right ear:	☐	☐	☐	☐	☐
Left ear:	☐	☐	☐	☐	☐

If your hearing aid howls, what is the cause of the howling?

Movement of the jaw	Grimaces	Bending down	Turning the head	Other
☐	☐	☐	☐	☐

If other, please explain?

If you experience physical discomfort in the ear when wearing the hearing aid, how often does this discomfort occur ?

	Almost all the time	Severtal times every day	Dayly	Weekly	Very seldom or never
Right ear:	☐	☐	☐	☐	☐
Left ear:	☐	☐	☐	☐	☐

If you experience physical discomfort in the ear when wearing the hearing aid, what causes this discomfort ?

Movement of the jaw	Grimaces	Bending down	Turning the head	Insertion or removal of the hearing aid
☐	☐	☐	☐	☐

Other causes?

How well is the physical fit of the hearing aid?

	Very poor	Poor	Average	Good	Very good
Right ear:	☐	☐	☐	☐	☐
Left ear:	☐	☐	☐	☐	☐

List of Figures

List of Tables

Bibliography

[1] 3Shape. URL `www.3Shape.com`.

[2] Lyric hearing aid. URL `http://www.lyrichearing.com/`.

[3] Oticon. URL `www.demant.com`.

[4] H. Akaike. A new look at the statistical model identification. *IEEE Transactions on Automatic Control*, 19(6):716–723, 1974.

[5] E. Andreasen, F. Bierring, and J. Rostgaard. *De indre organers anatomi*. Munksgaard, 9 edition. ISBN 87-16-12164-3.

[6] P. Andresen and M. Nielsen. Non-rigid registration by geometry constrained diffusion. In *Proc. Medical Image Computing and Computer Assisted Intervention (MICCAI 99)*, pages pp. 533–543, 1999.

[7] L. Armijo. Minimization of functions having lipschitz continuous first partial derivatives. *Pacific Journal of Mathematics*, 16(1):1–3, 1966.

[8] R. J. Oliviera W. J. Staab B. Ballachanda, R. T. Miyamoto. *The Human Ear Canal*. Singular Publishing Group Inc., 1995. ISBN 1-56593-169-6.

[9] J. Bærentzen and H. Aanæs. Signed distance computation using the angle weighted pseudo-normal. *IEEE Transactions on Visualization and Computer Graphics*, 11(3):243–253, may 2005.

[10] S. Baker and I. Matthews. Lucas-Kanade 20 years on: A unifying framework. *International Journal of Computer Vision*, 56(3), 2004.

[11] S. Balci, P. Golland, and W. Wells. Non-rigid groupwiseregistration using b-spline deformation model. In *Proc. Statistivcal Image Registration Workshop (MICCAI 2007)*, pages 23–30, 2007.

[12] R. Barrett, M. Berry, T. Chan, J. Demmel, J. Donato, J. Dongarra, V. Eijkhout, R. Pozo, C. Romine, and HA Vorst. *Templates for the Solution of Linear Systems: Building Blocks for Iterative Methods*. Society for Industrial and Applied Mathematics, 1993.

[13] M. Belkin and P. Niyogi. Laplacian eigenmaps for dimensionality reduction and data representation. *Neural Comp.*, 15(6):1373–1396, June 2003.

[14] J. Besag. Towards bayesian image analysis. *Journal of Applied Statistics*, 16(3):395–407, 1989.

[15] P.J. Besl and N.D. McKay. A method for registration of 3-D shapes. *IEEE Transactions on Pattern Analysis and Machine Intelligence*, 14(2): 239–256, 1992.

[16] F.L. Bookstein. Principal warps: thin-plate splines and the decomposition of deformations. *IEEE Transactions on Pattern Analysis and Machine Intelligence*, 11(6):567–585, 1989.

[17] B. Boser, I. Guyon, and V. Vapnik. A training algorithm for optimal margin classifiers. *Fifth Annual Workshop on Computational Learning Theory*, pages 144–152, 1992.

[18] P. S. Bradley and O. L. Mangasarian. Feature selection via concave minimization and support vector machines. In *Proc. 15th International Conf. on Machine Learning*, pages 82–90. Morgan Kaufmann, San Francisco, CA, 1998.

[19] L. Breiman, J. Friedman, R. Olshen, and C. Stone. *Classification and Regression Trees*. Chapman and Hall, Monterey, CA, 1984. ISBN 0-412-04841-8.

[20] M. Bro-Nielsen and C. Gramkow. Fast fluid registration of medical images. In R. Hohne, K.H.; Kikinis, editor, *Visualization in Biomedical Computing. 4th International Conference, VBC '96 Proceedings*, pages 267–276. Springer-Verlag, 1996.

[21] P.J. Burt et al. Fast filter transforms for image processing. *Computer Graphics and Image Processing*, 16(1):20–51, 1981.

[22] J. Cadima and I. T. Jolliffe. Loading and correlations in the interpretation of principle compenents. *Journal of Applied Statistics*, 22(2):203–214, 1995.

[23] L. H. Clemmesen and S. Darkner. Classification in longitudinal studies. *Medical Image Analysis*, 2008. submitted.

[24] D. Comaniciu, V. Ramesh, and P. Meer. Real-time tracking of non-rigid objects using mean shift. In *Proc. of CVPR*, pages II:142–149, 2000.

[25] D. Comaniciu, V. Ramesh, and P. Meer. Kernel-based object tracking. *IEEE Transactions on Pattern Analysis and Machine Intelligence*, 25(5): 564– 577, 2003.

[26] K. Conradsen. *En Introduktion til Statistik*, volume 1B. Institute of Mathematical Modelling, Lyngby, Denmark, 1995.

[27] B. C. Cooper. Tmd diagnosis and treatment:the role of bioelectronic instruments in the management of tmd. *New York State Dental Journal*, pages 48–53, November 1995.

[28] T. F. Cootes, C. J. Taylor, D. H. Cooper, and J. Graham. Active shape models - their training and application. *Computer Vision and Image Understanding*, 61(1):38–59, 1995.

[29] T.F. Cootes and C.J. Taylor. Using grey-level models to improve active shape model search. In *Proceedings of International Conference Pattern Recognition*, pages A:63–67, 1994.

[30] T.F. Cootes and C.J. Taylor. Active shape models: Smart snakes. In *Proc. British Machine Vision Conference*, pages 267–275, 1992.

[31] T.F. Cootes and C.J. Taylor. Active shape models: Smart snakes. In *Proc. British Machine Vision Conference*, pages 267–275, 1992.

[32] T.F. Cootes and C.J. Taylor. Data driven refinement of active shape model search. In *Proc. British Machine Vision Conference*, pages 383–392, 1996.

[33] T.F. Cootes, C.J. Taylor, D.H. Cooper, and J. Graham. Training models of shape from sets of examples. In *Proc. British Machine Vision Conference*, pages 9–19, 1992.

[34] T.F. Cootes, C.J. Taylor, and A. Lanitis. Active shape models: Evaluation of a multi-resolution method for improving search. In *Proc. British Machine Vision Conference*, pages I: 327–336, 1994.

[35] T.F. Cootes, S. Marsland, C.J. Twining, K. Smith, and C.J. Taylor. Groupwise diffeomorphic non-rigid registration for automatic model building. In *European Conference on Computer Vision ECCV 04*, pages Vol IV: 316–327, 2004.

[36] T.F. Cootes, C.J. Twining, and C.J. Taylor. Diffeomorphic statistical shape models. In *Proc. British Machine Vision Conference*, volume 1, pages 447–456, 2004.

[37] L. Creel, Desporte, E.J., and R. P. Juneau. Soft-solid instrument a positive solution to the dynamic ear canal. *High performance hearing solutions*, 3: 40–43, 1999.

[38] S Darkner, M Vester-Christensen, R Larsen, R R. Paulsen, and C Nielsen. Automated 3D rigid registration of open 2D manifolds. In *Proc. From Statistical Atlases to Personalized Models Workshop, MICCAI 2006*, pages 19–22.

[39] S. Darkner, R. Larsen, M. B. Stegmann, and B. K. Ersbøll. Wedgelet enhanced appearance models. In Rasmus Larsen Arthur Pece and Alan Yuille, editors, *2nd International Workshop on Generative Model Based Vision (GMBV 2004), Washington, D. C., July, 2nd*, New Jersey, US, jul 2004. IEEE.

[40] S. Darkner, R. R. Paulsen, and R. Larsen. Analysis of deformation of the human ear and canal caused by mandibular movement. In *Medical Image Computing and Computer Assisted Intervention MICCAI 2007*, pages 801–8, B, oct 2007. Brisbane, Australia, Springer Lecture Notes.

[41] S. Darkner, M. Vester-Christensen, R. Larsen, and R. R. Paulsen. Evaluating a method for automated rigid registration. In Josien P. W. Pluim and Joseph M. Reinhardt, editors, *Proc. SPIE Medical Imaging 2007: Image Processing*, volume 6512, page 651225. SPIE, 2007.

[42] S. Darkner, M. R. Sabuncu, P. Golland, R. R. Paulsen, and R. Larsen. Analysis of surfaces using constrained regression models. In *Medical Image Computing and Computer Assisted Intervention- MICCAI 2008*, LNCS. New York, USA, Springer, September 2008. to appear.

[43] S. Darkner, M. Vester-Christensen, R. R. Paulsen, and R. Larsen. Non-rigid registration of 2D manifolds in 3D Euclidian space. In Joseph M. Reinhardt and Josien P. W. Pluim, editors, *Proc. Medical Imaging 2008: Image Processing*, volume 6914, page 69142R. SPIE, 2008.

[44] S. Darkner, D. Witzner Hansen, R. R. Paulsen, and R. Larsen. Robust registration for change detection. In Josien P. W. Reinhardt, Joseph M.; Pluim, editor, *Proc. SPIE Medical Imaging 2007: Image Processing*, volume 6914, pages 69142T–69142T–8. SPIE, April 2008.

[45] A. Dedner, M. Luthi, T. Albrecht, and T. Vetter. Curvature guided level set registration using adaptive finite elements. In *Die Deutsche Arbeitsgemeinschaft für Mustererkennung DAGM 07*, pages 527–536, 2007.

[46] E. J. Dierks. Temporomandibular disorders and facial pain syndromes. *Otolaryngology*, 1:849–864, 1991.

[47] H.Q. Dinh, G. Turk, and G.G. Slabaugh. Reconstructing surfaces by volumetric regularization using radial basis functions. *IEEE Transactions on Pattern Analysis and Machine Intelligence*, 24(10):1358–1371, October 2002.

[48] D. Donoho. Wedgelets: Nearly-minimax estimation of edges. Technical report, Dept. of Stat., Stanford Univ., 1997.

[49] I. L. Dryden and K.V. Mardia. *Statistical Shape Analysis*. Wiley, July 1998.

[50] R. O. Duda, P. E. Hart, and D. G. Stork. *Pattern Classification*. John Wiley & Sons, 2001. ISBN 978-0-471-05669-0.

[51] S. Durrleman, X. Pennec, A. Trouve, and N. Ayache. Measuring Brain Variability Via Sulcal Lines Registration: A Diffeomorphic Approach. In *Proc. Medical Image Computing and Computer Assisted Intervention (MICCAI)*, volume 4791, pages 675–682. Springer.

[52] B. Efron. Large-scale simultaneous hypothesis testing: the choice of a null hypothesis. *Journal of the American Statistical Association*, 99(465): 96–104, 2004.

[53] B. Efron and R. Tibshirani. Empirical bayes methods and false discovery rates for microarrays. *Genetic Epidemiology*, 23(1):70–86, 2002.

[54] D. P. Egolf, D. K. Nelson, H. C. III Howell, and V. D. Larson. Quantifying ear-canal geometry with multiple computer assisted tomographic scans. *Journal of the Acoustical Society of America*, 93:5:2809–2819, 1997.

[55] S. G. H. Erbou, S. Darkner, J. Fripp, S. Ourselin, and B. K. Ersbøll. Estimation of shape model parameters for 3D surfaces. In *5th IEEE International Symposium on Biomedical Imaging*, pages 624–627, may 2008.

[56] S. S. Ewing. The complexities of tmd. *RDH*, 27(10):58, 2007.

[57] E. Fisher, P. F. van der Stelt, and S. M. Dunn. 3D registration of surfaces for change detection in medical images. In K. M. Hanson, editor, *Proc. SPIE Medical Imaging*, volume 3034, 1997.

[58] A. W. Fitzgibbon. Robust registration of 2D and 3D point sets. *Image and Vision Computing*, 21(13-14):1145–1153, 2003.

[59] P. T. Fletcher, S. C. Joshi, C. Lu, and S. M. Pizer. Gaussian distributions on lie groups and their application to statistical shape analysis. In Christopher J. Taylor and J. Alison Noble, editors, *IPMI*, volume 2732 of *Lecture Notes in Computer Science*, pages 450–462. Springer, 2003.

[60] P. T. Fletcher, C. Lu, and S. Joshi. Statistics of shape via principal geodesic analysis on lie groups. In *Proceedings of the IEEE Computer Society Conference on Computer Vision and Pattern Recognition*, volume 01, page 95, Los Alamitos, CA, USA, 2003. IEEE Computer Society.

[61] K. Fukunaga and L.D. Hostetler. The estimation of the gradient of a density function. *IEEE Transactions on Information Theory*, 21:32–40, 1975.

[62] A. Genkin, D. L. David, and D. Madigan. Large-scale bayesian logistic regression for text categorization. *Technometrics*, 49(3):291–304, August 2007.

[63] E. Giles. Sex determination by discriminant function analysis of the mandible. *American Journal of Physical Anthropology*, 22(2):129–135, 1964.

[64] P. Golland. Discriminative direction for kernel classifiers. In *NIPS*, pages 745–752, 2001.

[65] P. Golland, W. E. L. Grimson, M. E. Shenton, and R. Kikinis. Small sample size learning for shape analysis of anatomical structures. In *Medical Image Computing and Computer-Assisted Intervention (MICCAI)*, volume 1935, pages 72–82. Springer-Verlag, 2000.

[66] JC Gower. Generalized Procrustes Analysis. *Psychometrika*, 40(1):33–51, 1975.

[67] S. Granger and X. Pennec. Multi-scale em-icp: A fast and robust approach for surface registration. In *European Conference on Computer Vision ECCV 02*, page IV: 418 ff., 2002.

[68] M. Graw. Significance of the classical morphological criteria for identifying gender using recent skulls. volume 3, page 1, january 2001.

[69] M. J. Grenness, J. Osborn, and W. L. Weller. Mapping ear canal movement using area-based surface matching. *JASA*, 111(2):960–971, 2002.

[70] M.H. Gross. Computer graphics in medicine: from visualization to surgery simulation. In *ACM SIGGRAPH Computer Graphics*, volume 32, pages 53–56. ACM Press New York, NY, USA, 1998.

[71] A. Haar. Zur theorie der orthogonalen funktionensysteme. *Mathematische Annalen*, 71(1):38–53, 03 1911.

[72] E. Haber and J. Modersitzki. Numerical methods for volume preserving image registration. *Inverse Problems*, 20(5):1621–1638, 2004.

[73] T. Hampton. Tmjd study. *JAMA: Journal of the Amarican Medical Association*, 295(4):377, 2006.

[74] M.F. Hansen, S.G. Erbou, M. Vester-Christensen, R. Larsen, B. Ersbøll, and L.B. Christensen. Surface-to-surface registration using level sets. In *Scandinavian Conference on Image Analysis 15*, pages 780–788. Springer.

[75] P. C. Hansen. The L-curve and its use in the numerical treatment of inverse problems. In P. Johnston, editor, *InviteComputational Inverse Problems in Electrocardiology*, Advances in Computational Bioengineering, vol.4. WIT Press, 2000.

[76] T. Hastie, R. Tibshirani, and J. Friedman. *The Elements of Statistical Learning: Data Mining, Inference, and Prediction*. Springer-Verlag, 2001. ISBN 0387952845.

[77] T. Hastie, S. Rosset, R. Tibshirani, and J. Zhu. The entire regularization path for the support vector machine. *J. Mach. Learn. Res.*, 5:1391–1415, 2004. ISSN 1533-7928.

[78] S. Haykin. *Neural Networks*. Prentice Hall, New Jersey, 1999.

[79] H. Hindi and P.A.R. Center. A tutorial on convex optimization. In *American Control Conference, 2004. Proceedings of the 2004*, volume 4, pages 3252–3265.

[80] A. E. Hoerl and R. W. Kennard. Ridge regression: Biased estimation for nonorthogonal problems. *Technometrics*, 12:55–67, 1970.

[81] J. L. Horn. A rationale and test for the number of factors in factor analysis. *Psychometrika*, 30:179–185, 1965.

[82] P.J. Huber. Robust regression: asymptotics, conjectures and Monte Carlo. *Annals of Statistics*, 1(5):799–821, 1973.

[83] A. Hyvarinen, J. Karhunen, and E. Oja. Independent Component Analysis. *IEEE Transactions on Biomedical Engineering*, 14:21–30, 2000.

[84] Kitware Inc. *VTK User's Guide 4.4*. Kitware Inc., 2004. URL `www.vtk.org`.

[85] I. Ito, M. Imada, M. Ikeda, K. Sueno, T. Arikuni, and A. Kida. A Morphological Study of Age Changes in Adult Human Auricular Cartilage With Special Emphasis on Elastic Fibers. *The Laryngoscope*, 111(5):881, 2001.

[86] N. S. Jensen and C. Nielsen. Auditory ecology in a group of experienced hearing-aid users: Can knowledge about hearing-aid users' auditory ecology improve their rehabilitation? In A N Rasmussen, T Poulsen, T Andersen, and C B Larsen, editors, *Hearing Aid Fitting - Proceedings of the 21st Danavox Symposium*, pages 235–259, 2005.

[87] O.G. Jørsboe. *Sandsynlighedsregning. Matematisk Institut DTU, Lyngby, Denmark, 1995.*

[88] F. Kahraman, M. Gokmen, S. Darkner, and R. Larsen. An active illumination and appearance (aia) model for face alignment. In *Proceedings of the CVPR 2007, IEEE Computer Society Workshop on Biometrics*, pages 1–7. IEEE Computer Society, jun 2007.

[89] H.F. Kaiser. The varimax criterion for analytic rotation in factor analysis. *Psychometrika*, 23(3):187–200, 1958.

[90] W.U. Kampen and B. Tillmann. Age-related changes in the articular cartilage of human sacroiliac joint. *Anatomy and Embryology*, 198(6): 505–513, 1998.

[91] W. Karush. Minima of functions of several variables with inequalities as side constraints. Master's thesis, Univ. of Chicago, 1939. M.Sc. Dissertation. Dept. of Mathematics.

[92] M. Kazhdan, T. Funkhouser, and S. Rusinkiewicz. Rotation invariant spherical harmonic representation of 3d shape descriptors. In *SGP '03: Proceedings of the 2003 Eurographics/ACM SIGGRAPH symposium on Geometry processing*, pages 156–164, Aire-la-Ville, Switzerland, Switzerland, 2003. Eurographics Association. ISBN 1-58113-687-0.

[93] S. Kochkin. MarkeTrak V: "Why my hearing aids are in the drawer": The consumers perspective. *The Hearing Journal*, 53(2):34–39, February 2000.

[94] S. Lanche, T. A. Darvann, H. Ólafsdóttir, N. V. Hermann, A. E. Van Pelt, D. Govier, M. J. Tenenbaum, S. Naidoo, P. Larsen, S. Kreiborg, R. Larsen, and A. A. Kane. A statistical model of head asymmetry in infants with deformational plagiocephaly. In *Proc. Scandinavian Conference on Image Analysis 2007*, page 898. Springer-Verlag, 2007.

[95] R. Larsen. Shape modelling using maximum autocorrelation factors. In Ivar Austvoll, editor, *Proceedings of the Scandinavian Image Analysis Conference (SCIA'01)*, pages 98–103, Bergen, Norway, jun 2001.

[96] R. Larsen, M. B. Stegmann, S. Darkner, S. Forchhammer, T. F. Cootes, and B. K. Ersbøll. Texture enhanced appearance models. *Computer Vision and Image Understanding*, 106:20–30, 2007.

[97] S. le Cessie and JC van Houwelingen. Ridge estimators in logistic regression. *Applied Statistics*, 41(1):191–201, 1992.

[98] F. Li, Y. Yang, and E. Xing. From lasso regression to feature vector machine. In Y. Weiss, B. Schölkopf, and J. Platt, editors, *Advances in Neural Information Processing Systems 18*, pages 779–786. MIT Press, Cambridge, MA, 2006.

[99] S. Liu, C.Y. Jia, and H. Ma. A new weighted support vector machine with ga-based parameter selection. In *Machine Learning and Cybernetics, 2005. Proceedings of 2005 International Conference on*, volume 7, pages 4351–4355, 2005.

[100] W.E. Lorenson. Marching cubes: a high resolution 3D surface construction algorithm. *Computer Graphics*, 21(4):163–169.

[101] B.D. Lucas and T. Kanade. An iterative image registration technique with an application to stereo vision. pages 674–679, 1981.

[102] E. Braverman M. Aizerman and L. Rozonoer. Theoretical foundations of the potential function method in pattern recognition learning. *Automation and Remote Control*, 25:821–837, 1964.

[103] E. C. Malthouse. Shrinkage estimation and direct marketing scoring models. *Journal of interactive marketing*, 13(4):10–23, 1999.

[104] J. Modersitski. *Numerical Methods for Image Registration*. Oxford University Press, 2004.

[105] P. Moon and D. E. Spencer. *Field Theory Handbook*. Springer-Verlag, New York, 1988.

[106] F. H. Netler. *Atlas der Anatomie des Menschen*. Novartis. ISBN 3-13-109023-5.

[107] T.E. Nichols and A.P. Holmes. Nonparametric permutation tests for functional neuroimaging: A primer with examples. *Human Brain Mapping*, 15 (1):1–25, 2002.

[108] M. Nielsen, P. Johansen, AD Jackson, and B. Lautrup. Brownian warps: A least committed prior for non-rigid registration. In *MICCAI*. Springer, 2002.

[109] M. Niethammer, M. Reuter, F. E. Wolter, S. Bouix, N. Peinecke, M.-S. Koo, and M. Shenton. Global medical shape analysis using the laplace-beltrami spectrum. In *Proceedings of the 10th Inernational Conference on Medical Image Computing and Computer Assisted Interventions, Part I, LNCS 4791*, pages 850–857. Springer, 2007. ISBN 978-3-540-75756-6.

[110] J. Nocedal and S.J. Wright. *Numerical Optimization*. Springer, 1999.

[111] H. Ólafsdóttir, M. B. Stegmann, and H. B. Larsson. Automatic assessment of cardiac perfusion MRI. In Pierre Hellier Christian Barillot, David R. Haynor, editor, *Medical image computing and computer assisted intervention, MICCAI*, volume 36 of *Lecture Notes in Computer Science*, pages 1060 – 1061. Springer, sep 2004.

[112] H. Ólafsdóttir, T. A. Darvann, N. V. Hermann, E. Oubel, B. K. Ersbøll, A. F. Frangi, P. Larsen, C. A. Perlyn, G. M. Morriss-Kay, and S. Kreiborg. Computational mouse atlases and their application to automatic assessment of craniofacial dysmorphology caused by the crouzon mutation fgfr2c̃342y. *Journal of Anatomy*, 211(1):37–52, jul 2007.

[113] R.J. Oliviera. The active earcanal. *Journal of the American Academy of Audiology*, 8:6:401–410, 1997.

[114] R.J. Oliviera and G. Hoeker. Ear canal anatomy and activity. *Seminars in hearing*, 24:4:265–275, 2003.

[115] R.J. Oliviera, B. Hammer, A Stillman, J. Holm, and R.H. Jons, C.and Margolis. A look at ear canal changes with jaw motion. *Ear and Hearing*, 13:6:464–466, 1992.

[116] R.J Oliviera, M. Babcock, M. Venemand, G. Hoeker, and B. Parish. The dynamic ear canal and its implications: The problem may be the ear, and not the impression. *Hearing Review*, 12(2):18–19, 2005.

[117] S. Osher and J.A.. Sethian. Fronts propagating with curvature dependent speed: Algorithms based on hamilton-jacobi formulations. *Journal of Computational Physics*, 79:12–49, 1988.

[118] N.C. Overgaard and J.E Solem. Separating rigid motion for continuous shape evolution. In *in Proc. International Conference on Pattern Recognition*. Hong Kong, 2006.

[119] M. Y. Park and T. Hastie. ell_1 Regularization Path Algorithm for Generalized Linear Models. *Journal of the Royal Statistical Society, Series B*, 69, part 4:pages 659–677.

[120] R. R. Paulsen. *Statistical Shape Analysis of the Human Ear Canal with Application to In-the-Ear Hearing Aid Design*. PhD thesis, Informatics and Mathematical Modelling, Technical University of Denmark, DTU, Richard Petersens Plads, Building 321, DK-2800 Kgs. Lyngby, 2004. Supervised by Rasmus Larsen (IMM), Søren Laugesen (Oticon), Herve Delingette (INRIA), and Knut Conradsen (IMM).

[121] R. R. Paulsen and K. B. Hilger. Shape modelling using markov random field restoration of point correspondences. In *Information Processing in Medical Imaging*, IPMI, 2003.

[122] R. R. Paulsen, R. Larsen, B. K. Ersbøll, C. Nielsen, and S. Laugesen. Testing for gender related size and shape differences of the human ear canal using statistical methods. In Knut Conradsen and Bjarne Kjær Ersbøll, editors, *Eleventh International Workshop on Matrices and Statistics*, Richard Petersens Plads, Building 321, DK-2800 Kgs. Lyngby, aug 2002. Informatics and Mathematical Modelling, Technical University of Denmark, DTU.

[123] R. R. Paulsen, R. Larsen, S. Laugesen, C. Nielsen, and B. K. Ersbøll. Building and testing a statistical shape model of the human ear canal. In *Medical Image Computing and Computer Assisted Intervention MICCAI 2002, 5th Int. Conference*, pages 373–380. Tokyo, Japan, Springer, 2002.

[124] R. R. Paulsen, C. Nielsen, S. Laugesen, and R. Larsen. Using a shape model in the design of hearing aids. In *SPIE - Medical Imaging*, The International Society for Optical Engineering - Medical Imaging, feb 2004.

[125] K. Pearson. On lines and planes of closest fit to systems of points in space. *Philosophical Magazine*, 2(6):559–572, 1901.

[126] C. Pirzanski. Despite new digital technologies, shell modelers shoot in the dark. *The Hearing Journal*, 59(10):28–31, Oct 2006.

[127] C. Pirzanski and B. Berge. An ear impression technique that works. *Hearing Review*, 11(12):24–27, 2002.

[128] C. Pirzanski and B. Berge. Is the end near for acoustic feedback. *Hearing Review*, 11(4):18–23, 2004.

[129] C. Pirzanski and B. Berge. Ear canal dynamics: Facts versus perception. *The Hearing Journal*, 58(10):50–58, October 2005.

[130] S.M. Pizer, D.S. Fritsch, P.A. Yushkevich, V.E. Johnson, and E.L. Chaney. Segmentation, registration, and measurement of shape variation via image object shape. 18(10):851–865, October 1999.

[131] G.M. Postelnicu, L . Zöllei, and B. Fischl. Combined volumetric and surface registration. *IEEE Transactions on Medical Imaging (TMI)*, July 2008. accepted.

[132] R.B. Potts. Some generalized order-disorder transformations. *Proceedings of the Cambridge Philosophical Society*, 48:106–109, 1952.

[133] K. T. Rajamani, M. A. Styner, H. Talib, G. Zheng, L. P. Nolte, and M. A. G. Ballester. Statistical deformable bone models for robust 3D surface extrapolation from sparse data. *Medical Image Analysis*, 11:99–109, 2007.

[134] A. Roche, G. Malandain, and N.J. Ayache. Unifying maximum likelihood approaches in medical image registration. 11(1):71–80, 2000.

[135] D. Rueckert, L. I. Sonoda, C. Hayes, D. L. G. Hill, M. O. Leach, and D. J. Hawkes. Non-rigid registration using free-form deformations: Application to breast mr images. *IEEE Transactions on Medical Imaging*, 18(8):712–721, 1999.

[136] D. Rueckert, P. Aljabar, R. A. Heckemann, JV Hajnal, and A. Hammers. Diffeomorphic Registration using B-Splines. In *9th International Conference on Medical Image Computing and Computer-Assisted Intervention (MICCAI 2006)*, October 2006.

[137] S. Rusinkiewicz and M. Levoy. Efficient variants of the icp algorithm. In *Proc. 3-D Digital Imaging and Modeling 3DIM 01*, pages 145–152, 2001.

[138] G. Schwarz. Estimating the dimension of a model. *The Annals of Statistics*, 6(2):461–464, 1978.

[139] J.A. Sethian. A Fast Marching Level Set Method for Monotonically Advancing Fronts. *Proceedings of the National Academy of Sciences*, 93(4): 1591–1595, 1996.

[140] J. Shawe-Taylor and N. Cristianini. *Kernel Methods for Pattern Analysis*. Cambridge University Press, UK, 2004.

[141] K. Sjöstrand and R. Larsen. The entire regularization path for the support vector domain description. In *Medical Image Computing and Computer-Assisted Intervention, MICCAI 2006, Copenhagen, Denmark*, Richard Petersens Plads, Building 321, DK-2800 Kgs. Lyngby, oct 2006. Informatics and Mathematical Modelling, Technical University of Denmark, DTU. Winner of best student paper award in the category of image analysis.

[142] K. Sjöstrand, M. B. Stegmann, and R. Larsen. Sparse principal component analysis in medical shape modeling. In *International Symposium on Medical Imaging 2006, San Diego, CA, USA*, volume 6144. The International Society for Optical Engineering (SPIE), feb 2006.

[143] K. Sjöstrand, M. S. Hansen, H. B. Larsson, and R. Larsen. A path algorithm for the support vector domain description and its application to medical imaging. *Medical Image Analysis*, 11(5):417–428, 2007.

[144] K. Sjöstrand, V. A. Cardenas, R. Larsen, and C. Studholme. A generalization of voxel-wise procedures for high-dimensional statistical inference using ridge regression. In Joseph M. Reinhardt and Josien P. W. Pluim, editors, *Medical Imaging 2008: Image Processing.*, volume 6914, pages pp. 69140A–69140A–12, April 2008.

[145] M. S. Sorensen, A. B. Dobrzeniecki, P. Larsen, T. Frisch, J. Sporring, and T. A. Darvann. The visible ear: A digital image library of the temporal bone. *ORL*, 64:378–381, 2002.

[146] S. Standring and H. Ellis. *Gray's anatomy*. Churchill Livingstone New York, 1995.

[147] M. B. Stegmann. Active appearance models: Theory, extensions and cases. Master's thesis, Informatics and Mathematical Modelling, Technical University of Denmark, DTU, Richard Petersens Plads, Building 321, DK-2800 Kgs. Lyngby, aug 2000.

[148] M. B. Stegmann. *Generative Interpretation of Medical Images*. PhD thesis, Informatics and Mathematical Modelling, Technical University of Denmark, DTU, Richard Petersens Plads, Building 321, DK-2800 Kgs. Lyngby, 2004. Awarded the Nordic Award for the Best Ph.D. Thesis in Image Analysis and Pattern Recognition in the years 2003-2004 at SCIA'05.

[149] M. B. Stegmann and K. Skoglund. On automating and standardising corpus callosum analysis in brain MRI. In *Proc. Svenska Symposium i Bildanalys, SSBA 2005, Malmø, Sweden*, pages 1–4. SSBA, mar 2005.

[150] M. B. Stegmann, H. Ólafsdóttir, and H. B. W. Larsson. Unsupervised motion-compensation of multi-slice cardiac perfusion MRI. *Medical Image Analysis*, 9(4):394–410, aug 2005.

[151] C. Studholme, DLG Hill, and DJ Hawkes. Incorporating connected region labelling into automated image registration using mutual information. In *Proc. of MMBIA*, volume 96, pages 23–31, 1996.

[152] M. Styner, K. Gorczowski, P. T. Fletcher, J. Y. Jeong, S. M. Pizer, and G. Gerig. Statistics of pose and shape in multi-object complexes using principal geodesic analysis. In Guang-Zhong Yang, Tianzi Jiang, Dinggang Shen, Lixu Gu, and Jie Yang, editors, *MIAR*, volume 4091 of *Lecture Notes in Computer Science*, pages 1–8. Springer, 2006. ISBN 3-540-37220-2.

[153] P. Switzer. Min/max autocorrelation factors for multivariate spatial imagery. *Computer Science and Statistics*, pages 13–16, 1985.

[154] T. Terriberry, S. Joshi, and G. Gerig. Hypothesis testing with nonlinear shape models. In *Information Processing in Medical Imaging (IPMI)*, pages 15–26. Springer.

[155] J.P. Thirion. Image matching as a diffusion process: an analogy with Maxwell's demons. *Medical Image Analysis*, 2(3):243–260, 1998.

[156] R. Tibshirani. Regression shrinkage and selection via the lasso. *J. R. Statist. Soc. B*, 58(No. 1):267–288, 1996.

[157] R. Tibshirani, M. Saunders, S. Rosset, J. Zhu, and K. Knight. Sparsity and smoothness via the fused lasso. *J. R. Statist. Soc. B*, 1(67):91–106, 2006.

[158] A. N. Tikhonov. Solutions of incorrectly formulated problems and the regularization method. *Soviet Math. Dokl.*, 4:1035–1038, 1963. English translation of Dokl. Akad. Nauk. SSSR, 151:501-504, 1963.

[159] G. Tolt, A. Wiklund, P. Andersson, T. Chevalier, C. Grönwall, F. Gustafsson, and H. Larsson. Registration and change detection techniques using 3D laser radar data from natural environments. In *Electro-Optical Remote Sensing II. SPIE (2006).*, volume 6396, October 2006. doi: 10.1117/12.690189.

[160] A. Tsai, A. J. Yezzi, W. M. Wells III, C. Tempany, D. Tucker, A. Fan, W. E. L. Grimson, and A. S. Willsky. A shape-based approach to the segmentation of medical imagery using level sets. *IEEE Trans. Med. Imaging*, 22(2):137–154, 2003.

[161] Z. Tu, S. Zheng, and A. Yuille. Shape matching and registration by data-driven EM. *Computer Vision and Image Understanding*, 109(3):290–304, 2008.

[162] H. C. van Assen, M. G. Danilouchkine, A. F. Frangi, S. Ordás, J. J. M. Westenberg, J. H. C. Reiber, and B. P. F. Lelieveldt. SPASM: A 3D-ASM for segmentation of sparse and arbitrarily oriented cardiac MRI data. *Medical Image Analysis*, 10:286–303, 2006.

[163] V. Vapnik. *The Nature of Statistical Learning Theory.* Springer-Verlag, New York, 2nd edition, 1999.

[164] M. Vester-Christensen, S. G. Erbou, S. Darkner, and R. Larsen. Accelerated 3D image registration. In Joseph M. Pluim, Josien P. W.; Reinhardt, editor, *Proc. SPIE Medical Imaging 2007: Image Processing*, volume 6512, page 65121W. SPIE, mar 2007.

[165] L. Wang, J. Zhu, and H. Zou. The doubly regularized support vector machine. *Statistica Sinica*, 16:589–615, 2006.

[166] S. Wang, Y. Wang, M. Jin, X. Gu, and D. Samaras. 3D Surface Matching and Recognition Using Conformal Geometry. In *Proceedings of the IEEE Computer Society Conference on Computer Vision and Pattern Recognition*, volume 2, pages 2453–2460, 2006.

[167] Y. Wang, B.S. Peterson, and L.H. Staib. 3D Brain surface matching based on geodesics and local geometry. *Computer Vision and Image Understanding*, 89(2-3):252–271, 2003.

[168] W.M. Wells, P. Viola, H. Atsumi, S. Nakajima, and R. Kikinis. Multi-modal volume registration by maximization of mutual information. *Medical Image Analysis*, 1(1):35–51, 1996.

[169] T. Whitted. An improved illumination model for shaded display. *Commun. ACM*, 23(6):343–349, 1980. ISSN 0001-0782.

[170] S.M. Yamany, MN Ahmed, E.E. Hemayed, and A.A. Farag. Novel surface registration using the grid closest point (GCP) transform. In *Proc IEEE, Int. Conf. on Img. Proc., ICIP*, volume 3, pages 809–813, 1998.

[171] P. Yu, B.T.T. Yeo, P.E. Grant, B. Fischl, and P. Golland. Cortical folding development study based on over-complete spherical wavelets. pages 1–8, 2007.

[172] L. Zollei, E. Learned Miller, W.E.L. Grimson, and W.M. Wells, III. Efficient population registration of 3d data. In *Proceeding of the Tenth IEEE International Conference on Computer Vision Workshop 2005; 10(WS) CVBIA 05*, pages 291–301, 2005.

[173] H. Zou and T. Hastie. Regularization and variable selection via the elastic net. *J. R. Statist. Soc. B*, 67(Part 2):301–320, 2005.

[174] H. Zou, T. Hastie, and R. Tibshirani. Sparse Principal Component Analysis. *Journal of Computational and Graphical Statistics*, 15(2):265, 2006.

[175] H. Zou, T. Hastie, and R. Tibshirani. On the "degrees of freedom" of the lasso. *Annals of Statistics*, 35(5):2173–2192, 2007.